EFFECTS OF MECHANICAL AND TEMPORAL PARAMETERS ON TACTILE PSYCHOPHYSICAL RESPONSES

by

Mustafa Zahid YILDIZ

B.S., Electrical and Electronics Engineering, Sakarya University, 2004.

M.S., Biomedical Engineering, Boğaziçi University, 2007.

Submitted to the Institute of Biomedical Engineering

in partial fulfillment of the requirements

for the degree of

Doctor

of

Philosophy

Boğaziçi University

2013

EFFECTS OF MECHANICAL AND TEMPORAL PARAMETERS ON TACTILE PSYCHOPHYSICAL RESPONSES

APPROVED BY:

Assoc. Prof. Dr. Burak Güçlü   . . . .
(Thesis Advisor)

Assoc. Prof. Dr.Can Yücesoy   . . . .

Assoc. Prof. Dr. Çağatay Başdoğan   . . . .

Asisst. Prof. Dr. Bora Garipcan   . . . .

Asisst. Prof. Dr. Özgür Kocatürk   . . . .

DATE OF APPROVAL: 15.05.2013

ACKNOWLEDGMENTS

I would love to express my sincere gratitude, first and foremost, to my advisor Assoc. Prof. Dr. Burak Güçlü for encouraging me and for continuous support during my PhD study and research. His guidance helped me during my research and writing of this thesis. I would like to thank to Dr. Çağatay Başdoğan from Koç University and Dr. Can Yücesoy from Boğaziçi University for their helpful comments during my thesis progress.

I also thank to my lab mates in Tactile Research Laboratory: İsmail Devecioğlu, Duygu Torun, Murat Özsaltık, Fatma Büşra Özkan and students who participated to the experiments of my study.

I would like to express my thanks to Mehmet Ayyıldız from Koç University, Nihal Bahar from Dokuz Eylül University for their help during the experiments. Part of the studies of this thesis was supported by Boğaziçi University BAP no: 10XP1 and Ministry of Development DPT project no: 09K120520 to Dr. Burak Güçlü.

ABSTRACT

EFFECTS OF MECHANICAL AND TEMPORAL PARAMETERS ON TACTILE PSYCHOPHYSICAL RESPONSES

Tactile feedback is becoming more important in clinical devices and engineering. Therefore, studies on basic sensory processing in the somatosensory system are essential. In this thesis, the mechanical and temporal parameters affecting the absolute tactile detection threshold of human Pacinian (P) channel were investigated. Temporal summation in P channel was found to be independent of stimulus frequency and the experimental results did not fit the classical model of temporal summation. The model needs to be modified to show the U-shaped Pacinian channel behavior. Additionally, the spatial summation property of the P channel was demonstrated on fingertip at three different contact locations and at three contactor sizes. The effects of skin mechanics on psychophysical thresholds of the P channel were studied by measuring mechanical impedance. A significant correlation was found between the thresholds and the dynamic modulus of the skin. Conventionally, somatosensory evoked potentials (SEPs) are measured on the scalp by applying electrically stimulating the peripheral nerves in the clinical setting. Here, SEPs were represented by different types of wavelet functions, which can be used in data compression. Non invasive recordings of scalp potentials were also investigated by applying strong mechanical stimulation on the fingertip. However, time-frequency analysis did not show much useful information about stimulus properties, which would be useful in understanding basic somatosensory processes. The results of this thesis may be useful in various fields such as haptics, robotics, prostheses, dermatology, cosmetics. Specifically, spatial and temporal summation should be incorporated in the high-frequency vibrotactile feedback in prosthetic arms.

Keywords: Touch, somatosensory, Pacinian channel, psychophysical threshold, temporal summation, spatial summation, skin mechanics, mechanical impedance, somatosensory evoked potentials.

ÖZET

MEKANİK VE ZAMANSAL PARAMETRELERİN PSİKOFİZİKSEL DOKUNMA CEVAPLARINA ETKİLERİ

Dokunsal geri besleme güncel klinik cihazlarda ve mühendislikte oldukça önemli olmaya başlamıştır. Bu yüzden bedenduyusu sistemindeki temel duyusal bilgi işlemeyi anlamak gerekmektedir. Bu tezde, insanda Pacini (P) kanalındaki mekanik ve zamansal parametrelerin psikofiziksel eşik değeri üzerindeki etkileri incelenmiştir. P kanalındaki zamansal toplama işleminin uyarı frekansından bağımsız olduğu gösterilmiştir. Aynı zamanda deneysel sonuçlar klasik zamansal toplama modeli ile uyuşmamaktadır. Bu model P kanalının U-eğrisi şeklindeki davranışını göz önüne almalıdır. Buna ek olarak, P kanalındaki uzaysal toplama özelliği de parmak ucundaki üç farklı kontakt bölgesi ve üç farklı kontakt ucu ile gösterilmiştir. Deri mekaniğinin P kanalı psikofiziksel eşik değerleri üzerindeki etkisi mekanik empedans ölçümleri ile incelenmiştir. Derinin dinamik modulus ve eşik değerleri arasında anlamlı korelasyon bulunmuştur. Klinik ortamda bedenduyusuna ilişkin uyarılmış potansiyeller kafa derisi üzerinden ölçülmekte ve genellikle periferik sinirlerin elektriksel olarak uyarılmasıyla oluşmaktadır. Burada, uyarılmış potansiyeller farklı dalgacık fonksiyonları cinsinden temsil edilmiştir. Ve bu sonuçlar veri sıkıştırma uygulamalarında kullanılabilir. Ayrıca, parmak ucundaki derinin mekanik uyarılmasıyla kafa derisi üzerinden ivnaziv olmadan ölçülen potansiyeller incelenmiştir. Ancak bu potansiyellerin zaman-frekans analizleri uyarı parametreleri hakkında anlamlı bilgi içermemektedir. Bu yüzden bedenduyusunda bilgi işlemeyi anlamak için kullanılması uygun değildir. Bu tezin genel sonuçları, haptik, robotik, protezler, dermotoloji ve kozmetik gibi birçok farklı alanda kullanılabilir. Örneğin, P kanalında gösterilen uzaysal ve zamansal toplama özelliği protez kollara yerleştirilecek yüksek frekanslı dokunsal geribesleme algoritmalarında kullanılabilir.

Anahtar Sözcükler: Dokunma, bedenduyusu, Pacini kanalı, psikofiziksel eşik değeri, zamansal toplama, uzaysal toplama, deri mekaniği, mekanik empedans, bedenduyusu korteksi uyarılmış cevaplar.

TABLE OF CONTENTS

LIST OF FIGURES

LIST OF TABLES

LIST OF SYMBOLS

d	Stimulus duration
A	Stimulus amplitude
k	Cycle/impulse index
f	Frequency
q	Threshold criterion
τ	Time constant
Z	Mechanical impedance
E^*	Dynamic modulus
σ	Stress
ε	Strain
F	Force
v	Velocity
w	Angular frequency
x_0	Static indentation
$R_{EKerror}$	Reconstruction error

LIST OF ABBREVIATIONS

SEP   Somatosensory evoked potential

P   Pacinian

PC   Pacinian channel

RA   Rapidly adapting

SA   Slowly adapting

NP   Non-Pacinian

SL   Sensation level

FFT   Fast Fourier transform

DWT   Discrete wavelet transform

1.   INTRODUCTION

1.1   Motivation

Somatic sensory system enables us to feel touch, pain and temperature on our bodies and to know where our limbs are and what they are doing. Among these senses, the sense of touch has a wide range of physical and emotional attributes for people of all age groups. It is sensitive to numerous kinds of stimuli such as pressure, vibration and stretch on the skin. The skin, as the touch organ, is embedded with mechanoreceptors and tactile fibers innervating these mechanoreceptors. With the help of information conveyed by these fibers, we are able to perform precise grip of objects without dropping them, to understand texture, shape and smoothness of objects.

Clinically, there are many conditions which affect sensory processes. However, most dramatically, loss of a limb results in a tremendous reduction in sensory feedback. Without sensory feedback, efficient motor control cannot be provided. In medical robotics and neural prostheses tactile feedback has vital importance. Additionally, visually impaired individuals depend on tactile feedback significantly. Therefore, understanding basics mechanisms of somatosensory processing is essential.

Tactile information is processed by four psychophysical tactile channels. Specifically, the Pacinian (P) channel has the lowest thresholds at high frequencies (e.g. 0.1 μm around 250 Hz). P channel has special psychophysical properties such as spatial and temporal summation. Additionally, the study of the stimulus parameters (i.e. stimulus contactor location, size, stimulus duration and frequency), that affect the sensitivity of the P channel may give us practical information for engineering and clinical applications in many areas. For example, these studies may be helpful for creating realistic (human-like) touch for neural prostheses. In this respect, I hypothesized that temporal summation is independent of stimulus frequency in the P channel and spatial summation is present at various location at the fingertip. Not only the stimulus pa-

rameters, but also the mechanical properties of skin may affect the sense of touch. This has numerous implications in dermatology, aging and cosmetics as well as designing artificial skin. In this thesis, I specifically studied the relationship between the tactile threshold in P channel and the dynamic modulus of the skin. Previous works showed that mechanical properties may affect the threshold.

Noninvasive clinical studies of the somatosensory system focused on somatosensory evoked potentials (SEPs) generated by electrical stimulation of the peripheral nerves. However, SEPs only give a limited amount of information (i.e. component amplitudes and latencies) on the general state of the somatosensory pathways. They do not tell us much about peripheral and central processing which occurs during natural mechanical stimuli. Therefore, I investigated whether mechanically evoked somatosensory potentials can give useful information about stimulus properties. Meanwhile, SEP measurements require substantial memory storage. Discrete wavelet transform was used to compress data and represent SEPs with a significantly reduced number of coefficients.

1.2   Skin anatomy

The sensation of touch begins at skin. Skin performs an essential protective function and prevents the evaporation of body fluids into dry environment we live in. But skin also provides our most direct contact with the world; indeed, skin is the largest and heaviest sensory organ of human body (1.2-2.3 m^2 of surface area, around 16% of total body weight)[1].

There are three major types of skin, specialized for mechanical stimuli: glabrous skin (hairless skin on the surface of our palm, the soles), hairy and mucocutaneous skin which lines the entrance to the inside of the body [2]. Glabrous skin is characterized by a regular array of ridges formed by folds of the epidermis. The ridges are arranged in curved patterns called fingerprints and contain a dense matrix of mechanoreceptors. Glabrous skin has a relatively thick epidermis and lack hair follicles [3].

Skin has a multilayered structure consisting of the epidermis, the dermis and the hypodermis. The epidermis forms an uninterrupted barrier that ranges in thickness from 0.07 mm to 0.12 mm over much of the body surface [4]. Epidermis consists largely of outward moving cells, the keratinocytes, that are formed by division of cells in the basal layer of the epidermis. The most superficial layer, the stratum corneum consists of 15-20 layers of dead a nucleate cells that are hexagonally thin and flat squames. At this stage, the cells are terminally differentiated keratinocytes, called corneocytes [4].

Below the epidermis is the dermis, which is 1 mm to 4 mm thick. The dermis is composed of the papillary and reticular layers. Human dermis makes up the bulk of the human skin and contributes to 15-20 % of the total body weight. It contains a lot of irregularities such as blood vessels, lymph vessels, nerve endings and the skin appendages such as hair follicles, small hair muscles, sebaceous glands and sweat glands. The papillary dermis forms the upper layer, which comprises about 10% of the full dermal thickness [4]. It contains collagen fibrils 20-40 nm in diameter that are packed into thicker collagen fibers 0.3-3.0 μm in diameter. Below the papillary layer is found the reticular layer, which contains collagen fibrils 60-100 nm in diameter. Reticular collagen fibrils are composed primarily of type I collagen and have fiber diameters between 10 and 40 μm. Type III collagen accounts for only about 15% of the dermal collagen, much of which is found in the papillary layer [5].

The dermis also contains elastin and minute quantities of reticulin and a supporting matrix or ground substance. Collagen comprises about 75% of the fat free dry weight and 18-30% of the volume of dermis [6]. The third layer, the hypodermis (or subcutaneous layer) is composed of loose fatty connective tissue. Its thickness varies considerably over the surface of the body. It acts as an insulating layer and a protective cushion and constitutes about 10% of the body weight [4].

The sensory receptors are responsible for tactile sensation located in this multi-layered organ (Figure 1). All mechanoreceptors have specialized end organs surrounding the nerve terminal. The sensitivity of these receptors is shaped both by the nerve terminal membrane and the outer structures [3].
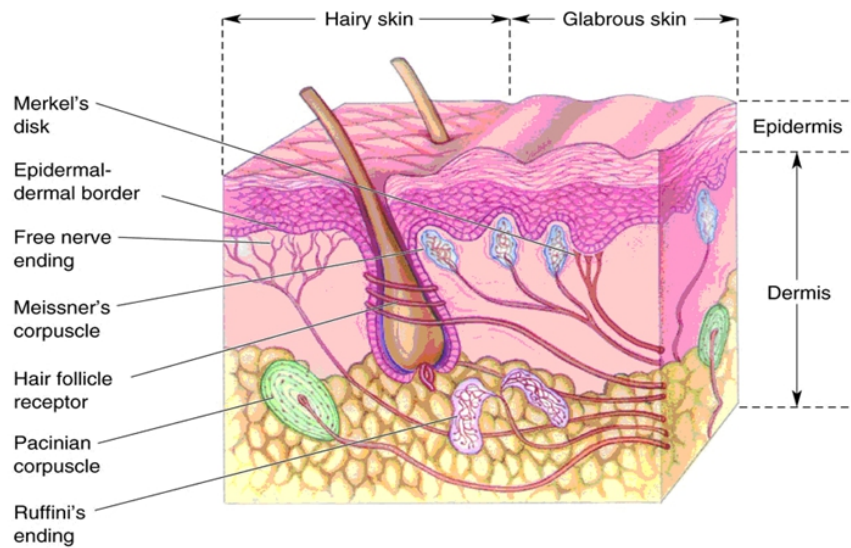
Figure 1.1 Mechanoreceptors in the glabrous and the hairy skin [2].

1.3 Mechanoreceptors in the glabrous skin

In human glabrous skin, there are four types of mechanoreceptors; Pacinian corpuscles, Meissner corpuscles, Merkel discs and Ruffini endings [7, 8]. The associated mechanoreceptive nerve fibers are typically classified according to their receptive field sizes and adaptation of their responses to ramp-and-hold stimulation. Specifically, rapidly adapting (RA) fibers innervate Meissner corpuscles, Pacinian (PC) fibers innervate Pacinian corpuscles. Slowly adapting type I fibers (SA I) are associated with Merkel cells. Slowly adapting type II (SA II) fibers form Ruffini endings. Mechanoreceptors are located in the superficial skin, at the junction of the dermis and epidermis, and more deeply in the dermis and subcutaneous tissue (Figure 1).

When a mechanical stimulus is applied on the skin, the accessory structure of the receptor acts as a mechanical filter, transmitting the stress to the unmyelinated membrane. The strain at the level of the membrane induces stretch sensitive channels to respond by increasing their conductances to certain ions, Na^+ ions in particular, although a contribution from K^+ ions may also occur. This causes a passive local depolatizaton of the membrane, called the receptor potential. If the passive spread of the receptor potential is sufficient, an action potential will ve generated at the first
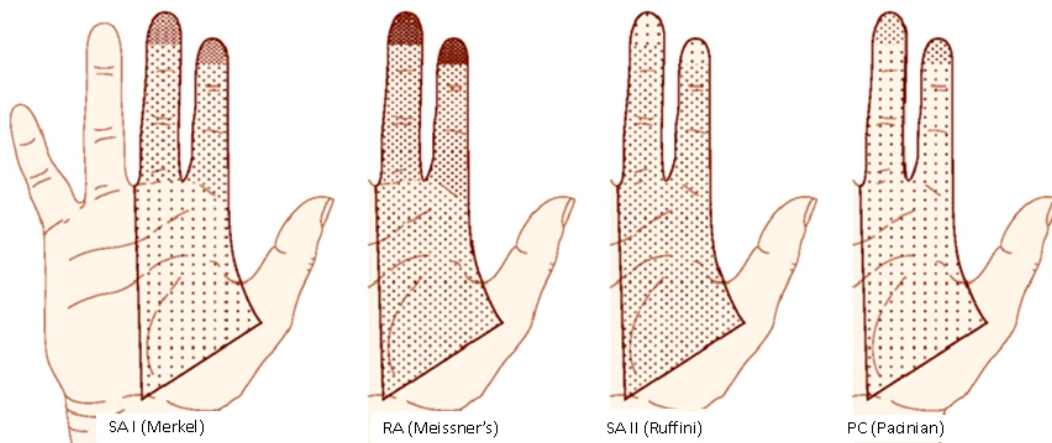
Figure 1.2 The distribution of mechanoreceptor types in the human hand varies [3].

node of Ranvier and propagated along the peripheral nerve [3].

In Figure 2, the number of sensory nerve fibers innervating an area is indicated by the stippling density, with the highest density of receptors shown by the heaviest stippling. Meissner corpuscles and Merkel disk receptors (SA I) are the most numerous receptors; they are distributed preferentially on the distal half of the fingertip. Pacinian corpuscles and Ruffini endings are less common; they are distributed more uniformly in the hand (Figure 2).

The size and structure of receptive fields differ depending on the fiber type. A single dorsal root ganglion neuron innervating the superficial layers of the skin receives input from a cluster of 10-25 Meissner corpuscles or Merkel disk receptors. The afferent fiber has a receptive field that spans a small circular area with a diameter ranging from 2 to 10 mm (Figure 3). In contrast, the afferent fibers innervating the deep layers of skin are connected to a single Pacinian corpuscle or Ruffini ending. Consequently, the receptive fields of these receptors of these afferents cover large areas of skin, and their borders are indistinct (Figure 3). Usually, receptive fields have a single or multiple hot spots where sensitivity to touch is greatest, located directly above the receptors. The large receptive fields result from the ability of these receptors to sense mechanical displacement at some distance from the end organ [3].

The differences in size of afferent receptive fields play an important role in the
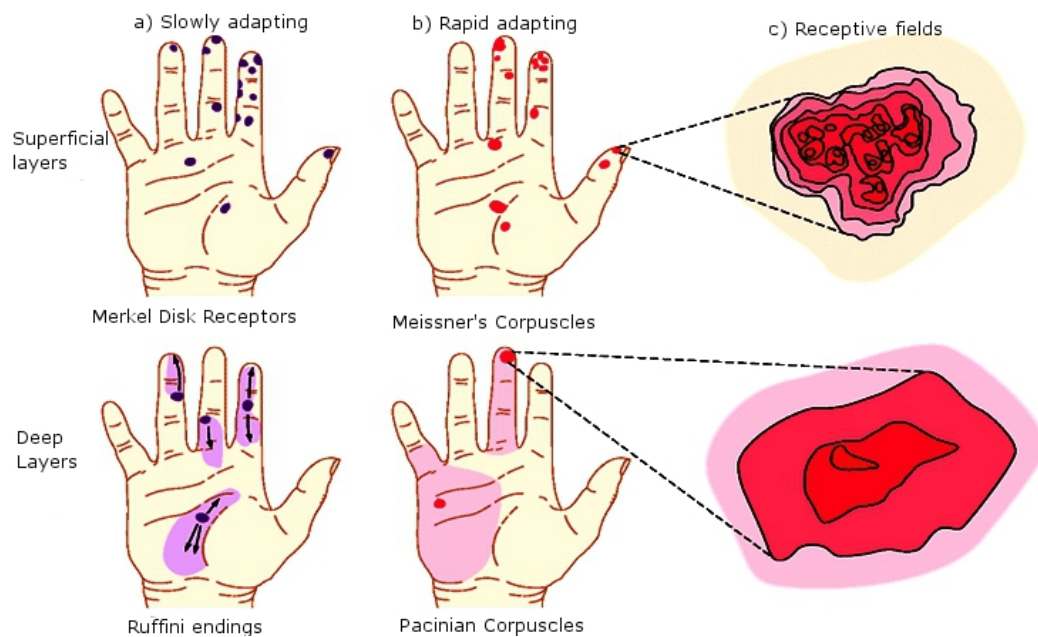
Figure 1.3 Mechanoreceptors in the glabrous skin and the structure of their receptive fields [3].

tactile sensation. Meissner corpuscle and Merkel disk receptors resolve fine spatial differences because they transmit information from a restricted area of skin. As these receptors are smaller in diameter than the fingerprint ridges of glabrous skin, individual receptors can be stimulated by very small bumps on a surface. This high spatial resolution allows humans to perform fine tactile discrimination of surface texture and to read Braille. Pacinian corpuscles and Ruffini endings resolve only coarse spatial differences. They are poorly suited for accurate spatial localization or for discriminating fine spatial detail. They sense more global properties of objects and detect displacements from a wide area of skin.

The temporal response properties of mechanoreceptive fibers are different. Meissner and Pacinian corpuscles are fast adapting, in other words they generate action potentials only during high frequency components of the mechanical stimulus (Figure 4). Merkel disks and Ruffini endings are slowly adapting and they can generate a sustained response of action potentials during the stimulus period. PC fibers are most sensitive for 40-300 Hz vibrotactile stimulation. RA fibers respond mostly stimuli at 3-40 Hz. The anatomy, physiology and psychophysics of Pacinian tactile system have been studied extensively due to easier accessibility [9, 8, 10, 11, 12] . Adaptation properties,
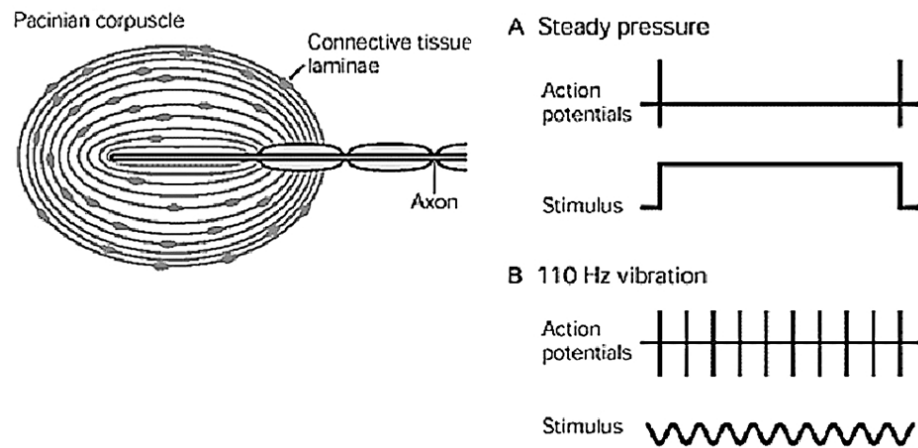
Figure 1.4 Rapidly adapting response of Pacinian corpuscles. a) Rreceptor only responds at the beginning and end of the steady stimulus. b) Receptor responds every cycle of vibration within a frequency range [3].

densities and receptive field sizes of the mechanoreceptor fibers are shown in Figure 5.

1.4 Skin mechanics

Quantitative measurement of mechanical behavior of human skin has crucial importance for many areas, such as dermatology, cosmetics and for tissue engineering. Mechanical properties of skin depend on the nature and organization of a) dermal collagen and elastic fiber network, b) water content, proteins and macromolecules embedded in the extracellular matrix c) cellular layers in the epidermis.

Collagen is a group of naturally occurring proteins found in animals, especially in the flesh and connective tissues of vertebrates. It is the main component of connective tissue, and is the most abundant protein in mammals, making up about 25% to 35% of the whole-body protein content. Collagen, in the form of elongated fibrils, is mostly found in fibrous tissues such as tendon, ligament and skin, and is also abundant in cornea, cartilage, bone, blood vessels, the gut, and intervertebral discs. The fibroblast is the most common cell which creates collagen.

Changes in collagen fibril orientation during deformation of dermis are critical
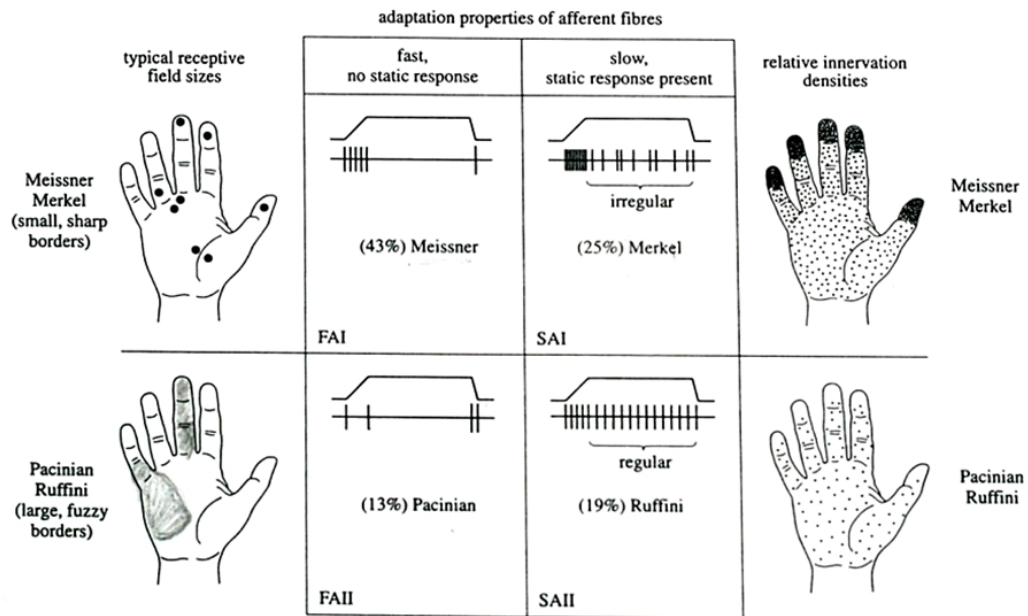
Figure 1.5 Receptive field sizes, adaptation properties, and innervation densities of tactile afferent fibers [8].

for maintaining the large extensibility of human skin. The mechanical properties of skin are related to the structure and properties of the collagen and elastic fibers and the proteoglycans that are found in the skin. Collagen fibers are form an irregular network of wavy coiled fibres that run almost parallel with the skin surface [13]. Collagen is characterized by high stiffness (Young's modulus approximately 0.1 GPa [14] to 1 GPa [15] in the linear region) and low extensibility (rupture at strains in the order of 5-6%) [4].

Elastin is a protein in connective tissue that is elastic and allows many tissues in the body to resume their shape after stretching or contracting. Elastin helps skin to return to its original position when it is poked or pinched. Elastin is also an important load-bearing tissue in the bodies of vertebrates and used in places where mechanical energy is required to be stored. Elastin serves an important function in arteries as a medium for pressure wave propagation to help blood flow and is particularly abundant in large elastic blood vessels such as the aorta. Elastin is also very important in the lungs, elastic ligaments, the skin, and the bladder, elastic cartilage. Elastin fibers are the second main component of the dermis (4% of the fat-free dry weight). They are

less stiff than collagen and show reversible strains of more than 100% [5].

Reticulin is found in much smaller amounts: only 0.4% of the fat-free dry weight. Mechanical properties of reticulin are not exactly known, but since reticulin has a similar molecular structure and morphology as collagen, the properties are likely to be similar to that of collagen. The ground substance is responsible for the viscoelastic behavior of the dermis. It is unlikely that it contributes to the tensile strength of the dermis.

The stress-strain curve for the skin can be divided in four to stages (Figure 6). In the first stage, the contribution of the undulated collagen fibers can be neglected and elastin is responsible for the skin stretching. In this stage, the stress-strain relation is approximately linear with a Youngâs modulus of approximately 5 kPa [4, 16]. Up to strains of about 0.3 the collagen network offers little resistance to deformation and behavior is dominated by elastic fibers [5]. In the second stage, a gradual straightening of an increasing fraction of the collagen fibers causes an increasing stiffness. Between strains of about 0.3 and 0.6 the collagen fibrils begin to offer resistance to deformation. In the third stage, all collagen fibers are stretched and the stress-strain relation becomes linear again. Beyond this phase (strain over 0.6), yielding and rupture of the fibers occur [4, 5] (Figure 6).

Skin is also viscoelastic and as a results, the mechanical response to loading involves both a viscous components associated with energy dissipation and an elastic component associated with energy storage. Energy applied to skin is partially dissipated through viscous sliding of collagen fibrils during alignment with the force direction while the elastic behavior of skin is important in ensuring shape recovery after deformation [5].
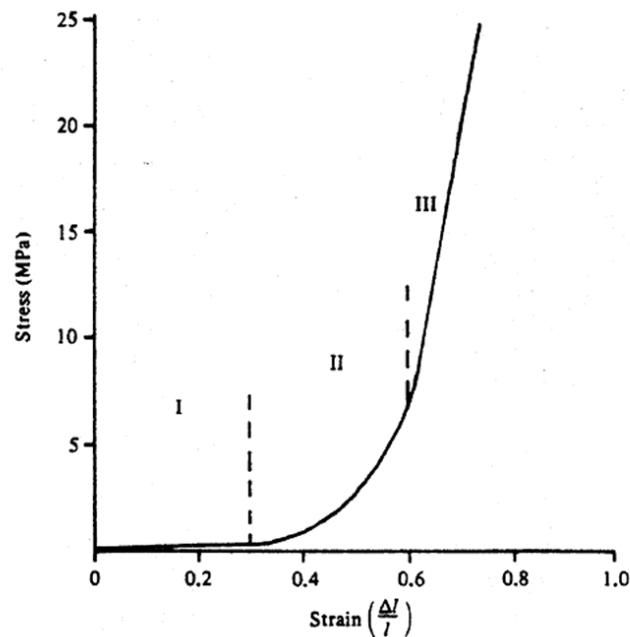
Figure 1.6 Stress-strain diagram of skin showing the different behaviours [16].

1.4.1 Viscoleastic properties of the skin

A viscoelastic material contains a combination of solid (storage of elastic energy) and liquid (viscous losses) property. For a purely elastic material, all the energy stored in the sample during loading is returned when the load is removed. As a result, loading and response curves for elastic materials move completely in phase (Figure 7.a). A purely viscous material does not return the energy stored during loading (Figure 7.b). All the energy is lost as pure damping once the load is removed.

Viscoelasticity is related with materials that exhibit both elastic and viscous behaviors. Some of the energy stored in a viscoelastic material is recovered upon removal of the load, and the remainder is dissipated in the form of heat. Therefore, a phase difference occurs between loading and response curves (Figure 7.c) [17].

The mechanical properties of viscoelastic materials are characterized by performing simple laboratory tests. Once the properties are characterized, one can integrate them into mathematical models to simulate the viscoelastic behavior. Since time plays
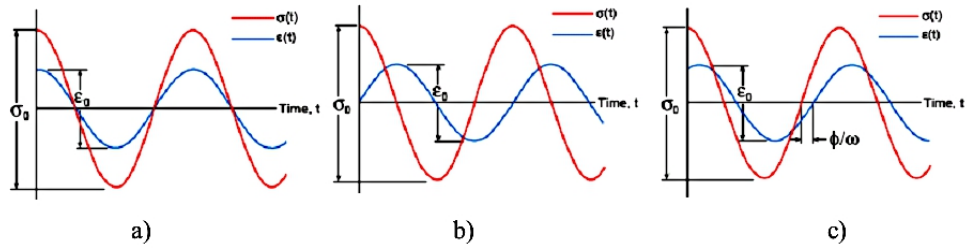
Figure 1.7 Cycling loading and response curves for a) elastic material, b) viscous material, c) viscoelastic material [17].
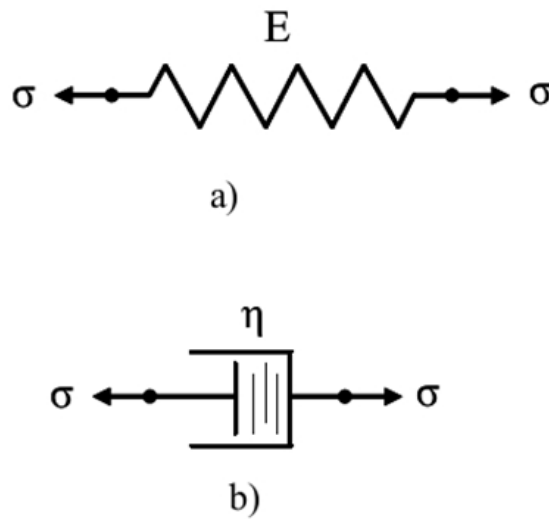
Figure 1.8 Viscoelestic elements. a) Linear spring. b) Linear dashpot.

an important role in the behavior of viscoelastic materials, these materials are also called time-dependent materials. This time-dependency is explained by the phenomena of creep under constant stress and stress relaxation under constant strain [17]. Viscoelastic materials somehow keep a record of their response history and they are said to possess memory. This memory can clearly be seen in the constitutive relationship between the stress and strain. As a result, mathematical models of viscoelastic behavior can take the form of partial differential Volterra equation problems.

Time dependency of the stress relaxation function E can also be given by spring and dashpot models (Figure 8). In these models, the stress carried by the spring is proportional to the strain in the spring and is given by Hooke's law;

$$\sigma = \varepsilon E \tag{1.1}$$

where E is the stiffness of the spring and ε is the strain of the spring, is the ratio of the change of length of the spring to its original length.

$$\varepsilon = \frac{\Delta L}{L_0} \tag{1.2}$$

σ and are analogous to the spring force and displacement, and E is the Young's modulus. The stress carried in the dashpot is proportional to the strain rate and is given by Newton's law of viscosity

$$\sigma = \eta \frac{d\varepsilon}{dt} \tag{1.3}$$

Viscoelastic materials then can be modeled as combination of springs and dashpots in series or parallel. The most common model elements are Maxwell Model, Voigt Model and Generalized Maxwell Solid (Figure 9).

1.4.2   Mechanical impedance measurement

The mechanical impedance (Z) of an element is the ratio of a sinusoidal driving force (F) and the resulting velocity (v). Its mechanical mobility is the reciprocal of the mechanical impedance. Consider a sinusoidal driving (F) that has a magnitude of F_0 and an angular frequency of ω:
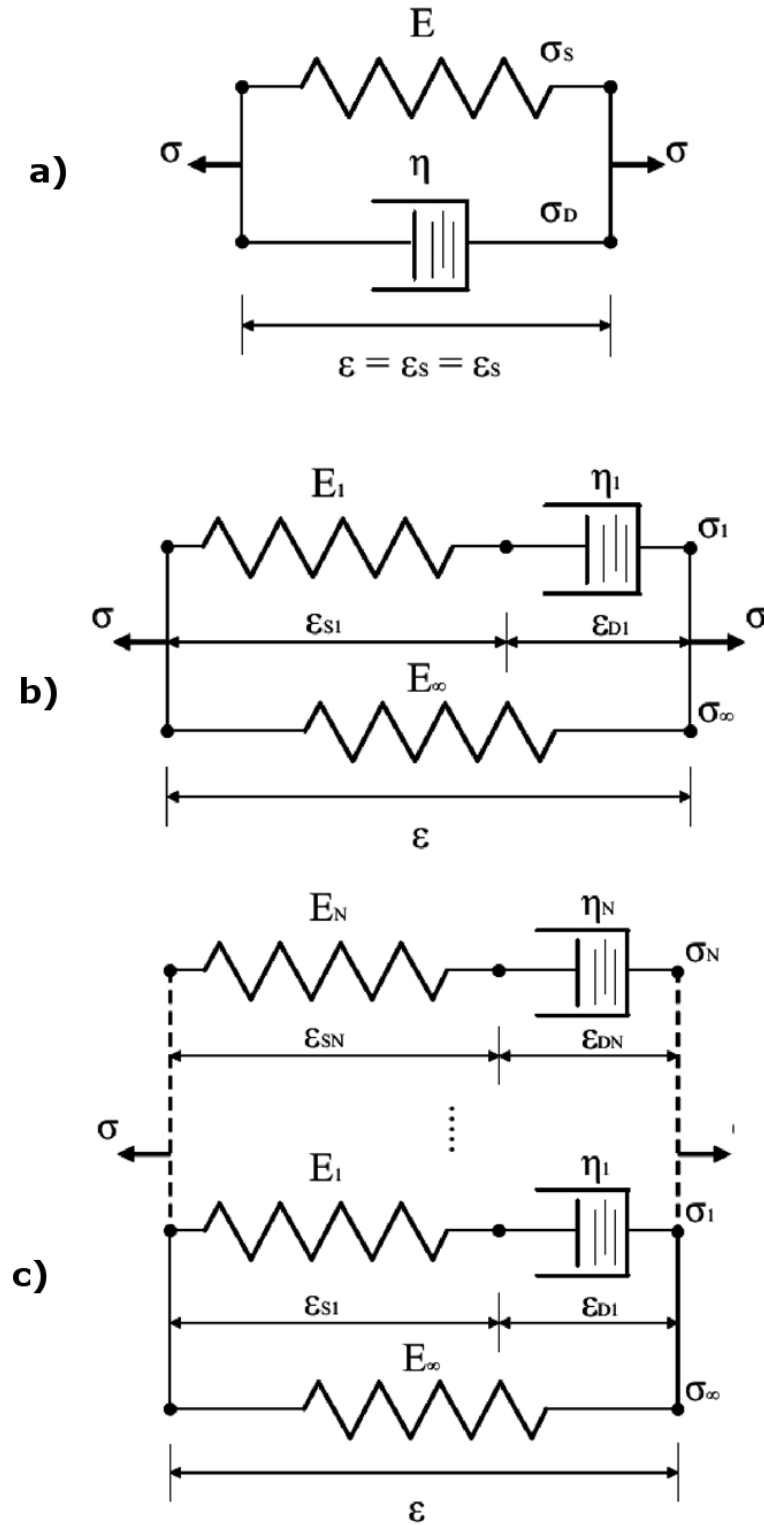
Figure 1.9 Viscoelastic Models. a)The Voigt model, b)Maxwell model, c)Generalized Maxwell solid.

$$F = F_0 e^{jwt} \tag{1.4}$$

The application of this force to a linear mechanical system results in a velocity v:

$$v = v_0 e^{jwt+\phi} \tag{1.5}$$

where v_0 is the magnitude of the velocity and ϕ is the phase angle between F and v. Then the mechanical impedance (Z) is given by

$$Z = \frac{F_0}{v_0} e^{j\phi} \tag{1.6}$$

The unit of impedance is Ns/m. Usually the velocity is not measured but calculated from acceleration integration.

In our measurements, we used Brüel and Kjær Impedance Head type 8001, which can measure force and velocity (Figure 10). Force and acceleration signals were amplified and filtered by a Nexus Type 2692 conditioning amplifier (Brüel and Kjær, Nærum, Denmark).

Because the amplified signal is relatively low, lock-in amplifiers (Ithaco, Inc., Ithaca, NY) are used (Figure 11). Lock-in amplifiers are used to detect and measure very small AC signals all the way down to a few nanovolts. Accurate measurements may be made even when the small signal is obscured by noise sources many thousands of times larger.

In amplifiers, a technique that known as phase-sensitive detection to single out the component of the signal at a specific reference frequency and phase is used. Noise signals, at frequencies other than the reference frequency, are rejected and do not affect the measurement. Therefore lock-in amplifiers require a frequency reference, which was provided by the mechanical stimulus signal we generated in the experiments. In Figure 12, the reference signal is a square wave at frequency ω_r. The signal is $V_{sig}\sin(\omega_r t+\theta_{sig})$. Lock-in amplifiers generate their own internal reference signal by a phase-locked-loop locked to the external reference. In Figure 12, the external reference, the measured signal and the amplifierâs internal reference are shown. The internal reference is $V_L\sin(\omega_L t+\theta_{ref})$.

The device amplifies the signal and then multiplies it by its internal reference using a phase-sensitive detector (PSD) or multiplier. The output is simply the product of two sine waves.

$$
\begin{aligned}
V_{psd} &= V_{sig}V_L sin(w_r t+\theta_{sig})sin(w_L t+\theta_{ref}) \\
&= \frac{1}{2}V_{sig}V_L cos([w_r-w_L]t + \theta_{sig}-\theta_{ref}) \\
&- \frac{1}{2}V_{sig}V_L cos([w_r + w_L]t + \theta_{sig} + \theta_{ref})
\end{aligned}
\tag{1.7}
$$

The PSD output contains two AC signals, one at the difference frequency (w_r-w_L) and the other at the sum frequency $(w_r + w_L)$. The PSD is passed through a low pass filter, the higher frequency component is removed. When w_r equals w_r, the resultant voltage will be

$$
V_{psd} = \frac{1}{2}V_{sig}V_L cos(\theta_{sig}-\theta_{ref})
\tag{1.8}
$$

As given in equation 8, this voltage is proportional to the phase difference.

In this thesis, I measured the mechanical impedance. However, I presented the results based on the dynamic modulus (E^*) which is the complex ratio of stress to strain. Which is the ratio of stress to strain. It has units of Pascal or N/m^2 [18], and it can be easily converted to mechanical impedance as the following:

$$E^* = \frac{\sigma}{\varepsilon} = \frac{F}{A}\frac{x}{x_0}$$

$$Z = \frac{F}{v} = E^*\frac{A}{iwx_0}$$

(1.9)

where σ (N/m^2) is the stress, ε is the strain (dimensionless), F (N) is the force, A (m^2) is the contactor area, x is the displacement (m), x_0 is the static indentation (m), v is the velocity (m/s), w is the angular frequency, and i is the imaginary number. The term iw has units of 1/s and implies the differentiation of the displacement to yield the velocity. Since E^* is a complex number, it can be represented as $E^* = E_1 + iE_2$ where E_1 is the storage modulus, and E_2 is the loss modulus.

In biomechanics literature, the dynamic moduli parameters were extensively used in the studies on aging [19, 20], cosmetics and clinical research [5, 21], skin related diseases [22]. The components of dynamic modulus are more intuitive for interpreting material properties.

The measuring side of the impedance head records information about everything that is mechanically connected to it (Figure 13). This means that even the adapter and the snap coupling, as well as the impedance headâs own mass before force gauge, are included in the impedance measurements. Therefore, a mass compensation should be performed on the results. Here, the masses of these additional components were measured and simply subtracted from the impedance calculations.
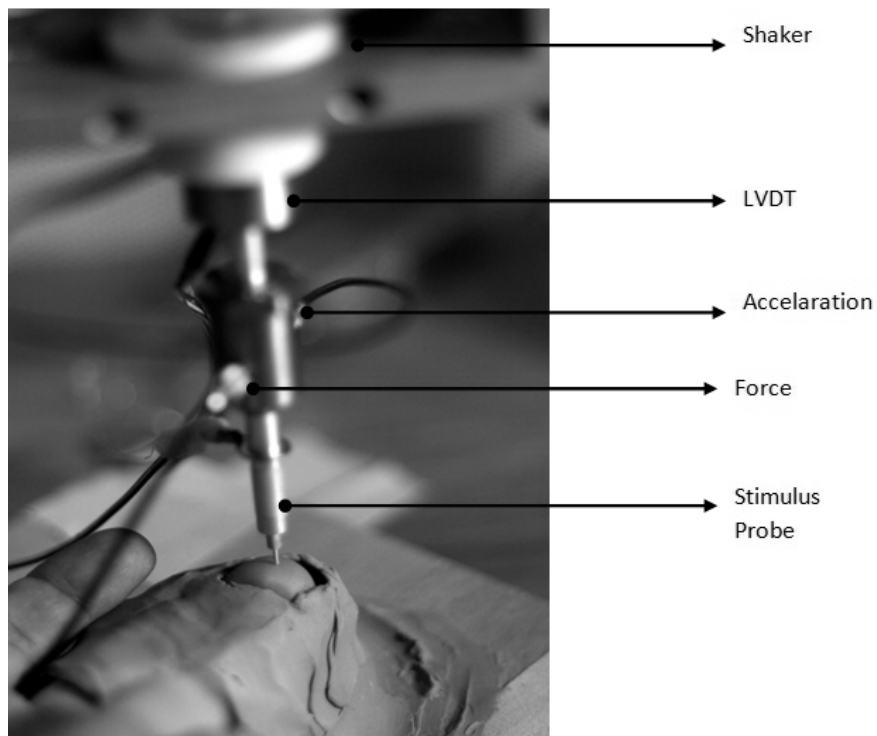
Figure 1.10 Impedance head for mechanical impedance measurement.
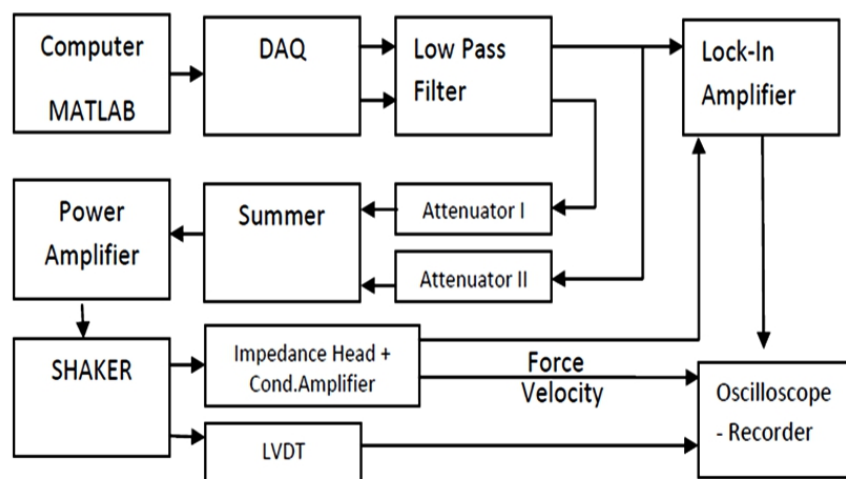
Figure 1.11 Block diagram of the instrumentation for mechanical impedance measurement.
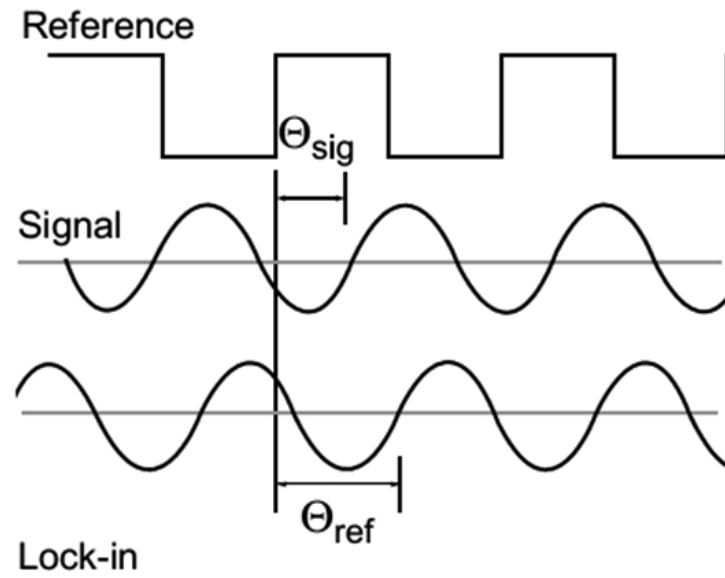
Figure 1.12 Lock-in amplifier working principle.
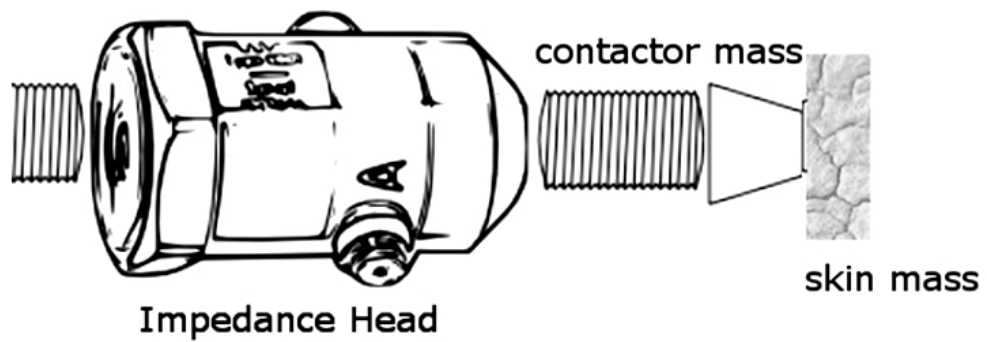
Figure 1.13 Mass compensation is needed for correct measurement
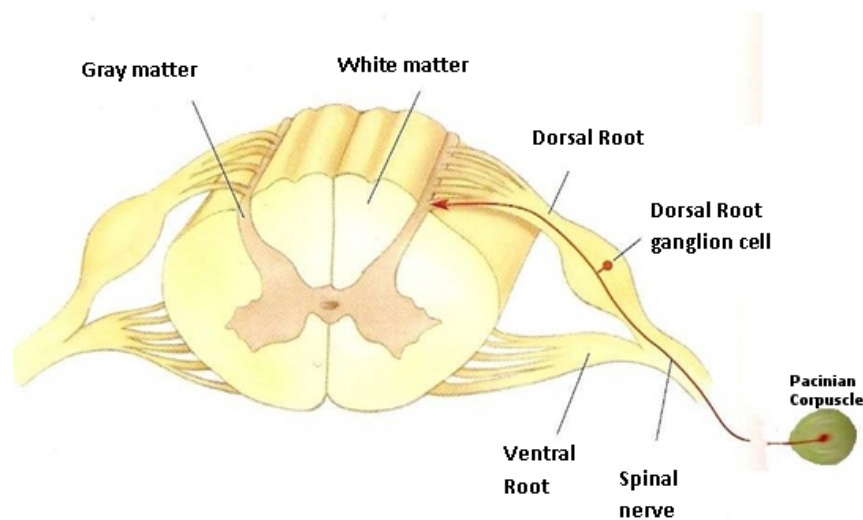
Figure 1.14 Structure of a segment of the spinal cord and its roots [3].

1.5 Somatosensory pathway

Axons bringing information from the somatic sensory receptors to the spinal cord are the primary afferent axons. Stimulation of receptors initiates signals that are transmitted through a series of relay nuclei to higher centers in the brain. The primary afferent axons enter the spinal cord through the dorsal roots; their cell bodies lie in the dorsal root ganglia [2] (Figure 14).

Each segment of the spinal cord receives innervation from a different part of the body. In Figure 15, three fibers in a peripheral nerve branch to receive input from three different, but overlapping, areas on the skin surface, indicated by the vertical lines at the left side. Each nerve fiber enters a different segment of the spinal cord (Figure 15).

Axons of the dorsal root ganglions ascend in the dorsal columns of the spinal cord and first synapse in the brain stem. Nerve fibers conveying different types of sensory information have different diameters. Large-diameter, myelinated nerves such as those from the mechanoreceptors conduct action potentials rapidly (Aβ fibers, diameter: 13-20 μm, conduction speed: 80-120 m/s). Small unmyelinated nerves from the free nerve endings conduct action potentials slowly (C fibers, diameter: 0.2-1.5 μm, conduction speed: 0.5-2 m/sec) by fibers that run in the spinothalamic tracts of the spinal cord and anterolateral pathway in the brain.
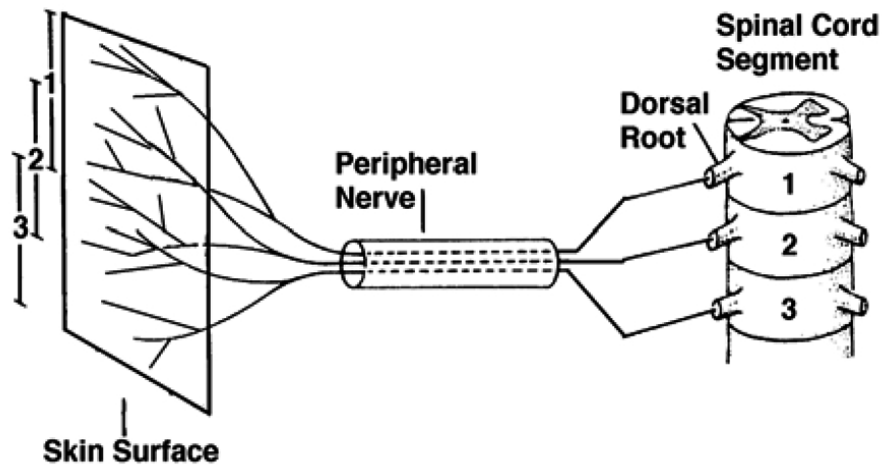
Figure 1.15 Peripheral fibers entering the spinal cord [2].

The dorsal column-medial lemniscal system is the principal pathway for touch and proprioception. The organization of this pathway is summarized in Figure 16. The primary somatic sensory cortex integrates information about touch. Afferent fibers synapse in the caudal medulla, where they terminate in the gracile or cuneate nuclei. Next, the sensory information is sent to thalamus and finally reaches to the somatosensory cortex. The information from the nociceptors and thermoreceptors are transmitted in a different system, through the spinothalamic tract (Figure 16).

The somatic sensory cortex has three major divisions: the primary and secondary somatic cortices and the posterior parietal cortex. Figure 17 is the illustration of the somatic sensory areas of the cortex. Each region of the somatic sensory cortex receives inputs from primarily one type of receptor in a columnar organization (Figure 18). The primary somatosensory cortex is subdivided in to Brodman's areas (3a, 3b, 1 and 2). Inputs from overlapping receptive fields of RA and SA fibers project to distinct column in area 3b ([3].
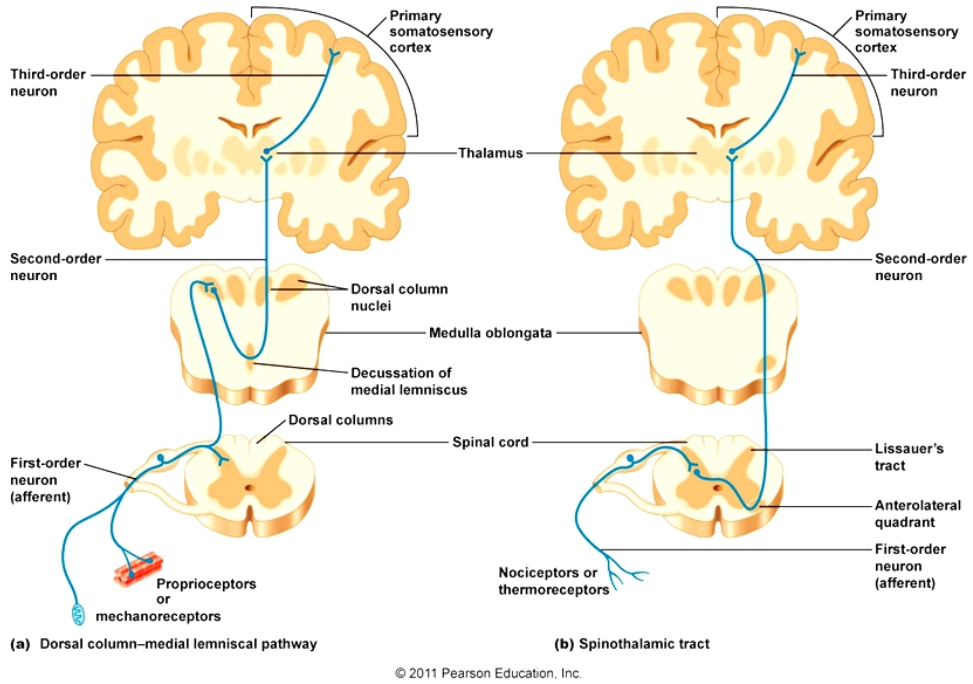
Figure 1.16 Somatosensory pathways, from the receptors to the somatosensory cortex [2].
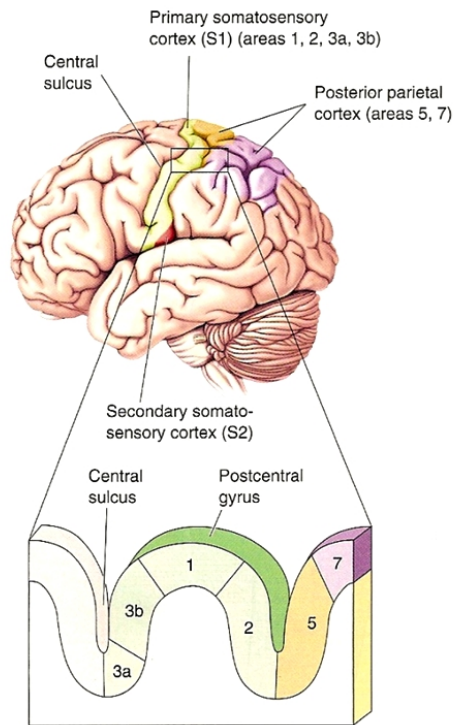
Figure 1.17 Somatosensory cortex [2].
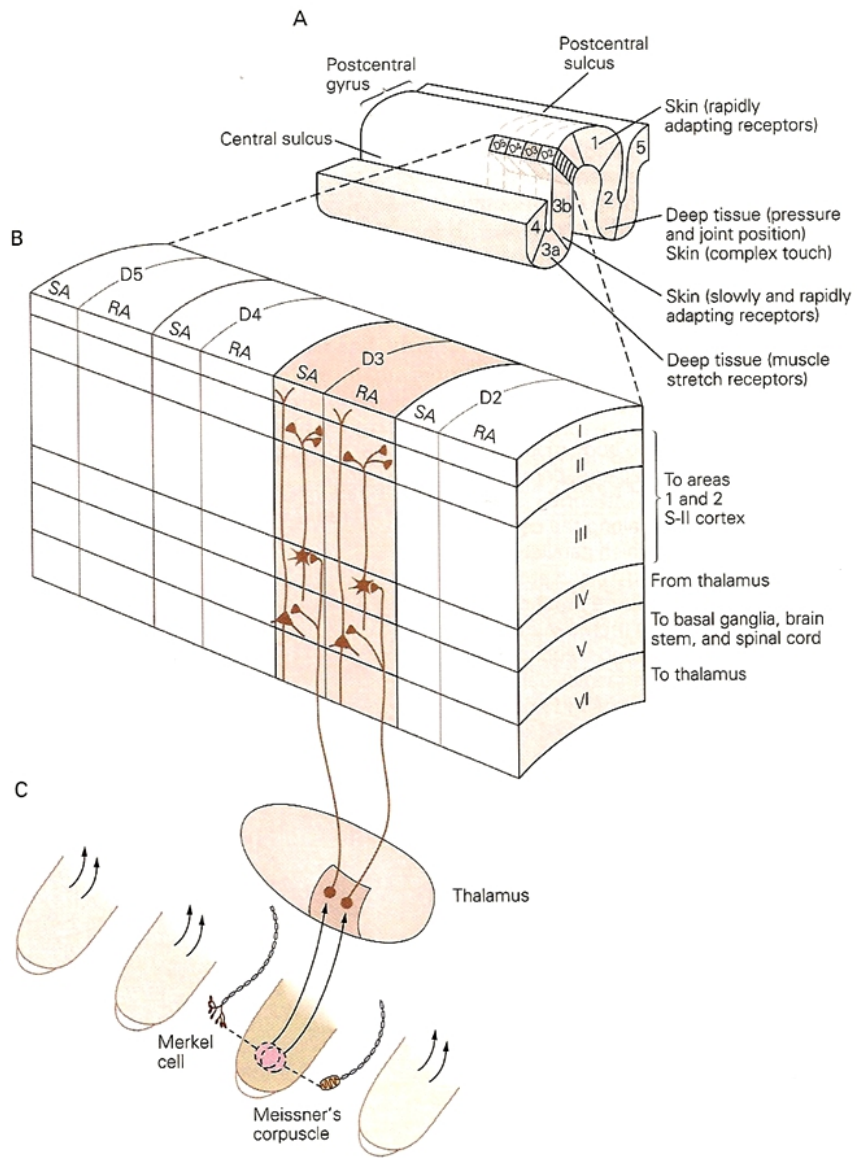
Figure 1.18 Cortical columns in the somatosensory cortex [3].

1.6   Tactile psychophysics

1.6.1   Tactile psychophysical channels

Tactile perception is based on the four psychophysical information channels, mediated by receptor systems [23]. The channels have been described as the Pacinian (P) channel and Non-Pacinian I, II and III channels (NP I, II, III) [8, 24, 25, 26, 27]. Because of the frequency sensitivity of Pacinian corpuscles [9], the P channel has lowest detection thresholds in the range of 200-300 Hz [28, 27].

The absolute detection threshold can be described as the lowest level at which a stimulus can produce a sensation. However, because detection is probabilistic, a more accurate definition for threshold is the stimulus level which produces a given detection probability. Because the sensitivity to the stimuli fluctuates, successive threshold measurements are averaged to reach at an accurate estimation of the absolute threshold [29]. The thresholds are measured by appropriate procedures which minimize the effects of response bias [30, 8, 31, 32].

Measurement of absolute thresholds has led to many significant advances in understanding sensory systems (e.g. vision, audition, touch). Vibrotactile thresholds depend on stimulus factors such as the locus of stimulation, the size of the stimulated skin area, the duration of the stimulus, and the frequency of vibration. An experiment by Verillo (1963) may serve to illustrate the relationship which is found for the absolute threshold for vibration and the frequency of the vibratory stimulus (Figure 19).

In Figure 19, it is clearly seen that when the stimulator was larger than 0.02 cm^2, vibrotactile sensitivity was a U-shaped function of frequency and that sensitivity was greatest in the frequency region around 250 Hz (threshold: 0.1 μm). Here, the stimulus was applied to the thenar eminence of the hand. However, smaller contactor sized resulted contant threshold as function of frequency. Increasing the size of contactor greater than 0.02 cm^2 resulted in a proportional decrease in the threshold. This finding indicated that the tactile system is capable of summating stimulation over a
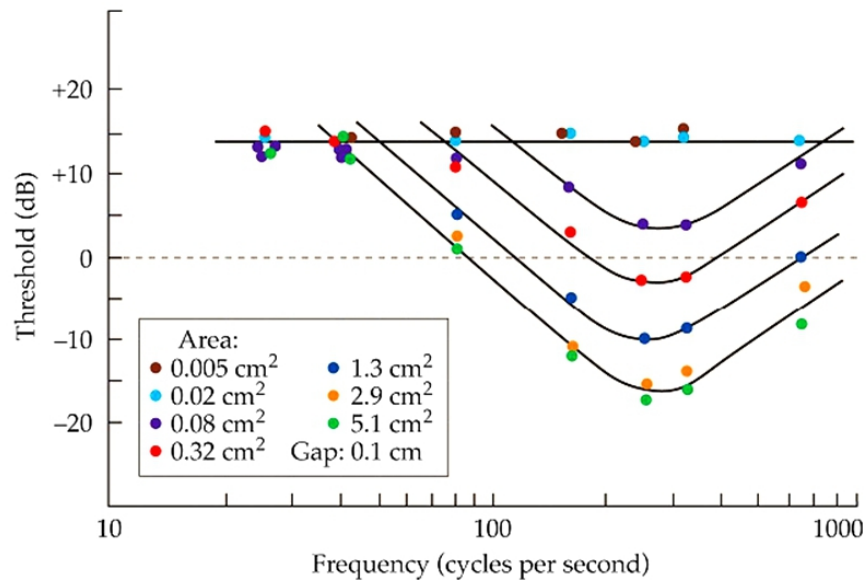
Figure 1.19 Vibrotactile thresholds for different contactor sizes as a function of vibration frequency [33].

relatively large area. From these findings, Verillo (1963) concluded that at least two receptor systems exist in the skin [33]. One system summates stimulus over space and accounts for the U-shaped frequency response. The other system is not capable of spatial summation, and has a flat frequency function. By comparing psychophysical data with data on the electro-physiological response of individual tactile receptors, Verillo (1966) was able to identify the Pacinian corpuscle as the receptor responsible for spatial summation[34] (Figure 20).

Vibrotactile threshold measurements for stimuli presented within a much wider frequency range and different parameters resulted in four channel model of mechanoreception [8] (Figure 21). In current literature, the non-Pacinian systems (Figure 21) correspond to the other receptors in the glabrous skin (Meissner, Merkel, Ruffini).

1.6.2 Absolute threshold measurement techniques

Early psychologists recognized the statistical nature of thresholds and developed several methods for quantitative measurement: method of constant stimuli, method of
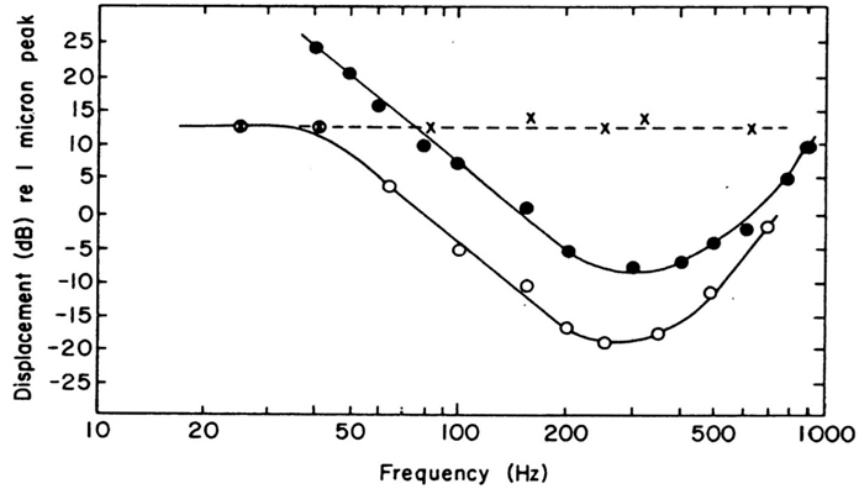
Figure 1.20 Human psychophysical thresholds and physiological threshold of Pacinian corpuscles in the cat [34].
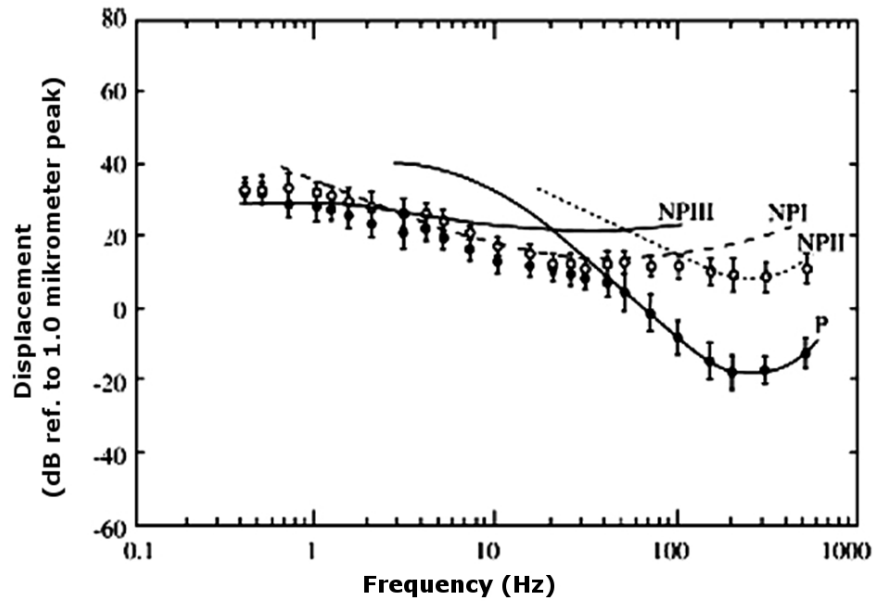
Figure 1.21 Four channel model of tactile sensation with extended frequency ranges of tuning curves [8].
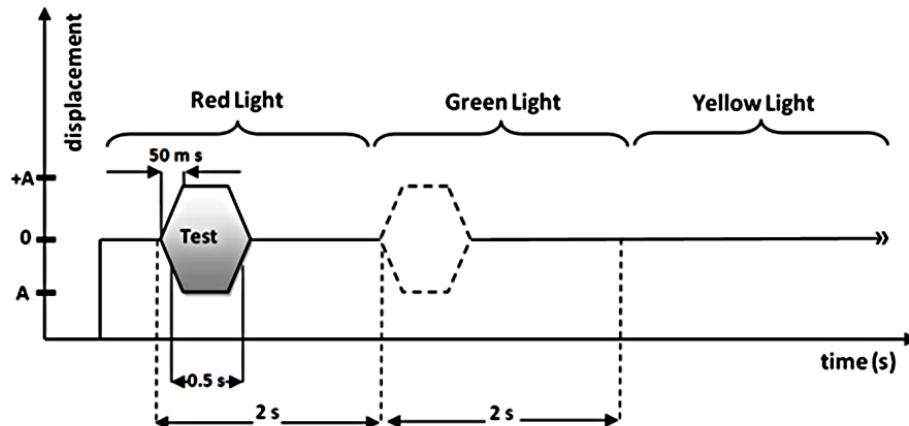
Figure 1.22 Timing diagram for the detection threshold experiments.

limit, method of adjustment, etc. The method of limits perhaps the most frequently used technique for determining sensory thresholds [29]. This method is less precise than the method of constant stimuli, but it is far less time consuming. The method of limit is typically combined with an adaptive up and down (staircaise) methold. The staircase method resembles the tracking method Beckesy (1947) first used with an audiometer to test hearing [35]. In this thesis, we used the modern criterio-free two interval forced-choice method. This method requires the subject to select an interval (in which the stimulus is presumed to occur) among two alternatives. A timing diagram for the two interval forced-choice method is given in Figure 22. Since the subject must select an interval, the result is either a hit or a miss. Therefore, an observer's criterion is not defined based on signal detection theory.

In Figure 22, red and green lights indicate the two intervals. The stimulus randomly occurs only in one interval (here the first interval qued by red light). The yellow light indicates the period for the subject response typically a feedback is given after the subject presses a button for selecting the interval in which he or she thinks the stimulus has occurred.
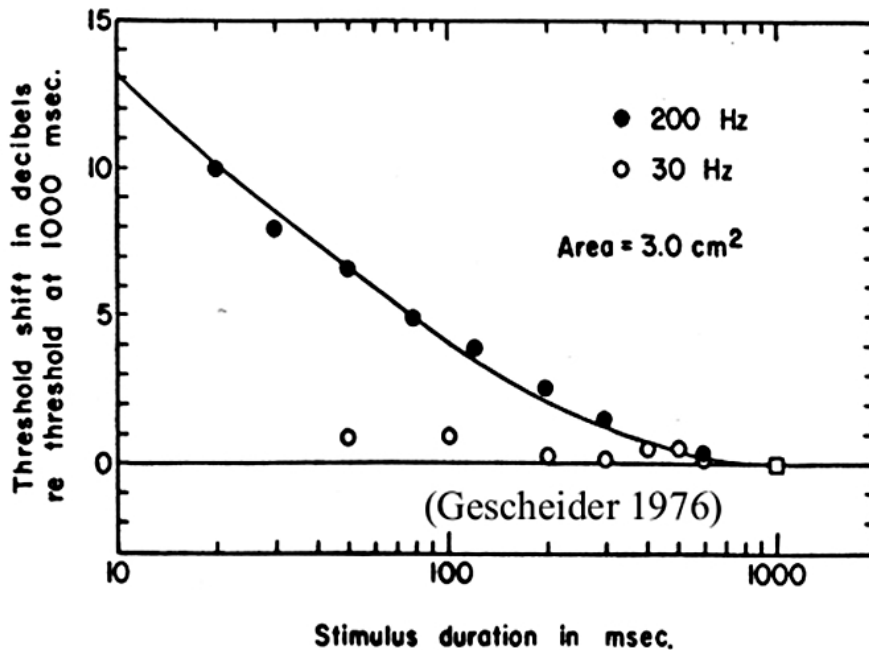
Figure 1.23 Temporal summation effect in the P channel at 200 Hz [40].

1.6.3 Temporal summation in the Pacinian channel

In many sensory systems, temporal summation can be explained as the improvement of the thresholds as the stimulus duration increases. In the sense of touch, this phenomenon occurs only in the Pacinian channel [36, 37, 38, 39]. This was tested mainly with high frequency stimuli delivered with large contactors. Gescheider (1976) and Green (1976) showed that temporal summation does not exist in NP channels at low frequencies [39]. In Figure 23, Gescheider (1976) showed the temporal summation effect at 200 Hz, but this effect did not exist at 30 Hz stimulation [40, 37].

The underlying mechanism of temporal summation in different modalities such as touch, hearing and vision has been proposed as the integration of neural responses to the stimulus over some critical duration of stimulus exposure [39]. Zwislocki (1960, 1965) developed a mathematical model of temporal summation based on neural integration [41, 42]. According to Zwislocki's theory, each cycle in a periodic stimulus generates neural activity which decay with a time constant of 200 ms. Additional stimulus cycles produce sequential neural activity which is superimposed on the decaying
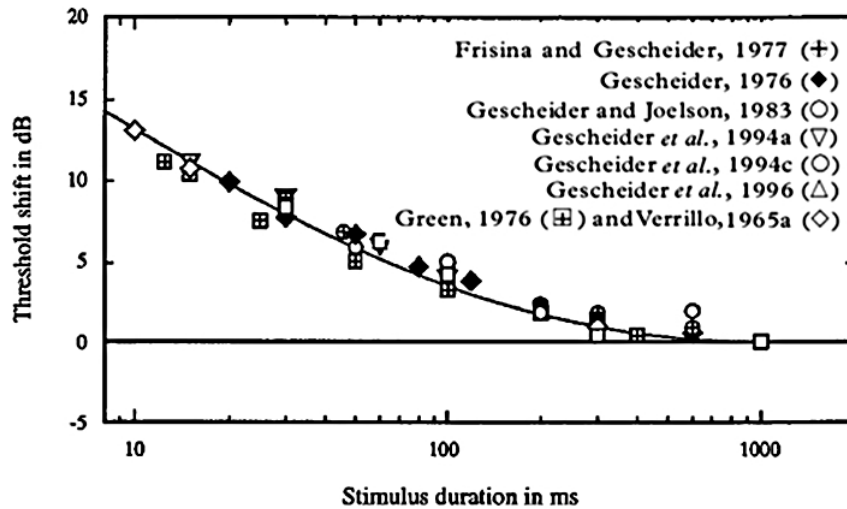
Figure 1.24 Threshold shift in dB for the 1000 ms stimulus detection threshold (adapted from [39]).

component. Support for the neural-integration model has mainly come from the findings of following cited studies [36, 40, 37, 38, 43]. Figure 24 shows these experimental resultsand the theoretical prediction of the Zwislocki's model.

Recently, Gescheider et al. (1999) suggested that probability summation also contributes to temporal summation by increasing the probability of receptor activation [39].

1.6.4   Spatial summation in the Pacinian channel

P channel has also been found to be capable of spatial summation of vibratory stimulation [33, 40, 8, 44]. When a mechanical vibration is applied to the skin containing Pacinian corpuscles the detection threshold decreases as the size of the stimulus contactor increases (Figure 26). However, this phenomenon was not detected at low frequencies, probably because another channel is activated below 80 Hz.

According to Gescheider et al. (2005), the spatial summation may be explained by a combination of neural integration and probability summation [44]. Neural inte-
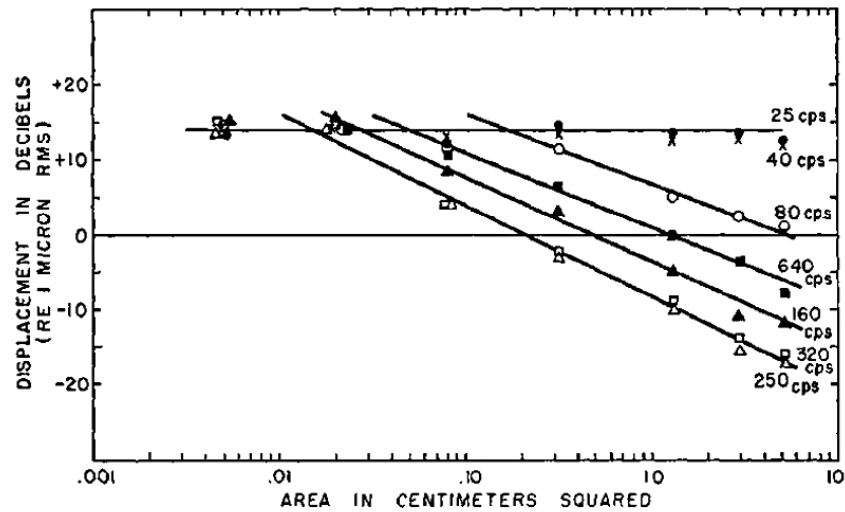
Figure 1.25 Vibrotactile threshold as a function of contactor area [33].

gration resulting in the adding up of the neural responses of an increasing number of tactile receptors as the physical extent of the stimulus increases. Probability summation operates because of the variability of the response properties [44]. As the stimulus area increases, the probability that the most sensitive receptors will be excited should be higher. This was recently simulated in a computation model [45]. In this thesis, I studied spatial summation in the P channel at different contact locations and correlated the threshold with mechanical measurements.

1.6.5 Masking in the Pacinian channel

In sensory systems, masking is the impairment of the detectability of one stimulus by the presentation of another stimulus [39]. Masking differs from adaptation during which the exposure to adaptation stimulus is considerably longer [46, 47, 48, 49]. In contrast, masking raises the detection threshold due to the presentation of the masking stimulus in a brief period of time [28, 50].

Masking, in general, can be applied before, during and after a test stimulus [51, 52, 50, 53]. Here, I studied forward masking in the P channel. In forward masking, the masking stimulus precedes the test. Previous studies showed that forward masking
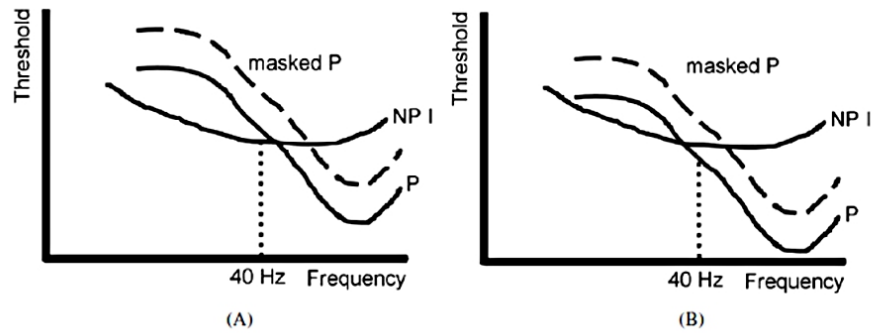
Figure 1.26 Forward masking in the P channel. a) The test stimulus is detected by the NP I channel. b) The detection is mediated by the P channel. If the P channel is masked (dashed line), the test stimulus is detected by the NP I channel [54]

occurs only when the intensity of a given masking stimulus is above the threshold of the channel 1985. Furthermore, the effect of forward masking decreases as the temporal interval between the masking and the test stimuli increases [48, 52].

To understand how the masking operates on tactile channels, the two possible scenarios regarding the detection of a 40-Hz stimulus are presented in Figure 27 [54]. There scenarios are discussed in detain by Güçlü and Bolanowski (2005). In brief, Figure 27.a shows that the threshold measured at 40 Hz is not affected by masking the P channel. Because, test stimulus is detected by the NP I channel. However, in Figure 27b, masking the P channel increases the threshold detected at 40 Hz. Because it was initially mediated by the P channel.

Figure 28 shows an example of a timing diagram for the forward masking procedure. The masking stimulus is applied before the test stimulus. The subjectâs task is to decide whether the test stimulus occurs in the first or the second time interval cued by red and green lights respectively. The masking stimulus is presented in both intervals, but the test stimulus is randomly presented in the first or the second interval. In the thesis, the masking stimulus duration and amplitude were adequate to produce forward-masking [25]. The time gap between the masking and test stimulus was 150 ms after the masking stimulus, according to Makous et al., 1996. A longer gap would decrease the effectiveness of masking.
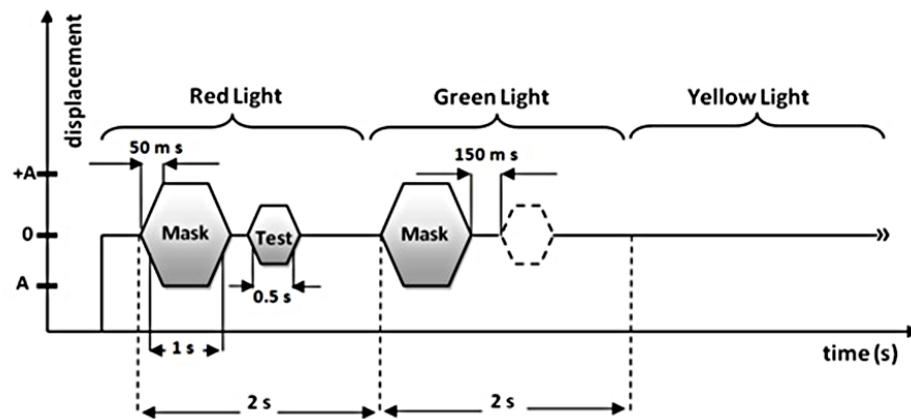
Figure 1.27 Timing diagram for threshold experiments with forward masking.

1.7   Somatosensory and evoked potentials

1.7.1   Electrical stimulation

SEPs are routinely used in the clinical setting for identifying lesions in the somatosensory pathway. They are obtained by electrical stimulation of the peripheral nerves (medial or tibial nerve). Depending on the clinical test, short-latency, mid-latency, and long-latency SEP components are analyzed after averaging 200-2000 sweeps (Figure 29). While the short-latency components reflect sub-cortical activity, the mid-latency components indicate the arrival of the afferent volley at the primary somatosensory cortex and long-latency SEP components reflect associated cortex areas. However, the generators of the different components are still debated [55]. SEPs, which are recorded at the contralateral electrode over the primary somatosensory cortex, usually extend over a time range of 20-70 ms after electrical somatosensory stimulation. The componenet peaks (N20, P25, N35, P45 and N50) labeled to their polarity and approximate latency. The exact latencies and amplitudes of components are used for clinical interpretation [55]. In Figure 30, a typical SEP as a response to median nerve stimulation in an adult subject is given. The recording shows the presitmulus interval, the stimulus artifact and major SEP components (N20, P25, N35, P45,N50).
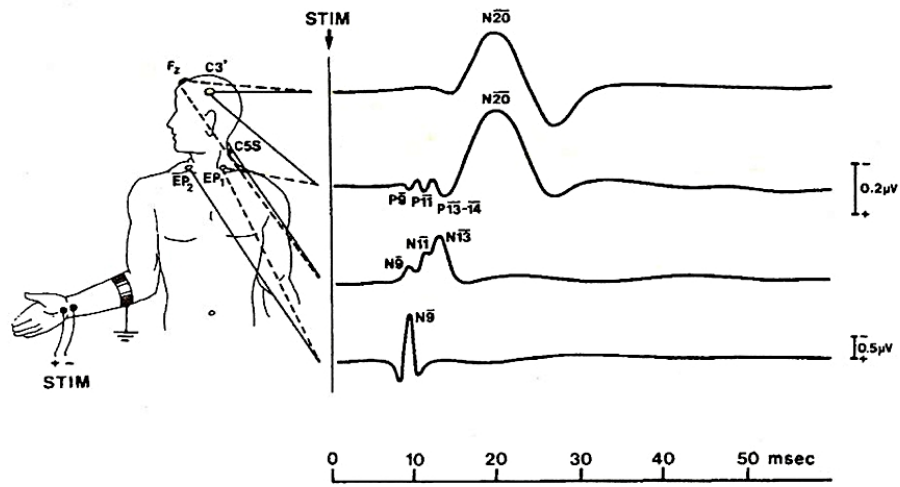
Figure 1.28 SEP recording with electrical stimulation of the median nerve [56].
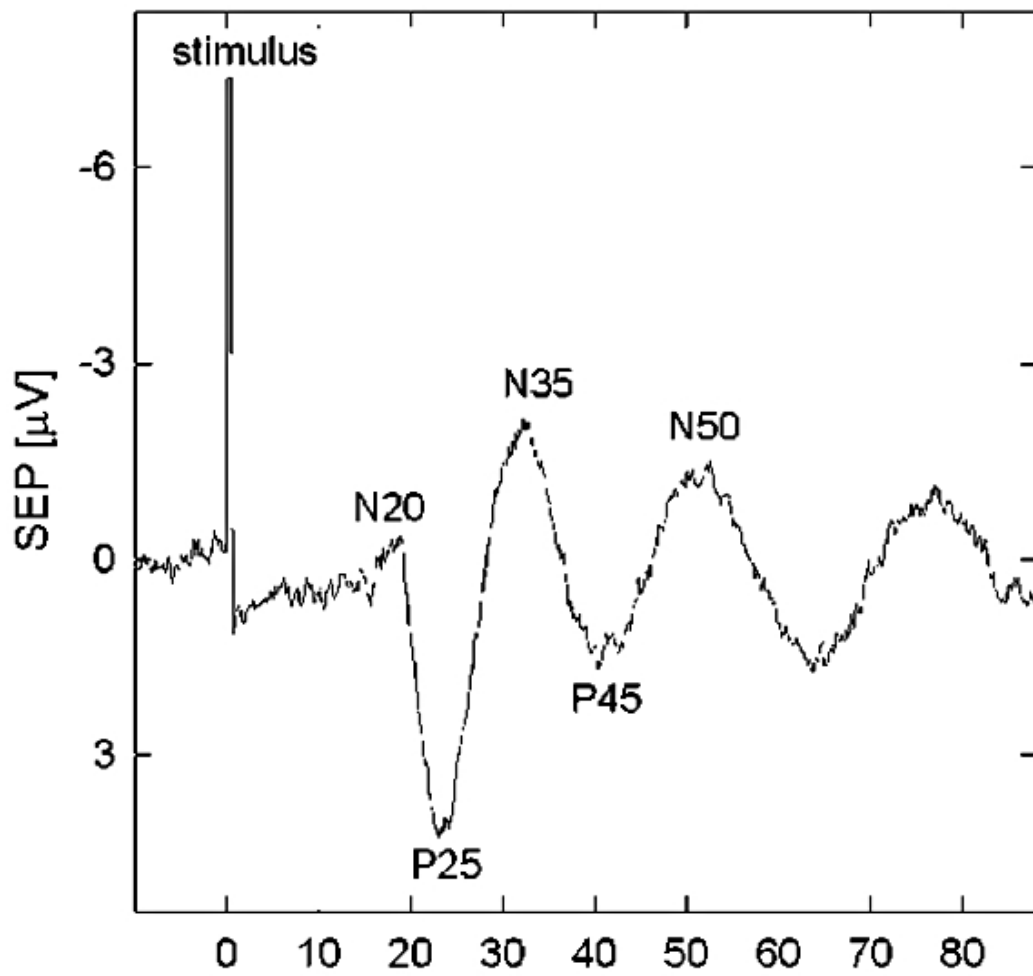
Figure 1.29 SEP components as a response to median nerve stimulation [55].

1.7.2 Mechanical stimulation

Electrically stimulating the peripheral nerves to record SEPs provides only a limited amount of information, mainly conduction velocities of fiber groups and their relative contributions carus1994. However, the somatosensory system is wired to process mechanical inputs and the information processing can only be understood by applying natural mechanical stimuli. Unfortunately, the number of neurons activated with mechanical stimuli is expected to be miniscule compared to the synchronized activation of thousand of neurons by electrical stimulation. Crouse et al. (1994) applied electrical (5 to 15 mA, biphasic rectangular pulse during 0.2 ms) and tactile stimulation (square-wave, contactor size 2 mm in diameter, 0.5 mm static indentation, 10 μm/ms velocity) to the median nerve. Responses were averaged 256 or 512 times. The responses were measured near the nerve by platinum needle electrodes on the forearm. The amplitude of the mechanically evoked responses were lower much lower (0.25-1μV) compared to electrically evoked responses (1-5 μV) for electrical stimulation.

It would be desirable that stimulus properties such as amplitude, frequency and duration could be extracted by analyzing scalp potentials noninvasively. Kelly and Folger (1997, 1999) reported that this could be possible by applying mechanical stimulation in long durations (8-32 s). They used a high density array of surface electrodes placed on the scalp. By using frequency domain analysis, they could demonstrate voltage components following the frequency of the stimulus (33 Hz). In this experiment, the mechanical stimulus was sinusoidal with amplitude (200 μm very much higher than the psychophysical threshold) and applied to the fingertip. Their results are in the Figure 2.1.

It is known that cortical neurons in the somatosensory cortex may be partially synchronized with a periodic mechanical stimulus [57, 58]. However, almost all studies used invasive single unit spike recordings from cortical neurons. It was one of the major aims of this thesis to investigate the possibility of obtaining information regarding synchronization by noninvasive recordings and search for a noninvasive electrophysiological substrate for psychophysical phenomena such as forward masking.
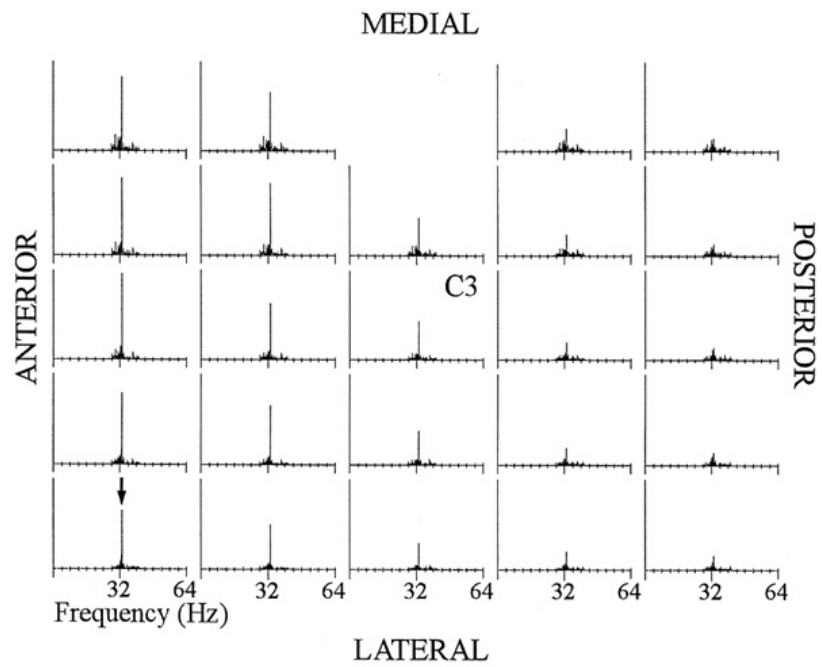
Figure 1.30 SEP recordings with mechanical stimulation [59, 60].

2.   EXPERIMENTAL STUDIES

2.1   Temporal summation is independent of frequency in the Pacinian (P) tactile channel

Mustafa Z. Yıldız, Murat Özsaltık and Burak Güçlü, Abstracts of the Psychonomic Society, 52nd Annual Meeting, USA, Abstract Book, pp. 105, 2011.

2.1.1   Background and Theory

Temporal summation is generally observed as the improvement of detection threshold as the stimulus duration is increased, and was previously shown to be effective in the tactile Pacinian (P) psychophysical channel.

A mathematical model for temporal summation was formulated by Zwislocki (1960), derived from the experiments in which the threshold of audibility was measured in response to various temporal patterns of stimulation [41]. The theory assumes that each pulse or a single cycle of a sinusoidal vibration produces a neural excitation which decays exponentially with time. And if the stimuli occur with an appropriate timing pattern, the resulting neural excitations summate to produce a graded response at the level of the temporal summator (Figure 2.1). In Zwislocki's study, the temporal summation was modeled by an integration having a time constant of 200 ms, the integration resulting in a decrease in threshold at a rate of - 3 dB/doubling of the duration (Figure 2.2). He showed that the slope of integration is independent of stimulus frequency. This model has proven useful in predicting threshold-duration functions for any temporal pattern of stimuli [41, 42].

In the introduction of this thesis, the temporal summation in the P channel was mentioned. Figure 2.2 shows a replot of Verillo's (1965) averaged results in which the
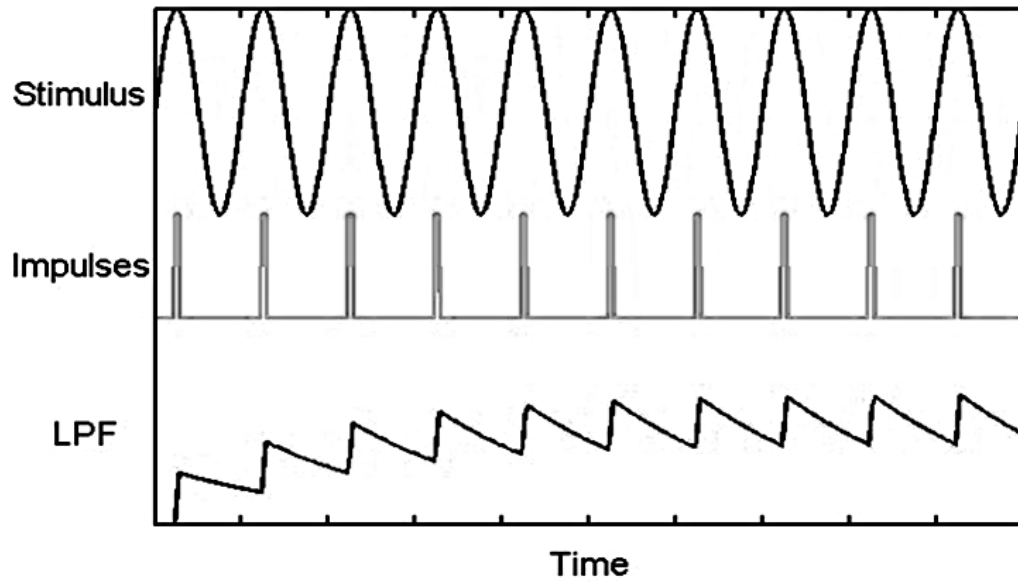
Figure 2.1 Timing diagram for threshold experiments with forward masking [36].
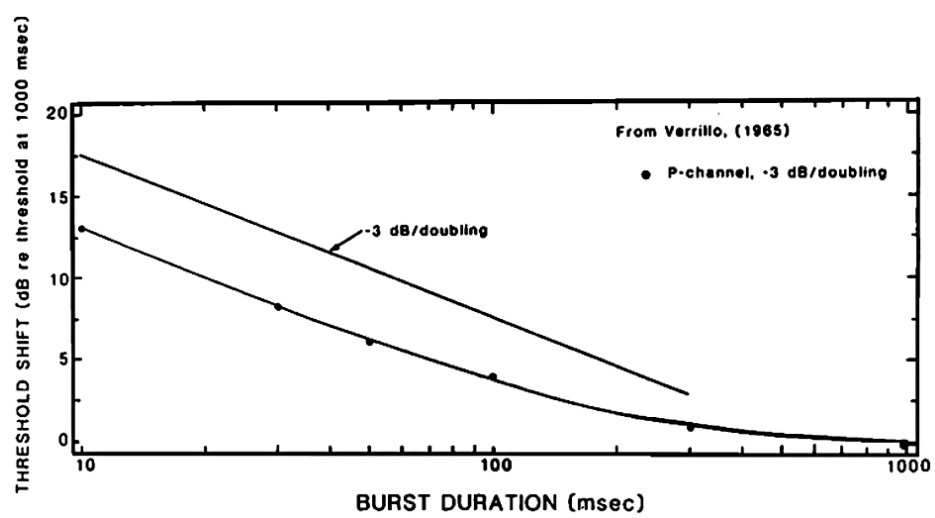
Figure 2.2 Timing diagram for threshold experiments with forward masking.
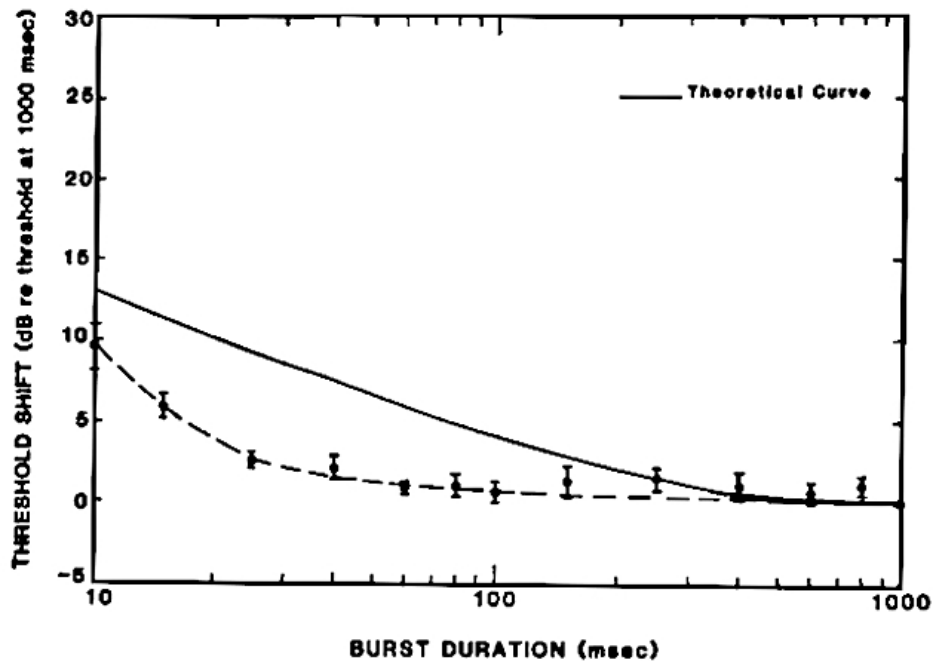
Figure 2.3 Theoretical threshold shifts versus simulated threshold shift [61].

amplitude of the stimulus required for threshold is plotted as a function of stimulus duration. The curve fitted to data matches the Zwislocki's theoretical formulation. In the study by Checkosky and Bolanowski (1992), the responses from single PCs were integrated by counting neural spike over the stimulus duration [61]. Furthermore, real-time responses were integrated with a low pass filter, more accurately modeling the central process. The amplitude-duration function obtained with the low-pass filter, however, resulted in a function which did not follow that obtained psychophysically (Figure 2.3). According to their results, the model temporal integrator does not account for the occurrence of neural impulses with respect to time; the pattern of firing probably plays a significant role in signaling threshold.

In the study by Checkosky and Bolanowski (1994), they wanted to explain the certain discrepancies in the psychophysical-physiological model for the sense of touch in P channel. The model was based on correlations among the psychophysical frequency response obtained on human glabrous skin and physiological frequency-response functions measured on two PC preparations: PC fibers innervating human glabrous skin [7] and PC isolated from cat mesentery. The frequency-response functions were qualitatively similar. Low frequency slope for human PC fibers differed from the slopes for
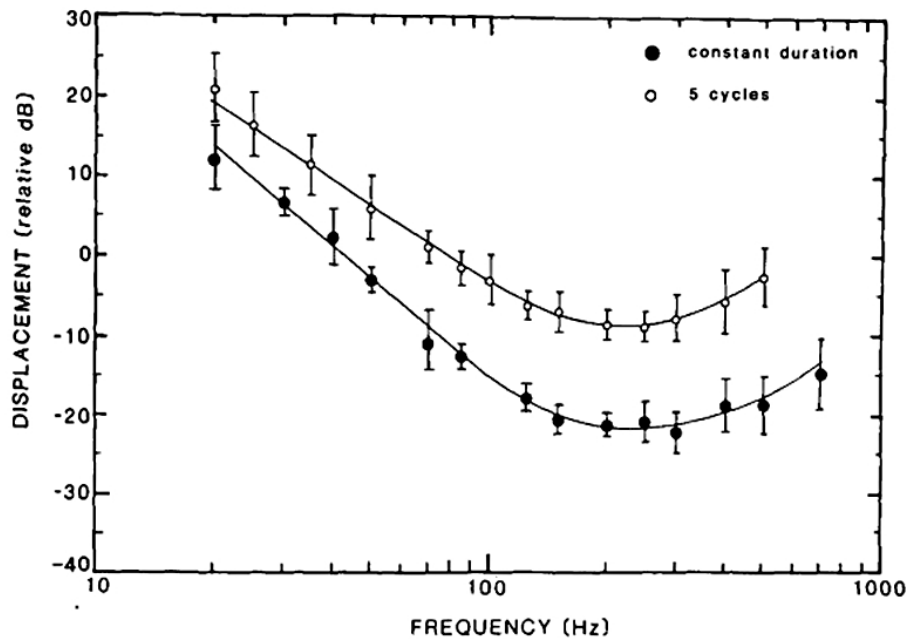
Figure 2.4 Average frequency-response functions of PCs isolated from cat mesentery. Displacement is plotted in relative decibel units, and the error bars signify the standard deviations: open circles, data obtained for a constant 5 cycles of stimulation across frequency; filled circles, data obtained for constant stimulus duration. The response criterion for both sets of data was 4 impulses stimulus. The numbers of PCs used in the averaging were 8 (open circles) and 6 (filled circles) [61].

the psychophysical and cat mesentery PC functions by being 3dB/octave less steep. To find out this discrepancy, experiments were performed using two methods of stimulation: a) a constant number of stimulus cycles (n=5) for each test frequencies, and b) a constant number of stimulus cycles (n = 5) for each test frequency as used by Johansson et al. The method of least squares was used to calculate the low-frequency (50 to 150 Hz) slopes of individual psychophysical and physiological functions. The mean slopes that resulted from using the two methods of stimulation were consistent with the theoretical expectations.

Since within each group the frequency responses of individual PCs were similar in form, the data were grouped and averaged to produce average frequency-response functions, which are shown in Figure 2.4. The averaging procedure in both cases, which involved normalization, was similar to that used by Bolanowski and Zwislocki (1984). For each set of functions, the normalization involved adding all the decibel displacement values required to elicit the 4 impulses/stimulus criterion response at every frequency for each receptor and dividing by the number of frequencies. Every individual mean

displacement value was then used as the normalization factor for the given receptor. Group means and standard deviations were calculated from the normalization values at each frequency. The two functions were separated by calculating the difference between the means of the normalization factors used in each of the two sets of functions, and by adding this value to the group means for the data obtained using fixed stimulus duration. Stimulus amplitude was expressed in relative decibel units, and the smooth curves through the data points were fitted by eye. The two curves have approximately the same best frequencies, about 200-300 Hz (Figure 2.4).

From the studies above, we constituted the temporal summation model (eqn. 13). In the classical apporach, each stimulus cycle produces an impulse of height A^2 (stimulus signal power $\sim$ energy in a spring), and impulses are integrated by a hypothetical neuron (low-pass filtering). Normalized threshold criterion was set according to frequency characteristic [62] obtained from PCs (Figure 2.4).

$$\theta = A^2 \sum_{k=1}^{df} e^{-\frac{df-k}{f\tau}}$$

(2.1)

$$A = \sqrt{\frac{\theta(e^{-\frac{1}{f\tau}} - 1)}{e^{-\frac{d}{\tau}} - 1}}$$

In equation 13, A is the stimulus amplitude, d is the duration (10-1000 ms), f is the stimulus frequency (50-500 Hz), τ is the time constant (200 ms), k is the cycle/impulse index and q is threshold criterion. We conducted psychophysical experiments to test the following hypotheses;

1- Temporal summation effect does not depend on frequency in the P channel. In other words, threshold improvement should stay constant as function of frequency.
2- We expected a threshold difference approximately $\sim$13 dB between 10-1000 ms as suggested in the previous studies.

3- Classical model would predict the improvement of thresholds as a function of frequency. But it would not reproduce the tuning curve of the P channel.

2.1.2 Methods

Subjects

Seven healthy adult subjects (four female and three male, age: 23-30 years) participated in the study. The experiments were approved by the Boğaziçi University Institutional Review Board for Research with Human Subjects. All the subjects were right handed by self-report and the tactile stimuli were applied on their left middle fingertips. Because temperature affects thresholds of the P channel [63, 54, 64], the experiments were performed with the skin surface temperature in a range of $30 - 34^0$ C. A temperature probe (PTC thermistor) connected to a multimeter monitored the skin surface temperature throughout the experiments. The mechanical stimuli did not pose any harm to the subjects.

Apparatus

The apparatus used for the psychophysical measurements were similar to the one used by Güçlü and Öztek (2007). Experiments were performed in a sound- and vibration-proof room (RE-242, ETS-Lindgren Acoustic Systems, Cedar Park, TX). The mechanical stimuli were applied by a V201 shaker (Ling Dynamic Systems Ltd., Royston, Herts, UK) with cylindrical contactor probe of radius 2 mm. A digital-to-analog converter card (DaqBoard/2000, IOtech, Cleveland, OH) connected to a personal computer generated the stimulus waveforms. The stimulus levels were adjusted by a PA5 digital attenuator (Tucker-Davis Technologies, Alachua, FL) and the output signal was amplified by an RA300 power amplifier (Alesis, Fort Lauderdale, FL) to drive the mechanical shaker. During the experiment, the mechanical vibrations were monitored by using a Schaevits ATA2001 LVDT (Lucas Control Systems, Pennsauken, NJ) and a TDS 2014 digital oscilloscope (Tektronix, Inc., Beaverton, OR). In order to prevent
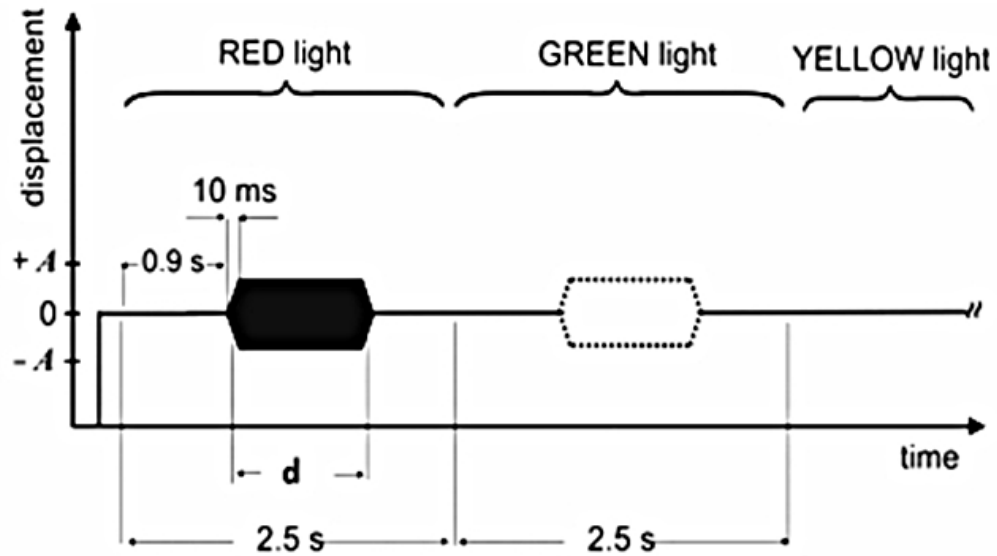
Figure 2.5 Stimulus timing diagram for temporal summation experiments.

movement, subjects' middle fingers were molded in modeling clay. The subjects were presented with auditory white noise by headphones to mask any sound emitted by the mechanical shaker, which would otherwise generate cues interfering with the task.

Stimuli

In the psychophysical experiments, the stimuli were bursts of 150, 250, 350 and 500 Hz sine waves superimposed on a 0.5 mm static indentation and applied on the left middle fingertips of the subjects. The bursts stimuli began and ended as cosine-squared ramps with 10 ms rise and fall times. The durations of the test stimulus were 10 and 1000 ms as measured between half-power points of the burst (Figure 2.5). The test stimulus was applied randomly in the first or the second interval (cued by red and green light in a two-interval forced choice task). The subjects responded after the yellow light was on by pressing buttons on a custom-made box. The subjects received feedback on the outcome of their decisions (yellow light blinking: correct, yellow light off: incorrect). The contactor radius was 2 mm and no contactor surround was used.

Psychophysical procedure

In the psychophysical experiments, a two interval forced-choice task was used with a three-down one-up rule to track detection thresholds. The test stimulus was presented randomly in either one of the two time intervals (duration: 2.5 s, see Figure 2.5). Then, the subject selected the interval in which he or she detected the stimulus by pressing the appropriate button. The stimulus level was decreased 1 dB for three correct responses (not necessarily consecutive) and increased 1 dB for every incorrect response. This rule yields the 75% probability point of the psychometric function [31]. The experiment stopped when the stimulus level was within ± 1 dB range for the last 20 trials [64]. This procedure was performed four times for each location and contactor, for every subject. The absolute thresholds were obtained by averaging the four measurements.

2.1.3   Results

This experiment was intended to provide the vibrotactile detection thresholds at 150, 250, 350 and 500 Hz during 10 and 1000 ms stimulation for all subjects using 2 mm contactor size. The average recorded threshold levels were between 5.53 and 9.40 dB (corresponding to 2.95 and 1.89 μm) for 10 ms and between -0.26 and 4.39 dB (corresponding to 0.96 and 1.65 μm) for 1000 ms stimulation (Figure 2.6). The threshold levels were consistent with the previous studies [40, 62]. There was a significant main effect of duration (Aligned Rank Transform, 2 way-Anova, p=0.003), and there was no significant main effect of frequency (Aligned Rank Transform , 2 way-Anova, p=0.155). There were no significant interaction (p=0.580).

The thresholds followed the typical U-shaped sensitivity curve of the P channel, and were significantly elevated for the 10 ms stimuli as compared to the 1000 ms stimuli. This duration difference ($\sim$6.6 dB) was almost constant as a function of frequency (Figure 2.7) and the duration difference was not significant (2-way Anova p=0.842), but significantly lower than the model-predicted difference of 13.1 dB. With the increase of
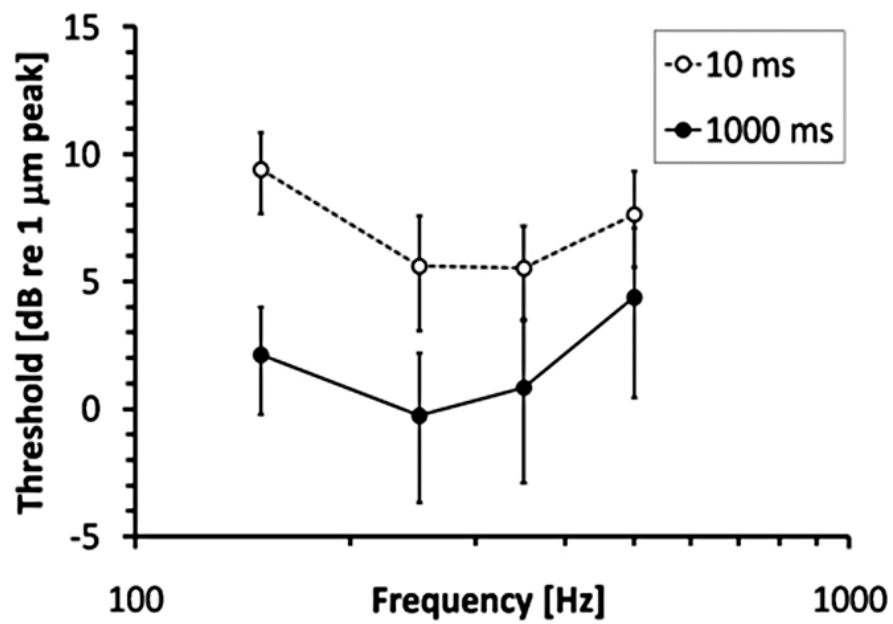
Figure 2.6 Temporal summation effect at different frequencies for 10 and 1000 ms stimulus duration.
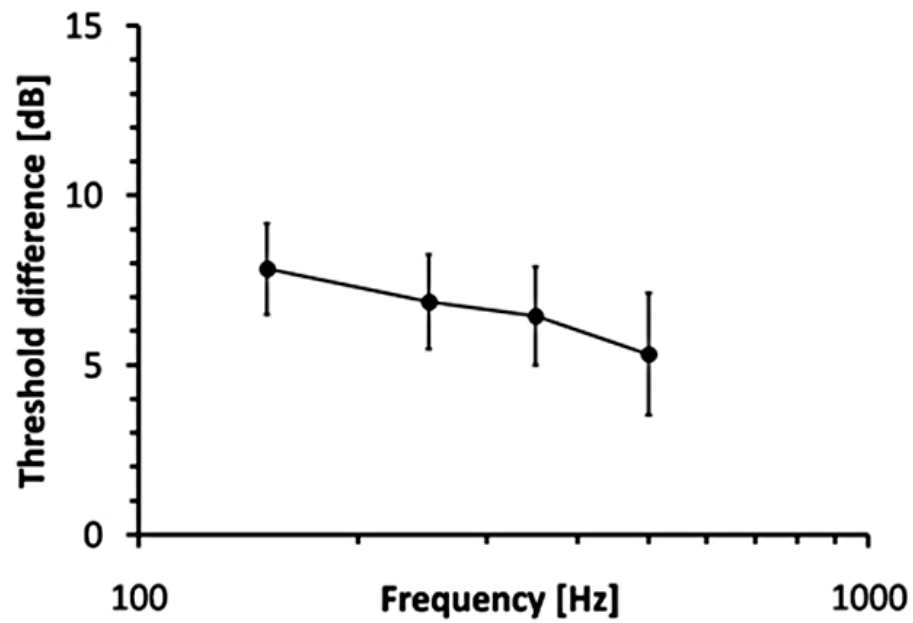
Figure 2.7 Mean threshold difference at different frequencies. Thresholds for 10 and 1000 ms duration were averaged.
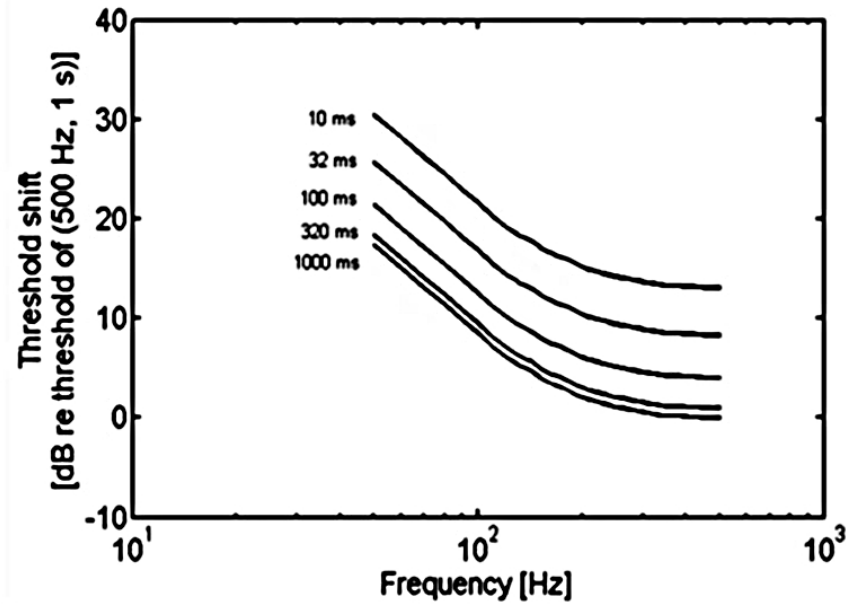
Figure 2.8 Simulation results of the classical temporal summation model as a function of frequency.

duration, the temporal summation effect was clearly seen at all frequencies. Specifically, the lowest thresholds were at 250 Hz for both 10 and 1000 ms for all subjects. Based on the classical model, we plotted the model predictions at different frequencies and durations. The threshold difference between 10 and 1000 ms at all frequencies was constant ($\sim$13.1 dB) and there was a decreasing trend as a function of frequency (Figure 2.8-2.9).

2.1.4 Discussion

The main objective of this study was to test the classical temporal summation model. The model states that for stimuli with longer durations, more neural impulses are integrated, which result in lower psychophysical thresholds. We obtained a similar improvement in our psychophysical experiments. In our results, the threshold difference between 10and 1000 ms was about 6.6 dB, on the other hand, it was about 13 dB in the studies by Verrillo (1965) and Gescheider (1976). In addition, we did not find an effect of frequency on this threshold difference which is a novel finding according to our knowledge.
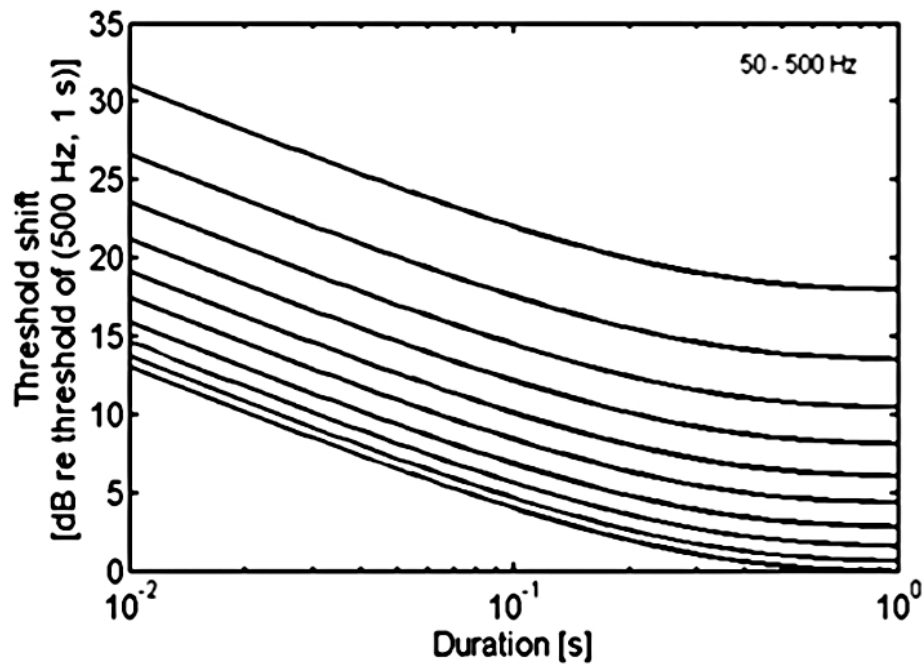
Figure 2.9 Threshold shifts in the simulation results between 10 and 1000 ms stimulus duration.

The actual threshold values were somewhat higher than those reported in the literature (i.e. -10 and -20 dB in [8, 38]). The difference with the previous literature may be due to ta spatial summation effect in P channel which we did not account for. The contactor area used in this study was 0.13 cm^2 but it was 2.9 cm^2 in the above cited studies.

This classical model does not include the tuning curve of the P channel. The threshold trend was not similar to the psychophysics. Therefore the model should be improved in this respect. Additionally, the threshold difference in the model was higher than our psychophysical results, probably due to the effect of contactor size. This effect may be incorporated into a revised temporal summation model which includes a population of receptors.

2.2 Relationship between vibrotactile detection threshold in the Pacinian channel and complex mechanical modulus of the human glabrous skin

Mustafa Z. Yıldız, Burak Güçlü, Somatosensory and Motor Research, 2013, 30:1, pg. 37-47.

2.2.1 Background and Theory

In human glabrous skin, there are four types of mechanoreceptors: Pacinian corpuscles, Meissner corpuscles, Merkel discs and Ruffini endings [65, 66, 67, 68, 7, 8]. The associated mechanoreceptive nerve fibers are typically classified according to their receptive field sizes and adaptation of their responses to ramp-and-hold stimulation. The frequency characteristics of mechanoreceptive fibers also differ when vibratory stimuli are used. For example, Pacinian fibers are most sensitive in the range of 40-300 Hz, whereas fast-adapting type I fibers linked to Meissner corpuscles respond mostly to stimuli at 3-40 Hz. The anatomy, physiology and psychophysics of the Pacinian tactile system have been studied extensively due to easier accessibility [69, 34, 70, 40, 10, 9, 71, 72, 8, 73, 11, 12].

Tactile perception is based on the four psychophysical information channels, mediated by the receptor systems [23]. The channels have been described as the Pacinian (P) channel and Non-Pacinian I, II and III channels (NP I, II, III) [8, 24, 26]. Because of the frequency sensitivity of Pacinian corpuscles [9, 71], the P channel has the lowest vibrotactile detection thresholds in the range of 200-300 Hz [74, 75, 28, 23, 8].

The absolute detection threshold can be defined as the lowest level at which a stimulus can produce a sensation. However, because detection is probabilistic, a more accurate definition for threshold is the stimulus level which produces a given detection probability. Because the sensitivity to the stimuli fluctuates, successive threshold mea-

surements are averaged to reach at an accurate estimation of the absolute threshold [29]. The thresholds are measured by appropriate procedures which minimize the effects of response bias [30, 29, 31, 32]. The vibrotactile detection thresholds may depend on the contact location [54, 76], contactor area [33, 34, 77, 40, 44, 76], pre-indentation of contactor in the skin [34], frequency of vibration [25, 23, 54], duration of stimulation [37, 34, 61, 62] and the density of mechanoreceptors [78, 45].

Specifically, only the P channel has the property of spatial summation [33, 77, 40, 8, 25, 44, 76] which is the decrease of the threshold by increases in the area of stimulation (e.g. threshold curves have a slope of -3 dB per doubling of area; Verrillo, 1966). Spatial summation was found to be a result of neural integration and probability summation in the P channel [25, 44, 45].

The density of mechanoreceptors varies considerably at different regions [78]. Whitehouse et al. (2006) stated that the density of fast-adapting type I fibers was greater distally within the terminal phalanx and they found that the vibrotactile thresholds at low frequencies were generally higher at proximal locations for a small contactor (diameter: 1 mm). On the other hand, Güçlü and Bolanowski (2005b) reported that the vibrotactile thresholds of the NP I channel were approximately constant at 40 Hz for a larger contactor (diameter: 4 mm) along the terminal phalanx, but the mechanical impedance of skin was not constant along this axis. This shows that the mechanical properties may also play a role in determining the psychophysical response. Interestingly, Johansson and Vallbo (1979) found that the density of Pacinian fibers shows little variation through the fingertip. However, Whitehouse et al. (2006) again found improvement of thresholds distally at 250 Hz.

The mechanical properties of the skin also varies from site to site (Lundström, 1984), changing the attenuation of vibration through the skin [79, 80, 81, 82, 83]. Therefore, skin impedance (or other mechanical variables) was studied in many physiological and psychophysical studies of the tactile sense [84, 85, 86, 45]. In this current study, we hypothesized that the vibrotactile detection thresholds should not vary significantly in the P channel when measured along the distal phalanx, because Pacinian

fiber density is approximately uniform. However, if the mechanical properties of the skin show significant differences, this may influence the psychophysical thresholds. In order to test this hypothesis, we measured absolute detection thresholds as a function of contactor size and contactor location. The thresholds were significantly affected both by contactor size (i.e. spatial summation effect) and contactor location (but with a different trend compared to Whitehouse et al. 2006). Additionally, we measured the mechanical impedance (specifically, the storage and loss moduli) at the contact locations and found a strong correlation between the thresholds and the loss modulus of the skin at 250 Hz, which is also a novel finding according to our knowledge.

2.2.2 Materials and Methods

Subjects

Seven healthy adult subjects (four female and three male, age: 23-30 years) participated in the study. The experiments were approved by the Boğaziçi University Institutional Review Board for Research with Human Subjects. All the subjects were right handed by self-report and the tactile stimuli were applied on their left middle fingertips. Because temperature affects thresholds of the P channel [63, 54, 64], the experiments were performed with the skin surface temperature in a range of 30-34^0 C. A temperature probe (PTC thermistor) connected to a multimeter monitored the skin surface temperature throughout the experiments. The mechanical stimuli did not pose any harm to the subjects.

Apparatus

The apparatus used for the psychophysical measurements were similar to the one used by Güçlü and Öztek (2007). Experiments were performed in a sound- and vibration-proof room (RE-242, ETS-Lindgren Acoustic Systems, Cedar Park, TX). The mechanical stimuli were applied by a V201 shaker (Ling Dynamic Systems Ltd., Royston, Herts, UK) with cylindrical contactor probes of radii 1, 2 and 3.5 mm. A

digital-to-analog converter card (DaqBoard/2000, IOtech, Cleveland, OH) connected to a personal computer generated the stimulus waveforms. The stimulus levels were adjusted by a PA5 digital attenuator (Tucker-Davis Technologies, Alachua, FL) and the output signal was amplified by an RA300 power amplifier (Alesis, Fort Lauderdale, FL) to drive the mechanical shaker. During the experiment, the mechanical vibrations were monitored by using a Schaevits ATA2001 LVDT (Lucas Control Systems, Pennsauken, NJ) and a TDS 2014 digital oscilloscope (Tektronix, Inc., Beaverton, OR). In order to prevent movement, subjects' middle fingers were molded in modeling clay. The subjects were presented with auditory white noise by headphones to mask any sound emitted by the mechanical shaker, which would otherwise generate cues interfering with the task.

To measure the mechanical impedance of the skin, a Type 8001 impedance head (Brüel and Kjær, Nærum, Denmark) was used. Force and acceleration signals were amplified and filtered by a Nexus Type 2692 conditioning amplifier (Brüel and Kjær, Nærum, Denmark). The acceleration signal was integrated twice by the same device to obtain the displacement signal. The voltages of the output signals and the phase angles between the force and displacement signals were measured by a 3962A single-phase lock-in amplifier (Ithaco, Inc., Ithaca, NY). The entire experimental system was calibrated with a highly accurate Fotonic Sensor (MTI-2100, MTI Instruments, Albany, NY).

Stimuli

In the psychophysical experiments, the stimuli were bursts of 250 Hz sine waves superimposed on a 0.5 mm static indentation [64]. The static indentation was applied to prevent skin-contactor decoupling and the stimulus levels were always out of the decoupling range [87, 25]. The burst stimuli began and ended as cosine-squared ramps with 50-ms rise and fall times. The duration of the test stimulus was 0.5 s as measured between half-power points of the burst (Figure 2.10.a). The test stimulus was applied randomly in the first or the second interval (cued by red and green light in a two-interval forced choice task). The subjects responded after the yellow light was on

by pressing buttons on a custom-made box. The subjects received feedback on the outcome of their decisions (yellow light blinking: correct, yellow light off: incorrect). In the mechanical measurements, the stimuli were continuous sine waves with amplitudes of 30 μm superimposed on a 0.5 mm static indentation. The stimuli were applied at three locations on the left fingertip (Figure 2.10.b).

The contact locations were normalized according to the length of the distal phalanx (L) of each subject measured from the fingernail to the joint line: L1 = 20% of L, L2 = 70% of L, L3= 90% of L. The locations were selected carefully to enable full contact for all contactor sizes (radius: 1, 2, 3.5 mm).

Psychophysical procedure

In the psychophysical experiments, a two interval forced-choice task was used with a three-down one-up rule to track detection thresholds. Two-interval forced-choice task is a commonly used technique in psychophysical experiments. The test stimulus was presented randomly in either one of the two time intervals (duration: 2 s, see Figure 2.11.a). Then, the subject selected the interval in which he or she detected the stimulus by pressing the appropriate button. The stimulus level was decreased 1 dB for three correct responses (not necessarily consecutive) and increased 1 dB for every incorrect response. This rule yields the 75% probability point of the psychometric function [31]. The experiment stopped when the stimulus level was within ± 1 dB range for the last 20 trials [64]. This procedure was performed four times for each location and contactor, for every subject. The absolute thresholds were obtained by averaging the four measurements.

Mechanical measurements

In this study, we do not report the conventional mechanical impedance (Z) which is the complex ratio of force to velocity. Instead, we analyze the dynamic modulus (E^*) which is the complex ratio of stress to strain. Dynamic modulus is a property of viscoelastic materials under sinusoidal loading conditions and it has units of Pa or
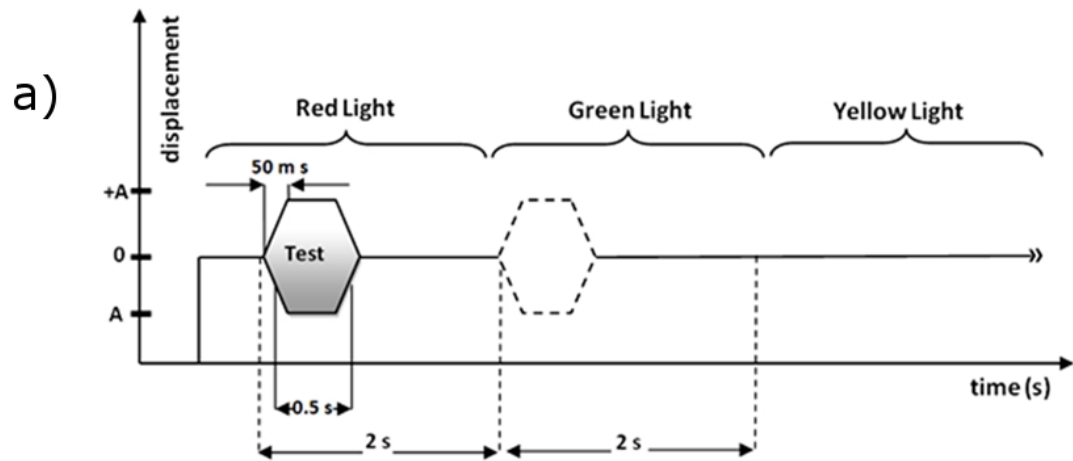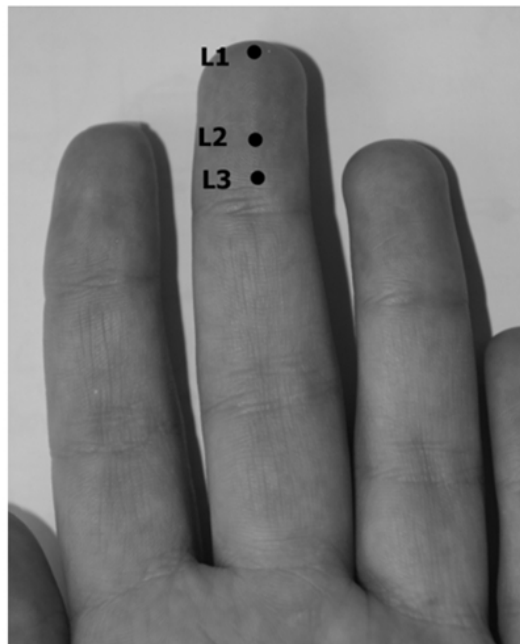
Figure 2.10 a)Stimulus timing diagram for the psychophysical experiments. b)Stimulus locations on the left middle-finger distal phalanx.

N/m^2 [18], and it can be easily converted to mechanical impedance as the following:

$$E^* = \frac{\sigma}{\varepsilon} = \frac{F/A}{x/x_0}$$

$$Z = \frac{F}{v} = \frac{E^*A}{(iwx_0)}$$

(2.2)

where σ (N/m^2) is the stress, ε is the strain (dimensionless), F (N) is the force, A (m^2) is the contactor area, x is the displacement (m), x_0 is the static indentation (m), v is the velocity (m/s), w is the angular frequency, and i is the imaginary number. The term iw has units of 1/s and implies the differentiation of the displacement to yield the velocity. Since E^* is a complex number, it can be represented as $E^* = E_1 + iE_2$ where E_1 is the storage modulus, and E_2 is the loss modulus. In phasor notation,

$$E^* = \frac{\sigma_p e^{i(wt+\delta)}}{\varepsilon_p e^{iwt}} = \frac{\sigma_p}{\varepsilon_p} e^{i\delta} = \frac{\sigma_p}{\varepsilon_p}(cos(\delta) + isin(\delta))$$

$$E_1 = \frac{\sigma_p}{\varepsilon_p} cos(\delta) = |E^*|cos(\delta)$$

$$E_2 = \frac{\sigma_p}{\varepsilon_p} sin(\delta) = |E^*|sin(\delta)$$

(2.3)

where $|E^*| = \sqrt{(E_1^2 + E_2^2)} = \sigma_p/\varepsilon_p$ is the magnitude of the dynamic modulus and $\delta = arctan(E_2/E_1)$ is the phase angle between stress and strain. Similar to psychophysical experiments, for the three contactors, the three contact locations were stimulated while the force and the displacement signals were measured. All measurements were repeated four times and the results were averaged. The mechanical measurements were obtained right after the psychophysical experiments without moving the contactor from the skin. According to the measured variables;

$$E_1 = \frac{(F_p/A)}{(x_p/x_0)}cos(\delta)$$

$$(2.4)$$

$$E_2 = \frac{(F_p/A)}{(x_p/x_0)}sin(\delta)$$

where F_p and x_p are the peak amplitudes of the force and displacement signals. δ is the phase angle $(\delta_F - \delta_x)$ between the two signals.

Analyses

Statistical analyses were performed in Matlab 6.5. First, four measurements (thresholds and moduli) from each subject were averaged. Separate 2-way ANOVAs were performed for the relevant variables: detection thresholds, storage and loss moduli. The factors in the ANOVAs were the location (L1, L2, and L3) and the contactor size (radius: 1, 2, 3.5 mm). Subject data were entered as repetitions. The Pearson correlations were found between the detection thresholds and the storage moduli, and between the same thresholds and the loss moduli.

2.2.3   Results

Psychophysical vibrotactile thresholds

The first experiment was intended to provide the vibrotactile detection thresholds at 250 Hz for all subjects using three contactor sizes. The average recorded threshold levels were between -8.0 and 3.5 dB (corresponding to 0.40 and 1.50 μm) and the standard errors were between 1.2 and 2.5 dB at the terminal phalanx (Figure 2.11). The threshold levels were consistent with the previous studies which used 250 Hz stimulation [8, 64]. There was a significant main effect of contactor size on the vibrotactile thresholds (2-way ANOVA, $p < 0.001$), and also a significant main effect
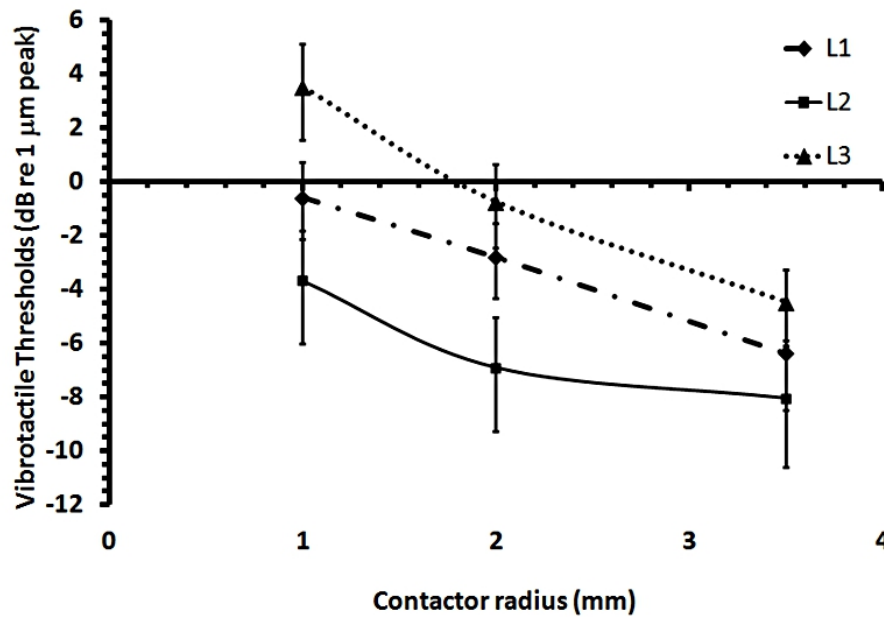
Figure 2.11 Average vibrotactile detection thresholds at locations L1, L2 and L3 for three contactor radii (1, 2 and 3.5 mm). Error bars are standard errors.

of location (2-way ANOVA, p = 0.001). There was no significant interaction between contactor size and location.

The vibrotactile thresholds had a decreasing trend with the increasing contactor size consistent with the literature [33, 77, 40, 8, 76]. In other words, with the increase of contactor area, the spatial summation effect was clearly seen at all contactor locations. Specifically, the middle point (L2), the location close to the whorl, had the lowest threshold level with the largest contactor (radius: 3.5 mm). The most proximal location (L3), the location close to the end of the terminal phalanx, had the highest thresholds at all contactor sizes. We used Tukey-Kramer method for multiple comparisons of the curves in Figure 2.11. The thresholds at L3 (average: 1.01 μm) were significantly higher than the thresholds at L2 (average: 0.50 μm) (confidence interval: 0.196, 0.812). Thresholds measured with 1-mm radius (average: 1.03 μm) were significantly higher than those measured with 2-mm radius (average: 0.70 μm) (confidence interval: 0.025, 0.641) and with 3.5-mm radius (average: 0.49 μm) (confidence interval: 0.232, 0.848).

Table 2.1

Storage and loss moduli of the glabrous skin at locations L1, L2 and L3 for three contactor radii (1, 2 and 3.5 mm).

Contactor Radius (mm)		Storage modulus (N/m^2)			Loss modulus (N/m^2)		
		L1	L2	L3	L1	L2	L3
1	mean	-1.07E+06	-1.04E+06	-1.00E+06	9.08E+04	5.52E+04	1.41E+05
	s.e.	2.81E+04	2.05E+04	9.73E+04	2.26E+04	1.29E+04	2.01E+04
2	mean	-2.35E+05	-2.38E+05	-2.42E+05	3.03E+04	2.38E+04	5.32E+04
	s.e.	5.76E+03	6.30E+03	8.34E+03	4.23E+03	4.45E+03	7.66E+03
3.5	mean	-7.48E+04	-7.63E+04	-7.02E+04	1.87E+04	1.26E+04	2.23E+04
	s.e.	3.44E+03	2.11E+03	3.67E+03	4.32E+03	1.81E+03	4.20E+03

Mechanical measurements

In the second experiment, we measured the force and displacement to calculate the storage and loss modulus of the glabrous skin. The calculated moduli are given in Table 2.1. For the storage modulus, only the contactor size had a significant main effect (2-way ANOVA, $p < 0.001$). The effects of the contactor location and the interaction between the factors were not significant. For the loss modulus, however, both factors (contactor location and size) had significant main effects (2-way ANOVA, p's < 0.001) and the interaction between them was significant ($p = 0.026$).

All measured storage moduli were negative due to the inertial (i.e. mass) effects (Figure 2.12.a). The storage modulus became less negative (i.e. more springiness) with higher contactor sizes. In addition, the middle point (L2) had the lowest loss moduli at all contactor sizes, whereas the most proximal location (L3) had the highest loss moduli (Table 2.1). Multiple comparisons of the data in Table 2.1 based on the Tukey-Kramer method yielded the following results. The storage moduli measured with the 1-mm radius contactor (average: -1.04 x 10^6 N/m^2) was significantly more negative than those measured with the 2-mm radius contactor (average: -2.38 x 10^5 N/m^2)(confidence interval: 0.73 x 10^6, 0.87 x 10^6) and those measured by the 3.5-mm

radius contactor (average: -7.38 x 10^4 N/m^2) (confidence interval: 0.90 x 10^6, 1.03 x 10^6). Additionally, the storage moduli measured with the 2-mm radius contactor was significantly more negative than those measured with the 3.5-mm radius contactor (confidence interval: 0.10 x 10^6, 0.23 x 10^6) (Figure 2.12a).

The loss moduli depended on both the contactor location and size (Figure 2.13.b). L2 (average: 3.05 x $10^4 N$/m^2) yielded loss moduli significantly lower than those measured at L3 (average: 7.22 x 104 N/m^2) (confidence interval: 1.89 x 10^4, 6.47 x 10^4). Similarly, the loss moduli measured at L1 (average: 4.66 x 10^4 N/m^2) were significantly lower than those measured at L3 (confidence interval: 0.28 x 10^4, 4.86 x 10^4). The loss moduli were lower for larger contactor sizes. Specifically, those measured with a 3.5-mm radius contactor (average: 1.79 x 10^4 N/m^2) were significantly lower than those measured with a 1-mm radius contactor (average: 9.57 x 10^4 N/m^2) (confidence interval: 0.55 x 10^5, 1.00 x 10^5). Again, those measured with a 2-mm radius contactor (average: 3.58 x 10^4 N/m^2) were significantly lower than those measured with a 1-mm radius contactor (confidence interval: 0.38 x 10^5, 0.83 x 10^5) (Figure 2.13b).

There was almost a significant moderate correlation between the absolute thresholds and the storage moduli (r = 0.650, p = 0.058) (Figure 2.14.a). However, the correlation between the absolute thresholds and the loss moduli was high and very significant (r = 0.951, p < 0.001) (Figure 2.14.b).

2.2.4 Discussion

The main goal of this study was to investigate the relationship between the psychophysical vibrotactile thresholds and the skin mechanics of the human fingertip. Because the vibrotactile threshold is lowest in the P channel at high frequencies, the stimuli targeted the P channel at 250 Hz. On the terminal phalanx of the left middle finger, three stimulus locations were selected carefully to enable full contact with different sized probes. The mechanical measurements were obtained from the same sites using the same contactors. There was no contactor surround which was sometimes
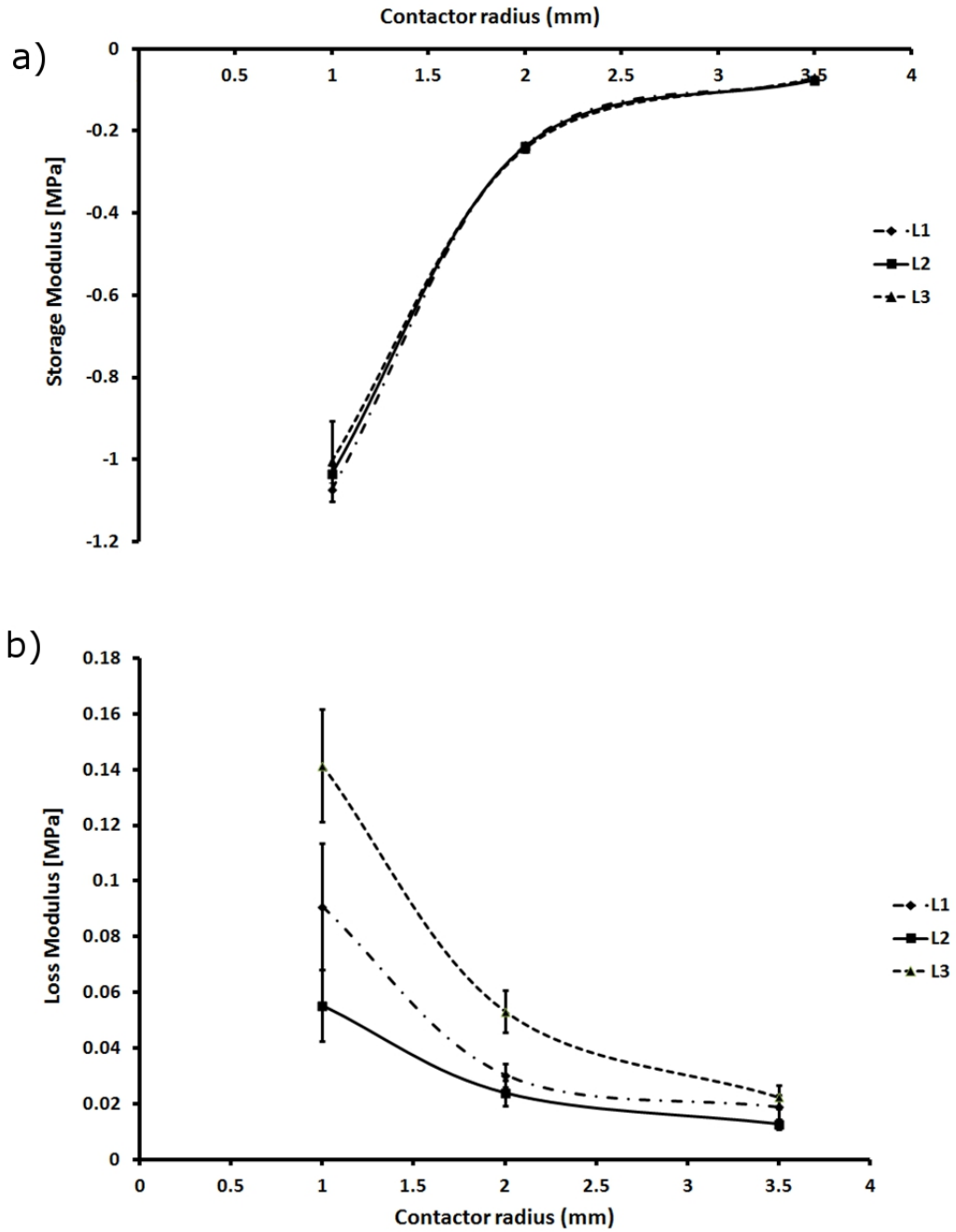
Figure 2.12 a) Storage moduli and b) loss moduli at locations L1, L2 and L3 for three contactor radii (1, 2 and 3.5 mm). Error bars are standard errors.
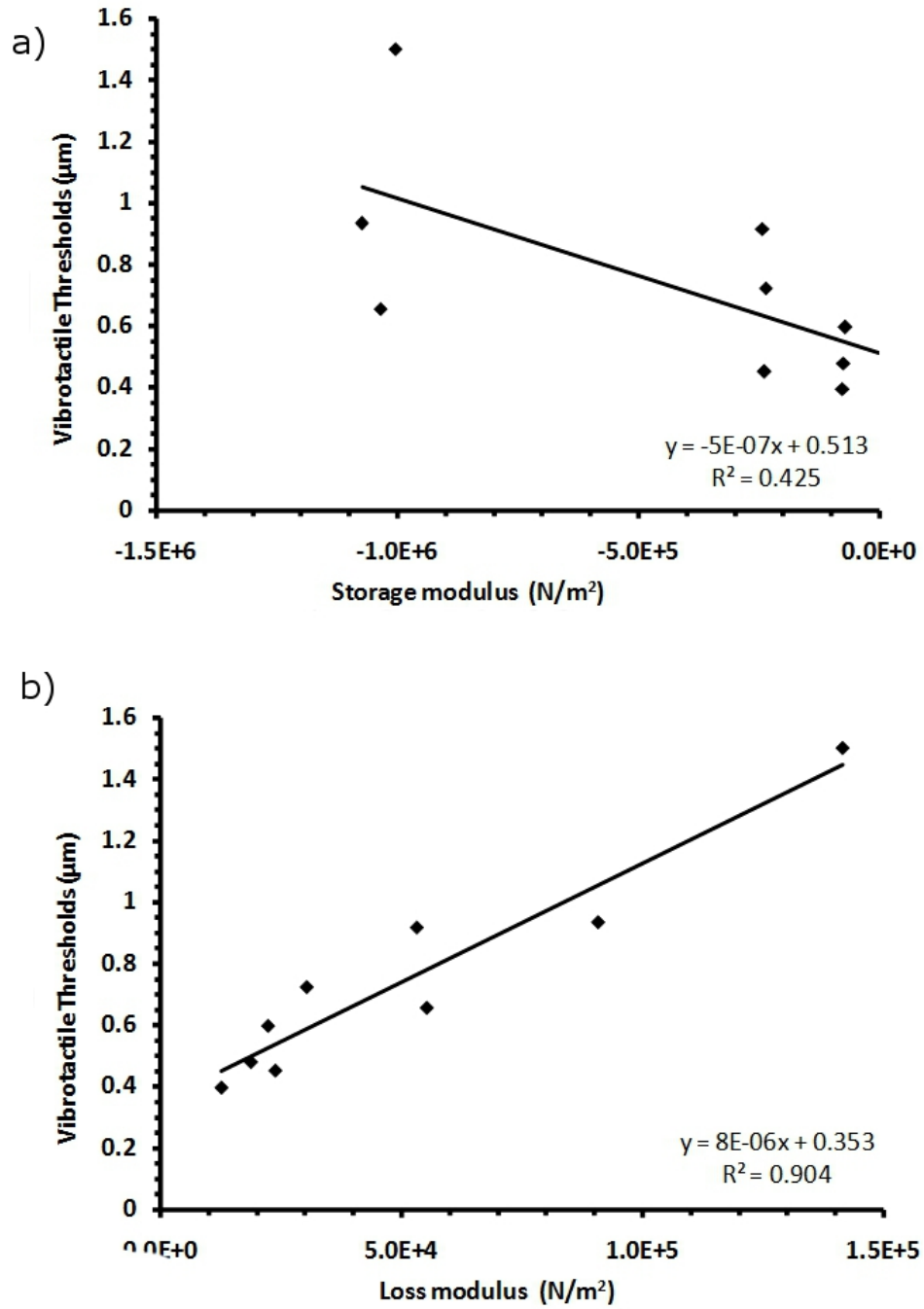
Figure 2.13 Correlation between a) the vibrotactile thresholds and the storage moduli (E_1), b) the vibrotactile thresholds and the loss moduli (E_2).

used in literature [8, 24, 76].

It was reported that the Pacinian fiber density is almost constant in the terminal phalanx [78]. Therefore, a significant vibrotactile threshold difference was not expected due to location at high frequencies (i.e. 250 Hz). According to our findings, however, there were significant differences. The location L2 (near whorl) had the lowest threshold level and L3 (proximal location) had the highest threshold level. In addition, spatial summation was observed significantly at all contact locations as expected from the P channel [33, 77, 40, 8, 25, 76].

Additionally, we found a strong positive correlation between the thresholds and the loss moduli of the skin at 250 Hz. Pacinian corpuscles in the skin have different sizes and shapes, and also they can be at different depths [88]. The reason for the correlation may be that when the energy loss as heat is low, the vibration amplitude through the Pacinian receptors becomes higher, and therefore, the detection threshold is measured lower. The inverse statement is expected to be correct as well. Similarly, the moderate correlation with the storage modulus may point out the elastic energy stored in the tissue due to its springiness which would also be used for excitation. Recall that as the springiness increased in the storage modulus, the thresholds decreased.

Previous psychophysical literature

The vibrotactile threshold measurements were consistent with the previous studies [74, 33, 77, 54, 64]. In those studies, 250-Hz thresholds of the P channel ranged from -7 to -13 dB. In the current study, we found -6.9 dB with a 2-mm contactor radius at location L2 (near the whorl). Previous studies with larger contactors yielded lower thresholds [74, 25]. Similarly, we measured lower threshold (-8.0 dB) with a 3.5-mm contactor radius. According to Verrillo (1971), the vibrotactile thresholds improve at a rate of 3 dB per doubling the contactor area. When we averaged results from the three locations, our thresholds decreased from 0.2 dB to -6.2 dB at a rate of 1.8 dB per doubling the area. This lower rate in the current study may be due to the difference in the duration of the stimulus which was much higher ($\sim$1 s) in the studies by Verrillo

(1962, 1963, 1971). As a matter of fact, Gescheider at al. (2002) reported that when a larger contactor is used (area $> 0.1\ cm^2$), the slope of the threshold improvement due to spatial summation becomes lower, which is in a good agreement with our results (see Figure 2.11). Gescheider et al. (2002) attributed this finding to the inclusion of probability summation, as well as neural integration, in the detection process. The interplay between neural integration and probability summation was shown by further experiments [44] and a population-response model [45].

As mentioned above, Johansson and Vallbo (1979) found that the density of Pacinian fibers is approximately uniform in the fingertip [78]. Therefore, we initially expected to find uniform thresholds, not depending on contact location in the P channel. However, Whitehouse et al. (2006) showed that the thresholds near the whorl are higher than those measured at other fingertip locations with a 3-mm radius contactor. There is a clear contradiction with our results which show the opposite, i.e. lowest thresholds near the whorl. On the other hand, Whitehouse et al. (2006) found a proximally increasing trend with a 0.5-mm contactor. We think that these inconsistencies may stem from the mechanical differences in the experimental conditions. For example, we did not use a contactor surround unlike most other researchers. Additionally, our contactor locations were slightly different. Güçlü and Bolanowski (2005b) showed that the mechanical impedance of the skin changes at different locations on the phalanx (at 40 Hz). Therefore, skin mechanics may play a role more important than we thought before [45].

Skin mechanics

Human skin is composed of several layers and behaves as an inhomogeneous, anisotropic, non-linear viscoelastic material [89, 5, 90, 21]. Viscoelastic materials have the property of viscous and elastic behavior when undergoing deformation. The storage and loss modulus in viscoelastic solids measure the stored energy representing the elastic portion (and the mass) and the energy dissipated as heat (dashpot-like behaviour) representing the viscous portion [18]. In the literature, there are many experimental and modeling studies on the static and dynamic behavior of the skin under various

stimulation conditions [80, 85, 14, 91, 92, 93, 90].

We measured the dynamic modulus at the fingertip. The storage part was negative because of the high inertial effects at 250 Hz (dependent on the square of the frequency), and its absolute value was in the range of 0.07-1.07 MPa. The loss modulus was in the range of 0.01-0.14 MPa at 250-Hz stimulation. Our results are consistent with some of the findings in the literature. For example, Xu and Lu (2008) found that under very low frequency stimulation (1 Hz) of the pig hairy skin [94], the storage modulus was approximately 2 MPa and the loss modulus was approximately 0.3 MPa. Furthermore, they showed that higher temperatures yielded higher moduli. Skin surface temperature was in the range of 30-34^{0}C in our experiments. On the other hand, Boyer et al. (2007) reported that the storage modulus was in the range of 0.01-0.03 MPa and the loss modulus was even lower than 0.01 MPa at 40-Hz stimulation in the human forearm.

In the study by Moore and Mundie (1972), an increase of the probe area resulted in an overall decrease in the reactance and the resistance which would correspond to a decrease in the dynamic modulus [80]. We found a similar decrease in both the absolute value of the storage modulus and the loss modulus as a function of contactor radius. In addition to stimulation parameters, the contact location and the type of skin stimulated most definitely have effects on the measured dynamic moduli. We found no significant difference in the storage modulus due to contactor location, but the proximal end had the highest loss modulus and the pad near the whorl had the lowest loss modulus. Devecioglu and Güçlü (2012) showed that, at 40-Hz stimulation, the distal end of the rat digit had the highest reactance (related with storage modulus) and the proximal end had the maximum resistance (related with loss modulus), which are partially in agreement with the current results. In the hairy skin, the epidermis is thinner than that in the glabrous skin. By using ultrasound and optical coherence tomography, Hendriks et al. (2006) estimated that the stiffness (related with storage modulus) of the human reticular dermis is 0.16 MPa [95]. The mechanical property of the epidermis, however, is expected to influence the overall mechanical properties of the glabrous skin which is currently being investigated in our laboratory.

Mechanics of Pacinian corpuscles

It is interesting to note that Lundström (1984) measured minimum mechanical impedance at 200 Hz in the human glabrous skin, and stated that this result may be the reason why humans have lowest detection thresholds around this frequency. The U-shaped threshold curve around this frequency is due to the P channel. Bolanowski and Zwislocki (1984a,b) showed that when the Pacinian receptors from the cat mesentery are completely isolated from the surrounding tissue and stimulated, the mechanoreceptive thresholds were still lowest around this frequency. Therefore, the U-shaped frequency sensitivity must be a characteristic of the Pacinian receptors and should not be attributed to skin mechanics.

Hubbard (1958) conducted experiments also with isolated Pacinian corpuscles from cat mesentery and viewed lamellar displacements [96]. The results showed that the static displacements in the corpuscles attenuated to zero before reaching the core and there was a nonlinear relation between the displacements and the indentation amplitude. The dynamic displacements showed less attenuation and were considered sufficient to excite the neurite in the core. Loewenstein and Skalak (1966) established a distributed-parameter model (with springs and dashpots) for the lamellae and fluid-filled spaces in the Pacinian corpuscles [97]. The predictions of this model were in good qualitative agreement with Hubbard's (1958) data. The model results showed that under static compression, the elastic forces were poorly transmitted to the core. However, under dynamic compression, the viscous forces were transmitted better. During release from load, energy stored in the spring elements was consumed by viscous flow, and this set up viscous forces again, which would cause re-excitation of the corpuscle. Therefore, increased loss modulus, i.e. viscous resistance, in the Pacinian corpuscle and the skin would hinder movement and considerably decrease dynamic displacements. The overall effect would be an increase of the vibrotactile thresholds as found in our results presented in this article.

According to the elastic semi-infinite continuum model studied by Güçlü et al. (2006), in a material with Poisson ratio of 0.25, the displacement at the contactor axis

and at a depth equal to the radius of the contactor is approximately 0.71 times the static indentation (see Equation (1) in that reference). This implies that for larger contactor sizes, a given static displacement can be achieved at greater depths in the skin. Therefore, a smaller static indentation would be adequate for exciting a single mechanoreceptor located at a more superficial level. If this general finding can be generalized to dynamic stimuli, it can partially explain spatial summation in the P channel. However, such an explanation does not rule out the possibility of contributions from multiple mechanoreceptors and/or mechanoreceptive fibers during the psychophysical detection process [45].

2.3 Reconstruction of somatosensory evoked potentials by using discrete wavelet transforms

2.3.1 Background and theory

The discrete wavelet transform (DWT) was developed to represent time signals by appropriate time-frequency windows. Similar to the FFT, the wavelet transform performs a least squares fit of an analysis function to the time domain data. For the discrete wavelet transform (DWT) considered here, a set of orthogonal basis functions is obtained by scaling and translation of a mother wavelet [55].

The Fourier transform can be used to measure oscillation amplitude across the whole frequency spectrum. However, the Fourier transform contains no temporal information. The windowed Fourier transform uses a fixed and arbitrarily defined window width, thus resulting in a fixed time-frequency resolution. When defining a narrow window, temporal resolution will be high. Wavelet transform are able to extract signal
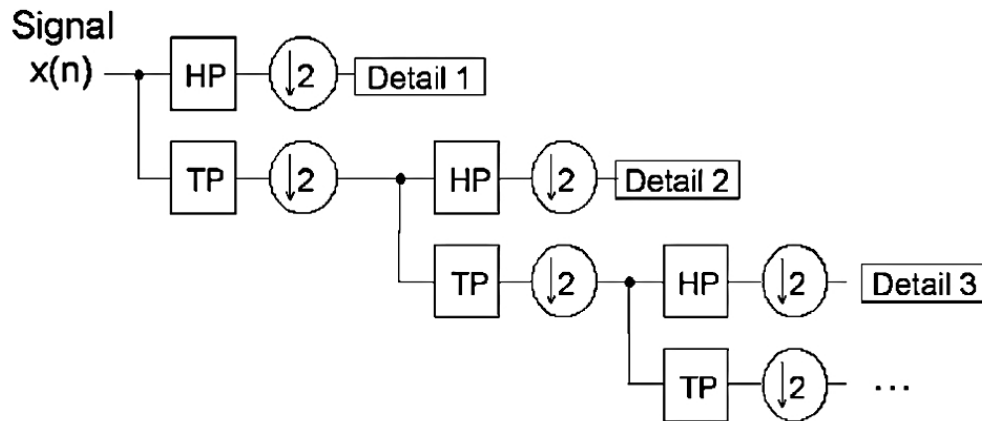
Figure 2.14 Discrete wavelet transform (DWT) implemented as an octave filter bank. The signal x(n) is decomposed by subsequent low-pass and high-pass filtering combined with sub-sampling (by 2). HP: High Pass Filter, TP: Low Pass Filter.

time and frequency information simultaneously. And give better results while decomposing noisy signal envelope [98].

An efficient calculation of the DWT coefficients in the case of discrete-time data can be performed using the multi-resolution analysis (MRA) [99]. The MRA is performed by filtering the signal to be analyzed with an octave filter bank as shown in Figure 2.14.

2.3.2   Methods

SEPs were recorded in Tactile Research Laboratory in Boğaziçi University Institute of Biomedical Engineering. 5 subjects were (3 male and 2 female, ages 26.4±2.3) participated in the study. The experiments were approved by the Boğaziçi University Institutional Review Board for Research with Human Subjects. All the subjects were right handed by self-report and electrical were applied on their left hand. The rectangular electrical stimulus was 4 mA and 4.7 Hz with 0.25 ms duration. The sampling frequency was 32.7 kHz. The SEPs were averaged 500 times for every subject. Gold-plated recording electrodes were placed over the somatosensory cortex (Cpi-Cpc). The Haar, Daubechies 6 and Meyer wavelet functions were tested. 8 Octave filter-bank method was applied to investigate a wide frequency range of SEPs.

We are interested in the reconstruction error ($R_{EKerror}$) , here defined as;

$$R_{EKerror} = \frac{\sum \left(x(n) - y(n)\right)^2}{\sum \left(x(n)^2\right)} \tag{2.5}$$

The error varies between the values 0 and 1, therefore indicating the quality of the reconstruction and providing a measure how good the information within the SEP can be parameterized within only few DWT coefficients. All analyses were performed in Matlab.

2.3.3 Results

Both the wavelet function and periodic extensions have to be chosen appropriately in order to achieve a good wavelet representation of the SEP. It is important to choose a wavelet function which offers good time domain localization properties and provides, at the same time, good frequency resolution. The first SEP component which is detectable is the N20 with a latency of about 20 ms after the stimulus. First 10 ms were discarded from the data to eliminate the artifact of electrical stimulation. For all subjects, the N20 peaks were visible (Figure 2.15).

Three different types of wavelet functions (Haar, Db6, Dmey) reconstructions were tested by using 8 octave filter-bank method. Total reconstruction errors and N20 latency errors were recorded (Table 2.2). We considered a latency error below 1% as an accurate representation for an SEP (Figure 2.16). As seen in the table 2.2, at the 6th octave reconstruction, the mean errors were 7.6% for Haar, 5.4% for Db6, and 5.3% for Dmey. At the same level, the mean latency errors were 3.4% for Haar, 1.2% for Db6, and 0.26% for Dmey. At the 7th octave, all the latency errors were above 1% (Table 2.3).
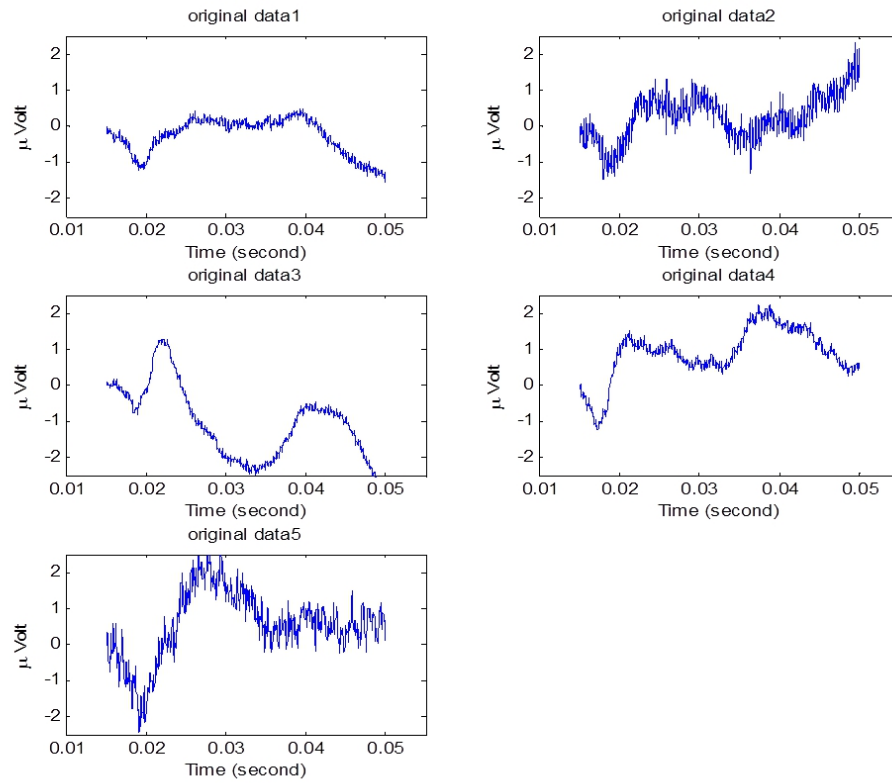
Figure 2.15 Raw data of SEPs from 5 subjects.
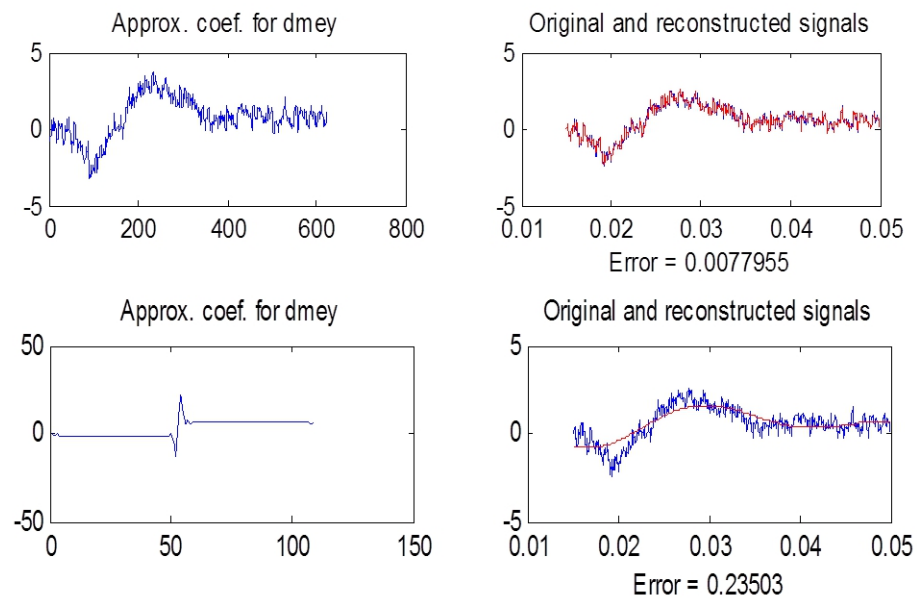
Figure 2.16 SEP reconstruction for subject no. 5 a) 1st Octave Dmey b) 8th Octave Dmey.

Mean Total Reconstruction Error			
1st	0.01028	0.00802	0.00792	544
2nd	0.0227	0.0221	0.02116	272
3rd	0.03354	0.03254	0.03248	136
4th	0.04344	0.0402	0.04018	68
5th	0.05232	0.04736	0.0456	34
6th	0.07686	0.05426	0.0531	17
7th	0.15404	0.08376	0.0834	9
8th	0.25034	0.176	0.15506	4

Table 2.2
Mean values of total reconstruction error for all subjects.

Δ **Latency= (Reconstructed Data Latency - Original Data Latency) [ms]**						
	7th Octave			6th Octave		
Latency(ms)	Haar	Db6	Dmey	Haar	Db6	Dmey
Data 1	1.7	0.7	0.2	0.67	0.38	0.1
Data 2	1.6	0.5	0.1	1	0.17	0.1
Data 3	1.8	1.19	1.8	0.9	0.14	0.03
Data 4	0.7	0.17	1.4	0.52	0.3	0.03
Data 5	1.41	0.67	0.1	0.32	0.2	0.1
mean	1.442	0.646	0.7	0.682	0.238	0.052
stdev	0.439	0.369	0.836	0.2766	0.099	0.045
% error	8.5	3.5	1	3.41	1.19	0.26

Table 2.3
Latency errors for the 6th and 7th octave reconstructions.

2.3.4   Discussion

As a quantitative measure for SEP representation by the reconstruction error, it was shown that the more coefficients are used, the higher is the accuracy for SEP representation. Therefore, the determination of SEP latencies will be more accurate.

When all the wavelet coefficients are used, the SEP can be reconstructed without any error. The number of DWT coefficients which are required for an adequate SEP representation depends upon the specific problem. From the clinical point of view the latencies can be regarded as the most important feature for SEPs. The wavelet decompositions of SEPs may be used for a large variety of applications. First, it may serve as a data reduction algorithm in order to minimize computer storage. Second, the DWT can be used to extract most prominent time frequency regions within the SEP signals. Third, the DWT maybe used as a preprocessing step for objective signal detection. In this case, only a few coefficients are needed [98].

These results show that SEPs can be accurately represented by using only 17 coefficients based on Dmey wavelet and 6th octave in the filter bank multi-resolution technique. In summary, it was shown that the wavelet representation of SEP may be a useful tool for any preprocessing step towards automatic evaluation.

2.4 Neural correlate of psychophysical forward masking in the tactile Pacinian Channel

Mustafa Z. Yıldız, Burak Güçlü, Society for Neuroscience Abstracts, 35, program no: 173.24, 2009.

2.4.1 Background and theory

Masking is the impairment of the detectability of one stimulus by the presentation of another stimulus [29]. Here, we focus on forward masking. For forward masking, the masking stimulus precedes the test. Previous studies showed that forward masking occurs only when the intensity of a given masking stimulus is above the threshold of the channel [51]. Furthermore, the effect of forward masking decreases as the temporal interval between the masking and the test stimuli increases [48, 52]. From the previous studies, we know that there is no masking in periphery of the tactile system. There are many studies on psychophysical masking in tactile system [28, 51, 8, 50], and there are also a lot of masking studies in auditory system [100, 48].

There is an extensive psychophysical literature on judgments of the presence, magnitude, and frequency of vibrotactile stimuli. However, non-invasive recording of evoked potentials on the scalp has mostly been determined for electrical stimuli. The evaluation of SEPs are not adequate to abtain detailed information about somatosensory processing. Therefore, our main goal was to find a correlate between mechanically evoked SEP and psychophysical response.

In the literature, there are few studies which reports mechanically evoked SEPs on the scalp. The frequency domain analysis revealed prominent frequency components in the signal corresponding to the frequency of vibrotactile stimulation, and sometimes its lower harmonics. This phenomenon may be due to the entrainment of cortical neurons [59, 60]. Note that Pacinian-like cortical neurons in S1 cortex do not generate spikes periodically as much as neurons associated with rapidly adapting afferents.

Therefore, at low stimulus level at which P channel is activated we obtain relatively low level of frequency-following response.

In this study, we present the parallel effects of forward masking on the psychophysical response and the frequency-following response in the mechanically evoked SEPs. Although there have been many studies on the psychophysics of forward masking, the neural correlate of the masking effect was not explicitly shown in the somatosensory cortex. Because the Pacinian channel is most sensitive at around 250 Hz, we used high frequency stimulation (230 Hz). In addition, to compare our results with previous literature [59, 60], we repeated the experiments with 40 Hz stimulation. For 40 Hz conditions, we did not investigate the masking effects; instead we measured only the test stimulus during 0.5 s stimulation. Overall, our findings indicate that mechanically evoked SEPs are not robust for studying somatosensory processing. Therefore, non-invasive scalp recordings offer little information about the psychophysical response.

2.4.2 Methods

Subjects

In this study, seven healthy adult subjects (ages 22-29 years) were involved. Experiments were approved by the Ethics Committee for Human Participants of Boğaziçi University. All the subjects were right handed and the tactile stimuli were applied on their left middle finger tips. The mechanical stimuli were applied by shaker with a cylindrical probe (radius =2 mm). Evoked brain potentials were recorded by a special amplifier (MicroMed) using gold-plated surface electrodes. The stimuli were burst of sine waves and they were superimposed on a 0.5 mm static pre-indentation [64]. In psychophysics experiments, the half power duration of test stimulus was 500 ms. In EEG recording experiments, there were three different amplitude levels (10, 20 and 30 dB Sensation Level (SL)).

Psychophysical Procedure

In the psychophysical experiments, two interval forced choice paradigm (see chapter 1.6.2) was used with a three-down one-up procedure to measure the absolute thresholds of the subjects. This procedure was performed four times for every subject and the absolute thresholds were obtained by averaging of four results for both 40 and 230 Hz stimulation.

In masked threshold experiments, just before the test stimulus, a high level mask stimulus was applied. The subject's task was to find the correct period in which a test stimulus occurred (Fig. 1.22). The threshold levels of the Pacinian channel were elevated by using a 230 Hz masking stimulus which proceeds with a 230 Hz test stimulus. The masking stimulus occurred in each interval but the test stimulus applied randomly. The intensities of the masking stimulus were SL10, SL20 and SL30 dB.

Evoked Potential Recording Procedure

First, the subjectâs electrically evoked SEPs were recorded to establish a baseline, and the N20 peaks were identified. Then, mechanically evoked SEPs were recordedon the scalp over the somatosensory cortex (Cpc-Cpi) and the inside elbow joint of the forearm ipsilateral to the stimulus served as the common reference for the recordings [56]. The sampling frequency was 1 kHz. The recording duration was 1 s. The evoked potentials were averaged 200 times to enhance the signal to noise ratio [98].

For 230 Hz stimulation, we recorded only over the somatosensory cortex (CH1) and we did not use a control channel as in the 40 Hz stimulation recordings. CH1 was the somatosensory cortex, the difference between ipsilateral and contralateral activities and CH2 was for the control channel, forehead (Figure 2.17). The recordings were repeated for no-stimulus (NS), 10 dB SL, 20 dB SL, 30 dB SL stimulus amplitude levels. When masking was used, the masking amplitude was the same as the test stimulus amplitude.
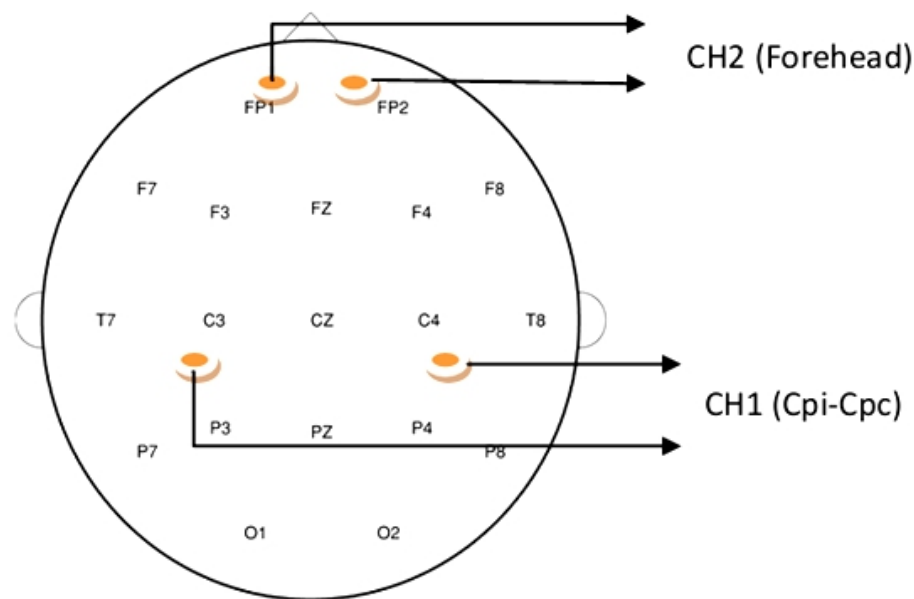
Figure 2.17 SEP measurement diagram. CH1: Electrodes over the somatosensory cortex, CH2: electrodes on the forehead for control measurements.

Analysis

To test the hypothesis of whether the mechanically evoked SEPsis related to the stimulus parameters, we performed the following analysis by using FFT. For 230 Hz mechanical stimulation measurements, the mechanically evoked SEPs were filtered to eliminate conventional EEG activities ($<$40 Hz). First, the total energy of the filtered data within the frequency band (50-500 Hz) was calculated. Secondly, the energy around the stimulus frequency (230$\pm$2 Hz) was calculated. For 40 Hz the mechanically evoked SEPs were filtered between 10-160 Hz. The energy in the filtered signal and the energy around stimulus frequency (40$\pm$2 Hz) were calculated. The analysis were performed in Matlab. We also applied frequency-time analysis (Complex Morlet wavelet transform) to the filtered data. Additionally, the temporal signal was divided into 12.5 ms bins. The total power of each bin was analyzed and Pierssonâs correlations were found between different channels.

2.4.3 Results

Psychophysics

The first experiment was intended to provide the absolute detection thresholds of each subject. The recorded threshold levels of the stimulus were between 5.8-22 dB (6.8-22.1 μm). With these results, the masking levels were not held fixed and adjusted according to each subject's absolute detection threshold levels. The detection threshold levels for masked thresholds at 10 dB SL and were between 2.8-16 dB (2.8-16 μm), at 20 dB SL were between 0.2-12.9 dB (0.8-10.9 μm), and at 20 dB SL were between 0.2-5.7 dB (0.2-5.8 μm). There were statistically significant differences for all masking levels (t-test p<0.001).

Figure 2.18 shows the average results for all participants for each condition (absolute threshold, masking at 10, 20 and 30 dB SL). The effect of masking stimulus varied among the participants. The linear function in Figure 2.19 is the best fit to the data. The high R^2 value (> 0.99) indicates that the masking function can be approximated by a linear function. The results are consistent with previous studies [54, 64].

Somatosensory responses

For 230 Hz mechanical stimulation recordings, the total area of power spectrum (50-500 Hz) during the masked test-stimulus and during the unmasked test-stimulus interval was significantly different for 20 dB SL and 30 dB SL masking level (Wilcoxon sign rank test p= 0.034 and p=0.013 respectively, Fig. 2.20). In addition, at driving frequency (at 230$\pm$2 Hz) masking and test period was significantly different from each other at 20 dB SL and 30 dB SL masking level (Wilcoxon sign rank test p=0.013 and p=0.019 respectively). For the 10 dB SL masking intensity level, there was no statistical difference for both total power spectrum and driving frequency spectrum area (Fig. 2.21).
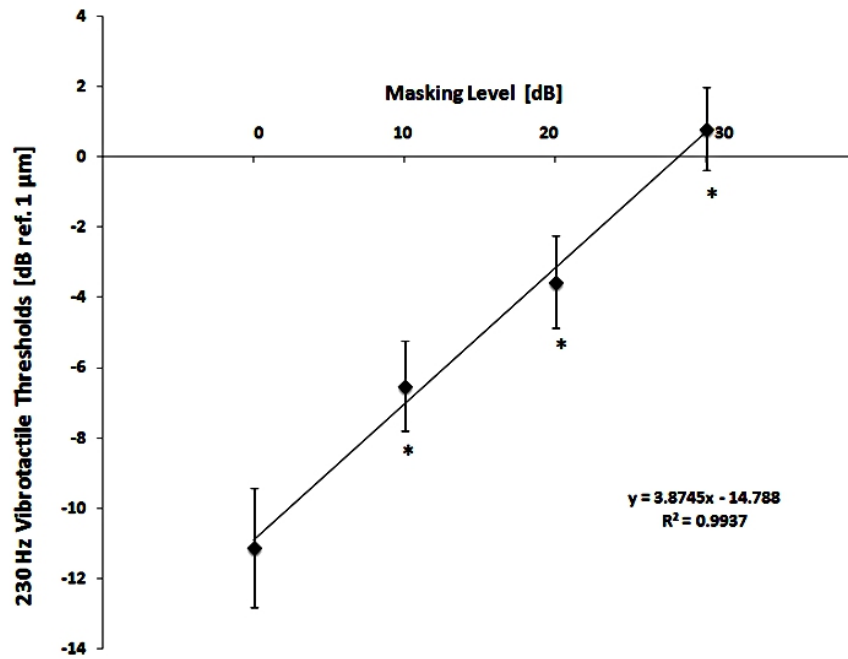
Figure 2.18 Psychophysical forward masking in the P channel at different masking levels (10, 20 and 30 dB SL).
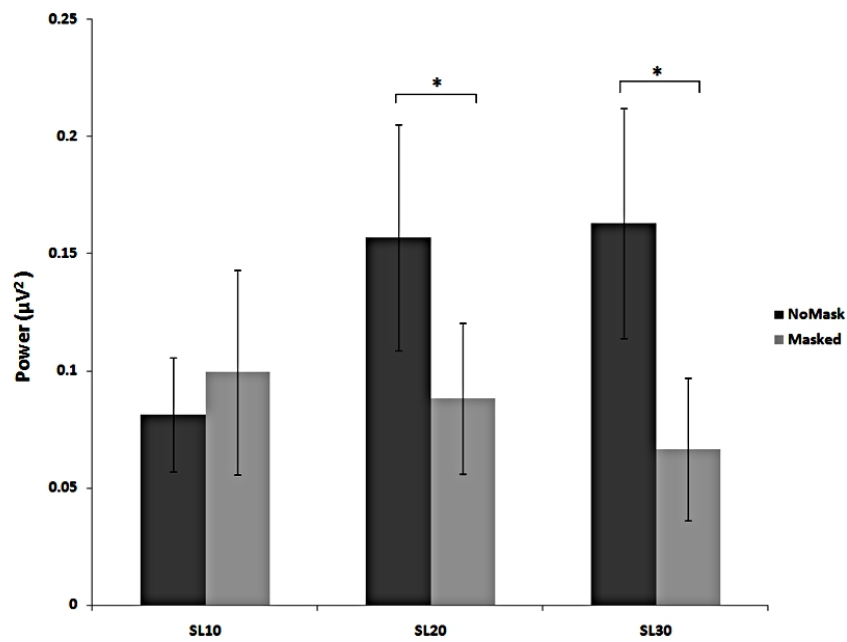
Figure 2.19 Signal power of mechanically evoked potentials between 50-500 Hz for No-Mask and Masked conditions, average of all subjects. The mechanical stimulus frequency was 230 Hz.
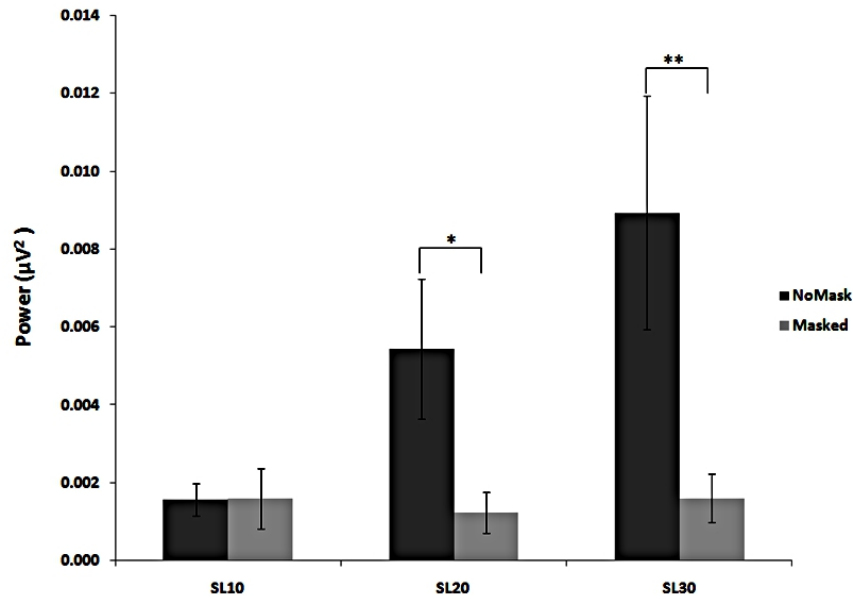
Figure 2.20 Signal power of mechanically evoked potentials at (230±2) Hz for No-Mask and Masked conditions, average of all subjects. The mechanical stimulus frequency was 230 Hz.

The dark gray bars in Figure 2.19 were replotted in Figure 2.21. There was a significant difference between the evoked responses of SL+10 and SL+20 dB stimulus levels (t-test p=0.017<0.05), and between SL+10 and SL+30 dB (t-test p=0.032<0.05), but not significant difference between SL+20 and SL+30 dB (t-test p=0.466) (Fig. 2.21).

Figure 2.22 shows the wavelet transform of two-second mechanically evoked SEPs recording including both the masking and test stimulus. In the same figure, the power spectrum of one-second masking-period and 0.5 second test-stimulus period is also given. The statistical analysis showed that for 30 dB SL stimulus intensities there was significant difference between mask and test stimulus periods within trials (p=0.019). In masking period, some subjects had a prominent stimulus frequency component in their mechanically evoked SEPs. However, the signal during the test stimulus did not include such a components, in fact, in subject no.2's data, there was more energy around 115 Hz.

For 40 Hz mechanical stimulation, the FFT's of mechanically evoked SEPs were calculated. The difference of the power spectrum area at stimulus frequency (at 40±2
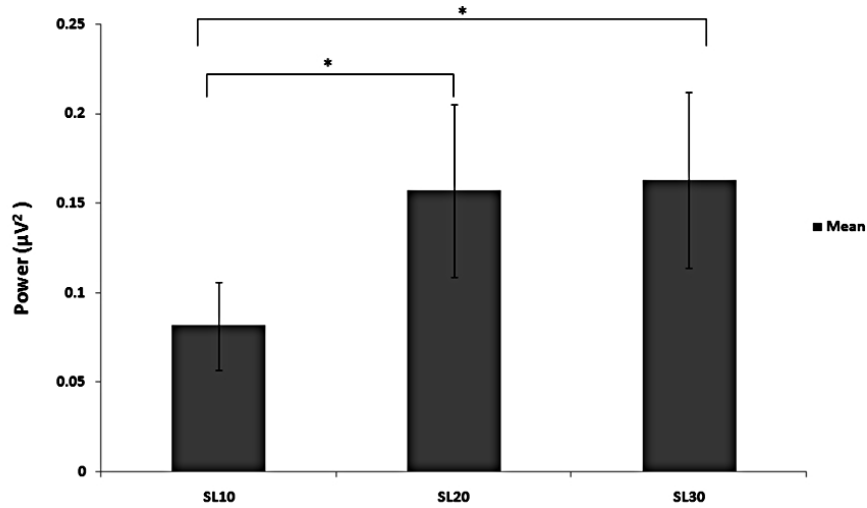
Figure 2.21 Amplitude dependency of mechanically evoked SEPs filtered between 50-500 Hz potentials (10, 20 and 30 dB SL). The mechanical stimulus frequency was 230 Hz.
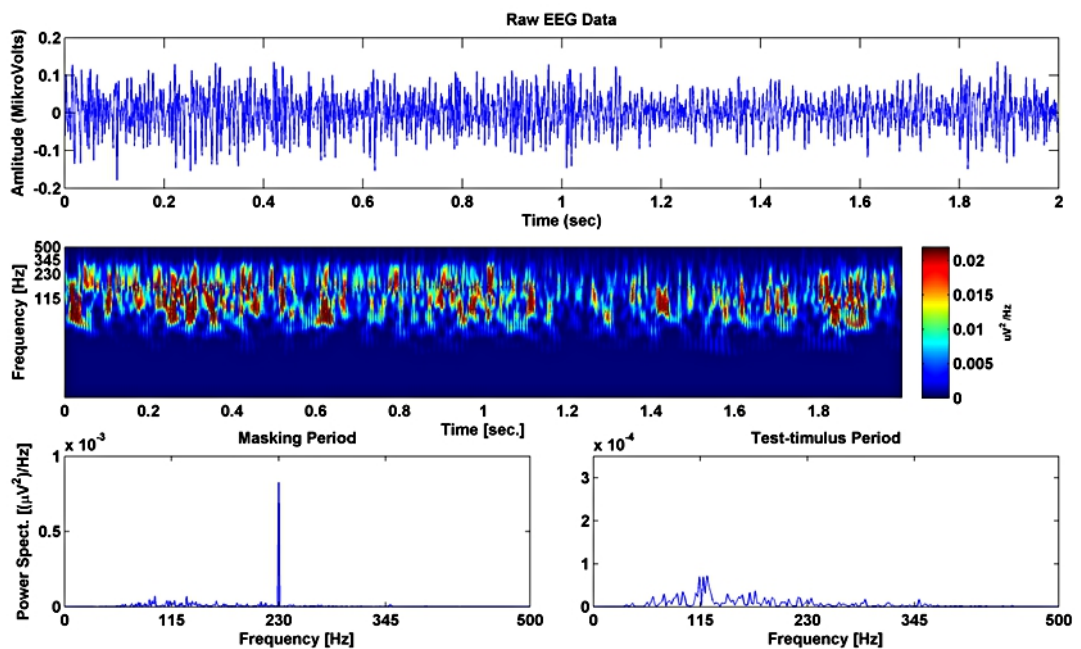
Figure 2.22 Mechanically evoked potantials with forward masking (subject no.2, 20 dB SL).

Hz) between two cases was significant for 30 dB SL and NS (Wilcoxon sign rank, p=0.0156), and for 10 dB SL and 30 dB SL (p=0.046) respectively (Figure 2.23.b). In other cases there were no significant differences. For filtered data within the 10-160 Hz band, there were no significant differences (Figure 2.23.a).

In 40 Hz stimulation recordings, Figure 2.24.a shows the no-stimulus period (NS) for CH1 activity and Figure 2.24.b shows the NS for CH2 activity. In Figure 2.25.c., power spectral density of mechanically evoked SEPs during stimulus period (0.5 s), and in Figure 2.25.d., the activity over forehead are seen. The stimulus amplitude was 30 dB SL ($\sim$100 μm) for subject no.1. The peaks were quite variable within and between subjects. Time averages of filtered data typically had in the range of 0.1-2 μV.

Time domain analysis

The time series data were divided into bins (12.5 ms) and the total power in each bin were averaged across subjects. Even though some trends are visible, the error bars are very high. The following correlations were performed based on these time bins. In Figure 25, the temporal change in power is shown for 100 ms bins for clarity; the stimulus period is between 200-700 ms. We could not reach any conclusions about any temporal trend in the signal power.

Additionally, the correlations between CH1 and CH2 at different stimulus amplitudes are given in the Table 2.4. The correlations were performed both for the entire recording period and only for the stimulus period. First, cross channel correlations for each stimulus level are presented. Specifically, for NS condition, when no stimulus were presented, CH1 and CH2 were not correlated during the stimulus period (r=0.03, p=0.825). The correlation increased in 10 dB SL stimulation, but still was not significant during the stimulus period. For the entire recording period, it was significant (r=0.24, p=0.029). For 20 dB SL, CH1 and CH2 activity was significantly correlated during the stimulus period (r=0.35, p=0.013). For 30 dB SL, CH1 and CH2 activities were significantly correlated both the entire recording and the stimulus period (respectively, r=0.36, p=0.001; r=0.32, p=0.026).
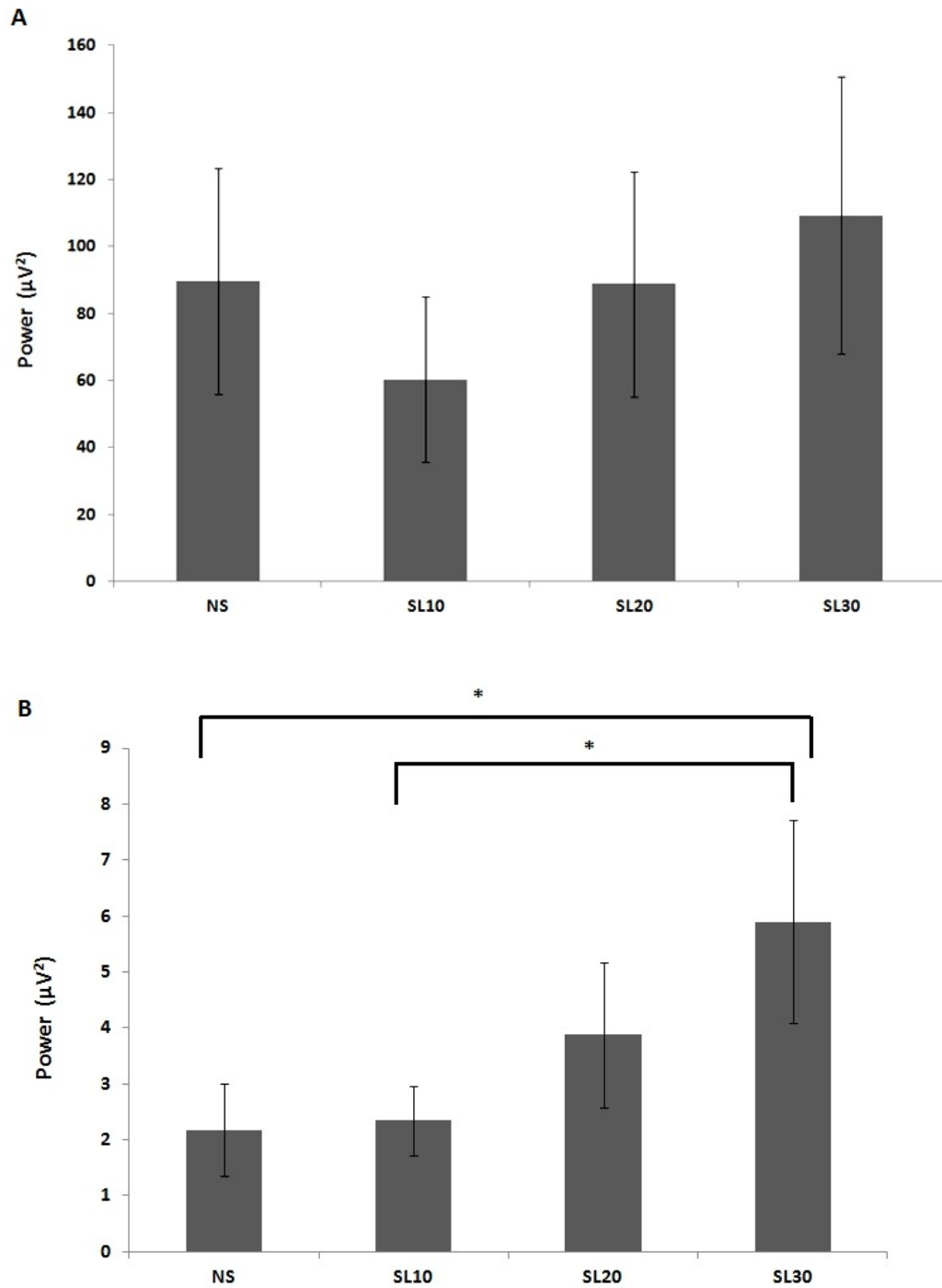
Figure 2.23 Signal power of mechanically evoked potentials. a) Analysis 10-160 Hz band, during stimulation period (500 ms). b) Analysis for 40 ± 2 Hz band. NS: No stimulus, SL10: 10 dB SL, SL20: 20 dB SL, SL30: 30 dB SL.
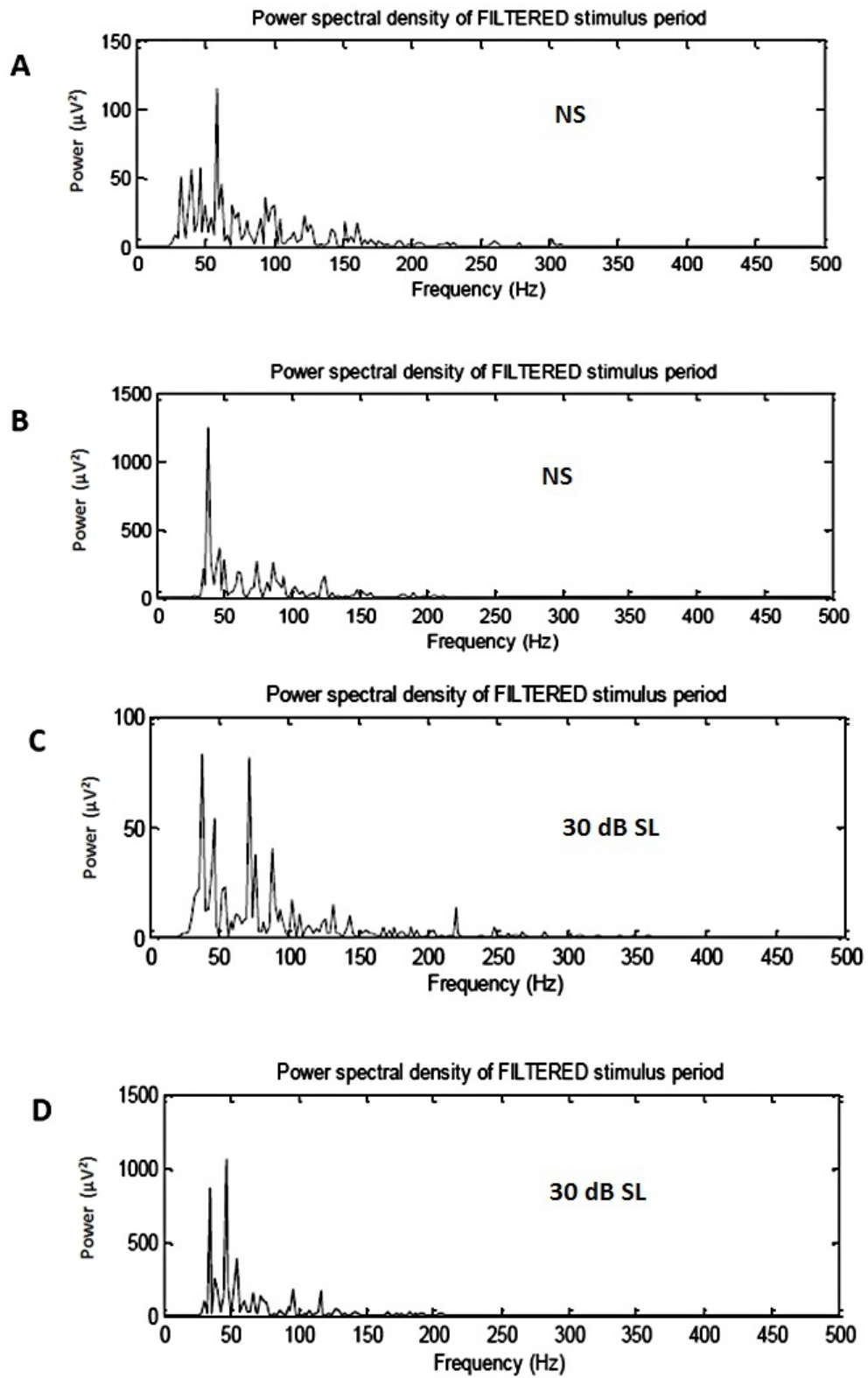
Figure 2.24 Power spectral density of mechanically evoked potentials during 0.5 s stimulation at 40 Hz. a)No stimulus period at CH1 b) No stimulus period at CH2 c) during stimulation at CH1 d) during stimulation at CH2.
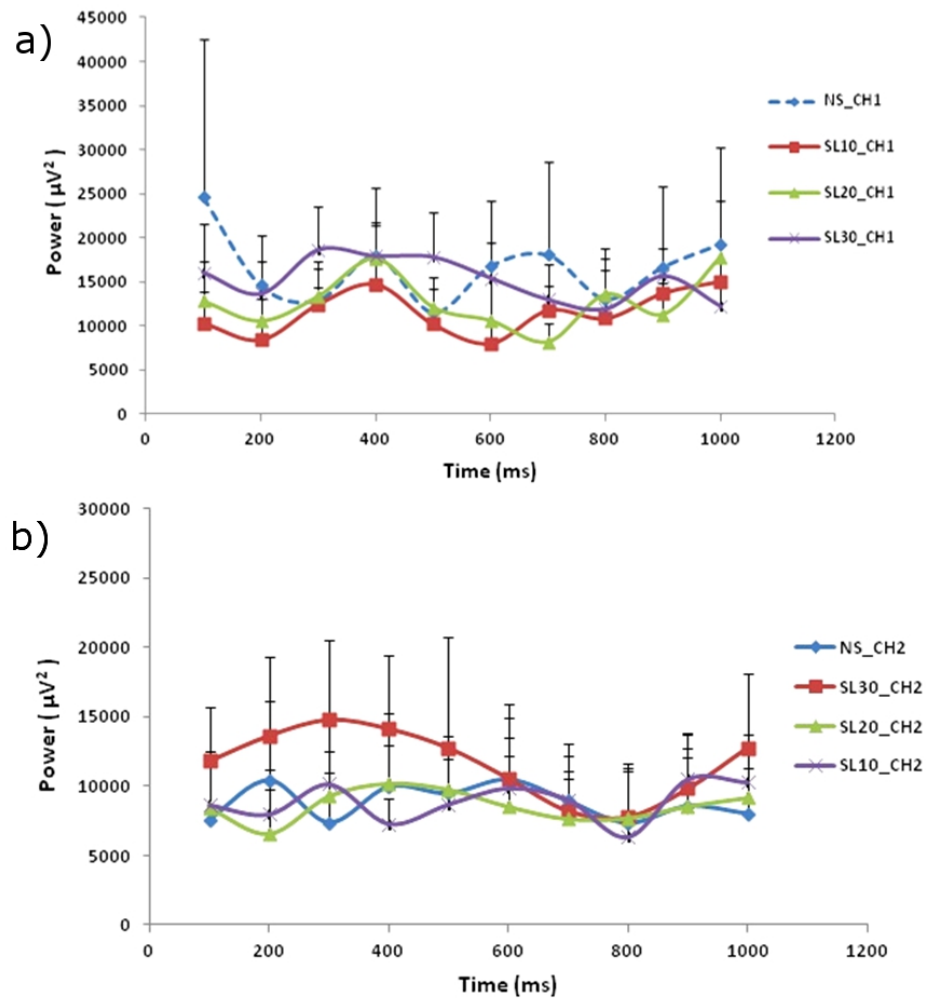
Figure 2.25 Signal power of mechanically evoked potentials over time. a) CH1: Electrodes over somatosensory cortex. b) CH2: electrodes over the forehead.

Table 2.4

Pearson's correlation coeffiecients between channels during 1 s recording or 0.5 s stimulation. Time window duration was 12.5 ms.

Category	Recording Channels (CH1:Somatosensory Cortex, CH2: Control-Forehead).			During recording 1 s	During stimulus 0.5 s
Cross-channel correlations for each stimulus level	NS_CH1	NS_CH2	r	0.022	0.032
			p	0.844	0.825
	SL10_CH1	SL10_CH2	r	**0.244**	0.25
			p	**0.029**	0.082
	SL20_CH1	SL20_CH2	r	0.169	**0.353**
			p	0.131	**0.013**
	SL30_CH1	SL30_CH2	r	**0.362**	**0.318**
			p	**0.001**	**0.026**
Within CH1, NS and different stimulus level correlations	NS_CH1	SL10_CH1	r	0.064	0.034
			p	0.57	0.811
	NS_CH1	SL20_CH1	r	-0.026	0.141
			p	0.812	0.332
	NS_CH1	SL30_CH1	r	0.054	0.09
			p	0.63	0.537
Within CH2, NS and different stimulus level correlations	NS_CH2	SL10_CH2	r	0.117	**0.363**
			p	0.299	**0.01**
	NS_CH2	SL20_CH2	r	-0.039	0.008
			p	0.726	0.956
	NS_CH2	SL30_CH2	r	-0.029	0.102
			p	0.793	0.481
Within CH1, cross correlations between different stimulus level	SL10_CH1	SL20_CH1	r	**0.291**	**0.281**
			p	**0.008**	**0.05**
	SL10_CH1	SL30_CH1	r	0.175	0.189
			p	0.119	0.191
	SL20_CH1	SL30_CH1	r	0.215	0.25
			p	0.055	0.082
Within CH1, cross correlations between different stimulus level	SL10_CH2	SL20_CH2	r	**0.276**	**0.405**
			p	**0.013**	**0.004**
	SL10_CH2	SL30_CH2	r	0.117	0.046
			p	0.296	0.748
	SL20_CH2	SL30_CH2	r	0.041	0.156
			p	0.712	0.281

Within CH1, the correlations between the NS condition and different stimulus levels were always not significant. On the other hand, within CH2, there was a significant correlation between the NS and SL 10 condition during the stimulus period (r=0.36, p=0.011).Additionally, within CH1, SL 10 and SL 20 conditions were significantly correlated both during the entire recording period and the stimulus period (respectively, r=0.29, p=0.009; r=0.28, p=0.051). Again, within CH2, SL 10 and SL 20 conditions were significantly correlated both during the recording period and the stimulus period (repectively, r=0.28, p=0.013; r=0.41, p=0.004).

2.4.4 Discussion

The mechanically evoked SEPs are different from the conventional signals recorded in the clinical EEG (α, β, δ oscillations), and electrically evoked SEPs. Electrically evoked SEP have been mostly used in the clinical setting for diagnosis of problems in neural pathways and for monitoring during spinal surgery [101]. During electrical stimulation, the number of neurons activated is high and also there is no differential activation of different afferent fibers. The evoked potentials are in the order of 5-20 μV. However, during mechanical stimulation, very little number of neurons is activated and the potential is in the order of 0.1-2 μV [102]. The electrically evoked SEP has little use for understanding somatosensory processing, except significant lesions. At the beginning of this study, we hoped instead that mechanically evoked SEPs may be useful for studying somatosensory processing and relating the psychophysical response and to the recorded potentials.

This study evaluated the mechanically evoked SEPs at different masking and test stimulus levels. We verified that masking elevates psychophysical detection thresholds consistent with previous studies. Similarly, we found a decrease in the mechanically evoked signal power during the test stimulus period after masking. This was found for 230 Hz stimulation. It is important to note that Pacinian-like cortical neurons in S1 do not generate spikes periodically as neurons associated with rapidly adapting fibers [103, 104]. This is probably why we did not see prominent frequency components at low

stimulus levels. At high stimulus levels, other neurons probably were also recruited.

On the other hand, RA-like neurons are more likely to fire periodically at high stimulus levels [105]. Unlike Kelly and Folger (1997, 1999), we did not find prominent peaks in the power spectral density plots for 40 Hz stimulation. However, there was a significant trend in the signal power around the stimulus frequency as the amplitude was increased. Still, the stimulus levels used were much higher than the threshold. Therefore, many different afferent types were probably recruited. Consequently, at this time, mechanically evoked SEP cannot give us detailed information about somatosensory processing.

In the time domain analysis showed that CH1 and CH2 get correlated as stimulus level is increased. This is reasonable due to spread of potentials on the scalp. On the other hand, the activity during stimulation was mostly not correlated with activity without stimulation which shows that mechanical stimulation evokes an activity pattern which is somehow not related to background activity. A significant finding was that, in both CH1 and CH2 the activity evoked with SL 10 and SL 20 was correlated. However, the activities evoked with other stimulus level combinations were not correlated. This suggests that the activity pattern somehow changes as the stimulus level is increased.

3.   CONCLUSIONS

3.1   Overview

In this thesis, the mechanical and temporal parameters affecting the psychophysical tactile thresholds of the P channel were investigated. Because the P channel has the lowest tactile thresholds at high frequencies it was attracted attention in many psychophysical studies. In addition, the P channel has properties such as temporal and spatial summation which are important in somatosensory processing and for haptics applications. In brief, my findings show that the temporal summation in the P channel is independent of the stimulus frequency. In other words, the amount of temporal summation more or less stays constant for any stimuli which activate the P channel. Additionally, it was shown that the classical temporal summation model should be extended to include the sensitivity characteristics of the P channel.

The mechanoreceptor and fiber innervation densities were studied extensively in the literature. It was known that the density of Pacinian corpuscles in human fingertip is approximately uniform longitudinally. Therefore, it was expected that the P channel thresholds should not vary along this axis. However, I found that the dynamic modulus of the skin changes, and probably as a result this affects the tactile detection thresholds. The loss modulus of the skin was found to be highly correlated with the psychophysical thresholds in the P channel. In this thesis, I applied three different contactor sizes at three different locations on fingertip. The spatial summation effect was clearly evident in the results.

As usual, in the forward masking protocol, the tactile thresholds increased as the masking level was increased. In this thesis, I tested whether this was reflected in the mechanically evoked SEPs. There was a significant decrease in the signal power during the test stimulus period probably due to the masking effect. This may be thought as the neural correlate of forward masking, which, according to our knowledge, was

not demonstrated before. However, mechanically evoked SEPs were not informative in every condition I tested. Therefore, they should be used with caution.

3.2   Implications

Tactile sensation can be impaired because of skin related diseases (scleroderma, morphoea, psoriasis, erysipelas and keloids that alters skin mechanics), due to aging, neurological conditions (multiple sclerosis), metabolic diseases (diabetic neuropathy), or due to complex disorders in psychiatric diseases (e.g. autism). This thesis may be useful for a detailed diagnosis of tactile sensitivity in these conditions, and to assess the effect of treatment.

Additionally, because of limb loss, some people may have to use prosthetics which typically lack tactile feedback today. According to a survey conducted by Lewis et al. (2012), most of prosthetics users rely on vision in order to control their movements. However, most of the users mentioned that they would prefer sensory feedback from their artificial limbs as temperature, vibration, electrical and pressure instead of visual or acoustical feedback. In order to provide a natural embodiment of the artificial limb, tactile feedback can be provided by indirect (mechanical or electrical stimulation of different area of skin) or direct (electrical stimulation of peripheral or central neurons) ways.

Indirect feedback systems are easy to implement because they are noninvasive. On the other hand, since tactile feedback is supplied to an alternate body part (i.e. residual limb) with respect to information from sensors in the prosthesis, patients need be trained to associate and utilize feedback signals that are physiologically relevant [106]. To create more biologically realistic tactile feedback systems it is imperative to stimulate either the peripheral nerve or the cortex.

The mechanical behavior of the skin may be important in some cosmetic applications. For example, the effectiveness of products such as creams can be tested;

new designs for electrical personal care products such as shavers can be developed. Additionally, plastic surgery may be improved by understanding more about skin mechanics.

3.3 Limitations

In this thesis a limited number of subjects could participate to the experiments, because our tests requires many sessions (25 hours/subject). Participants were mostly students in the University, therefore the subjects sample do not represent the entire population. However, we worked with participants in a narrow age range, because it was shown that tactile sensitivity decreases with age.

We did not control the skin surface temperature but we monitored it throughout the experiments and make sure that it was in a narrow range (30-34 ^{0} C). Although the Pacinian channel is sensitive to temperature, the variation in the measurements due to slight temperature changes is probably less than within subject variance.

The mechanically evoked SEPs measurements were done in a sound-proof booth. This structure was also electrically shielded. However, the signal to noise ratio in the recordings was very low. Even after averaging for 200 times, the signal was belove 1 μV. We observed that both the background noise and the signal supposedly due to the mechanical stimulus varied enormously between the subjects. In most of the trials, we could not obtain healthy recordings. Off-line analysis of the mechanically evoked SEPs data was often inconclusive regarding the presence of a mechanically evoked signal. Therefore, our findings need to be replicated. However, we obtained robust electrically evoked SEPs because of a larger recruitment of nerve fibers. The signal to noise ratio of mechanically evoked SEPs can be increased by using intra-dermal needle electrodes or direct recording on the cortex as in electrocorticogram.

The storage modulus was found to be negative probably because of inertial effects not accounted for. After measuring the force and displacement signals from the

impedance head conditioning amplifier, we subtracted the inertial contribution of the sensor tip and the contactor mass. This correction factor was always fixed and applied in the calculations. However, probably due to experimental measurement errors, the inertial effects were not entirely canceled, especially because of the high frequency (250 Hz) which has a squared contribution to the measurements.

For modulus calculations, I converted force measurement to stress by using a constant area, i.e. contactor area. However, the effective distribution of force changes due to indentation and is not constant. Specifically, the stress values are overestimated in this thesis, therefore, the moduli are also overestimated. The analyses can be improved by considering the contact problem in continuum mechanics.

APPENDIX A. LIST OF PUBLICATIONS

A.1 Journal Papers

Yıldız M.Z., Güçlü B. (2013), Relationship between vibrotactile detection threshold in the Pacinian channel and complex mechanical modulus of the human glabrous skin, Somatosensory and Motor Research, 30:1 ,pg 37-47.

Mehmet Ayyıldız, Burak Güçlü, Mustafa Zahid Yıldız, Çağatay Başdoğan. (2013) An Opto-Electro-Mechanical Tactile Sensor for Detection of Breast Lumps, IEEE Transactions on Haptics, vol. 6, no. 2, pp. 145-155, 2013.

1.2 International Conferences

Yıldız M.Z., Özsaltık M., Güçlü B. (2011), Temporal summation is independent of frequency in the Pacinial (P) Tactile channel, Psychonomic Society 2011, Seattle, W.A., Abstract Book, pp. 105.

Mehmet Ayyıldız , Burak Güçlü , Mustafa Z. Yıldız and Çağatay Başdoğan (2010) , A Novel Tactile Sensor for Detecting Lumps in Breast Tissue Haptics: Generating and Perceiving Tangible Sensations. Vol. 6191, A. Kappers, J. Van Erp, W. Bergmann Tiest, and F. Van der Helm, Eds., ed: Springer Berlin / Heidelberg, 2010, pp. 367-372.

Yıldız M.Z., Güçlü B. (2009) Neural correlate of psychophysical forward masking in the tactile Pacinian channel, Society for Neuroscience Abstracts, 35, program no.: 173.24.

Torun D., Yıldız M.Z., Güçlü B. (2009) Frequency following responses evoked

by vibrotactile stimulation of the distal phalanx in normal subjects, Türk Nöroloji Dergisi, 15 (Ek:1), 260-261.

Yıldız M.Z., Kahya Y., Güçlü B. (2008), Reconstruciton of Somatosensory Evoked Potentials by using Discrete Wavelet Transforms, X. International Conference on Cognitive Neuroscience, Bodrum.

1.3 National Conferences

Yıldız MZ, Güçlü B., (2010), The Effect of Psychophysical Forward Masking in the Pacinian Channel on Somatosensory Evoked Responses, Biyomut 2010, Antalya, Turkey.

Torun D., Yildiz M., Güçlü B. (2009) Parmak ucunun mekanik titresimle uyarılmasına karşın beyinden ölçülen frekans uyumlu cevaplar. Biyomut 2009, 14. Biyomedikal Mühendisligi Ulusal Toplantısı, ed. C. Güzeliş and M. Özgören, Izmir, Turkey, no: P43.

Yıldız M., Güçlü B. (2008), Optical Tactile Array Sensor for Lump Detection in Soft Tissue, Biyomut, ODTU, Anakara, Turkey.

REFERENCES

1. Schaefer, U. F., S. Hansen, M. Schneider, and J. L. Conteras, "Models for skin absorption and skin toxicity testing.," *Biotechnology: Pharmaceutical Aspects*, Vol. 7, pp. 3–33, 2008.

2. Bear, F. M., W. B. Connors, and A. M. Paradiso, "The somatic sensory system," in *Neuroscience, Exploring the Brain, Third edition.*, New York, USA: McGraw-Hill, 2006.

3. E R. Kandel, J. H. S., and M. J. Thomas, "Coding of sensory information," in *Principle of Neural Science 4th ed.*, pp. 411–429, New York, USA: McGraw-Hill, 4 ed., 2000.

4. Hendrix, F. M., "Mechanical behaviour of human epidermal and dermal layers in vivo," *PhD Thesis, Eindhoven University of Technology.*, Vol. 23, 2005.

5. Silver, F. H., J. W. Freeman, and D. DeVore, "Viscoelastic properties of human skin and processed dermis," *Skin Research and Technology*, Vol. 7, pp. 18–23, 2001.

6. Ebling, and R. Wilkinson, "Texbook of dermotology," *Blackwell Scientific Publ.*, 1992.

7. Johannson, R. S., U. Landström, and R. Lundström, "Responses of mechanoreceptive afferent units in the glabrous skin of the human hand to sinusoidal skin displacements," *Brain Research*, Vol. 244, pp. 17–25, 1982.

8. Bolanowski, S. J., G. A. Gescheider, and C. M. Checkosky, "Four channels mediate the mechanical aspects of touch.," *Journal of the Acoustical Society of America*, Vol. 84, pp. 1680–1694, 1988.

9. Bolanowski, S. J., and J. J. Zwislocki, "Intensity and frequency characteristics of pacinian corpuscles. i. action potentials," *Journal of Neurophysiology*, Vol. 51, pp. 793–811, 1984a.

10. Brown, A. G., R. E. Fyffe, and R. Noble, "Projections from pacinian corpuscles and rapidly adapting mechanoreceptors of glabrous skin to the catâs spinal cord," *Journal of Physiology*, Vol. 307, pp. 385–400, 1980.

11. Güçlü, B., E. A. Schepis, S. Yelke, C. A. Yücesoy, and S. J. Bolanowski, "Ovoid geometry of the pacinian corpuscle is not the determining factor for mechanical excitation," *Somatosensory and Motor Research*, Vol. 23, pp. 119–126, 2006.

12. Pawson, L., L. T. Prestia, G. K. Mahoney, B. Güçlü, P. J. Cox, and A. K. Pack, "Gabaergic/glutamatergicâglial/neuronal interaction contributes to rapid adaptation in pacinian corpuscles," *Journal of Neuroscience*, Vol. 29, pp. 2695–2705, 2009.

13. Lai, T. S. Y., and W. N. Findley, "Behaviour of nonlinear viscoelastic material under simultaneous stress relaxation in tension and creep in tortion," *J Appl Mech*, Vol. 36, pp. 22–27, 1969.

14. Manschot, J. F. M., and A. J. M. Brakkee, "The measurement and modeling of the mechanical properties of the human skin in vivo," *Journal of Biomechanics*, Vol. 19, pp. 511–515, 1986.

15. Maurel, W., Y. Wu, N. T. Magnenat, and D. Thalmann, "Biomechanical models for soft tissue simulation," *Esprit Basic Research Series*, Vol. 1, no. 1, pp. 79–83, 1998.

16. Daly, C., "Biomechanical properties of dermis," *The Journal of Investigative Dermatology*, Vol. 79, pp. 17–20, 1982.

17. Sedef, M., "Particleâbased modeling of nonlinear viscoelastic deformable objects based on experimental data," *Master Thesis, Koc University*, Vol. 1, pp. 32–60, 2008.

18. Findley, W. N., J. S. Lai, and K. Onaran, "viscoelasticity," in *Creep and relaxation of nonlinear viscoelastic materials*, Vol. 1, pp. 100–110, New York, USA: McGraw-Hill, 1 ed., 1976.

19. Silver, F. H., P. G. Seehra, J. W. Freeman, and D. DeVore, "Viscoelastic properties of young and old human dermis: A proposed molecular mechanism for elastic energy storage in collagen and elastin," *Journal of Applied Polymer Science*, Vol. 86, pp. 1978–1985, 2002.

20. Boyer, G., L. Laquieze, A. L. Bot, S. Laquieze, and H. Zahouani, "Dynamic indentation on human skin in vivo: ageing effects.," *Skin Res Technol.*, Vol. 15, no. 1, pp. 55–67, 2009.

21. Geerligs, M., C. W. J. Oomens, P. A. J. Ackermans, F. P. T. Baaijens, and G. W. M. Peters, "Linear shear response of the upper skin layers," *Biorheology*, Vol. 48, no. 3-4, pp. 229–245, 2011.

22. Dobrev, H., "Mechanical properties in other dermatological diseases," in *Bioengineering of the skin: skin biomechanics*, pp. 215–228, New York, USA: CRC Press, 2001.

23. Gescheider, G. A., S. J. Bolanowski, and R. T. Verillo, "Some characteristics of tactile channels," *Behavioral Brain Research*, Vol. 148, pp. 35–40, 2004.

24. Gescheider, G. A., S. J. Bolanowski, and K. R. Hardick, "The frequency selectivity of information-processing channels in the tactile sensory system," *Somatosensory and Motor Research*, Vol. 18, pp. 191–201, 2001.

25. Gescheider, G. A., S. J. Bolanowski, J. V. Pope, and R. T. Verillo, "A four-channel analysis of the tactile sensitivity of the fingertip: Frequency selectivity, spatial summation, and temporal summation," *Somatosensory and Motor Research*, Vol. 19, pp. 114–124, 2002.

26. Greenspan, J. D., and S. J. Bolanowski, "The psychophysics of tactile perception and its peripheral physiology basis," in *Handbook of Perception and Cognition* (Kruger, L., ed.), Vol. 7, pp. 25–103, San Diego, USA: McGraw-Hill, 4 ed., 1996.

27. Güçlü, B., and S. J. Bolanowski, "Frequency responses of cat rapidly adapting mechanoreceptive fibers," *Somatosensory and Motor Research*, Vol. 20, no. 3, pp. 249–263, 2003.

28. Gescheider, G. A., R. T. Verillo, and L. C. V. Doren, "Prediction of vibrotactile masking functions," *Journal of the Accoustical Society of America*, Vol. 72, pp. 1421–1426, 1982.

29. Gescheider, G. A., "Tactile psychophysics," in *Psychophysics: The Fundamentals*, McGraw-Hill, 4 ed., 1997.

30. Zwislocki, J. J., F. Maire, A. S. Feldman, and H. Rubin, "On the effect of practice and motivation on the threshold of audibility," *Journal of the Acoustical Society of America*, Vol. 30, pp. 254–262, 1958.

31. Zwislocki, J. J., and M. E. Relkin, "On a psychophysical transformed-rule up and down method converging on a 75Proceedings of the National Academy of Sciences of the USA, Vol. 98, pp. 4811–4814, 2001.

32. Morioka, M., and M. J. Griffin, "Dependence of vibrotactile thresholds on the psychophysical measurement method," *International Archives of Occupational and Environmental Health*, Vol. 75, pp. 78–84, 2002.

33. Verrillo, R. T., "Effect of contactor area on the vibrotactile threshold," *Journal of the Acoustical Society of America*, Vol. 35, pp. 1962–1966, 1963.

34. Verrillo, R. T., "Effect of spatial parameters on the vibrotactile threshold," *Journal of Experimental Psychology*, Vol. 71, pp. 570–575, 1966.

35. Bekesy, G. V., "The recruitment phenomenon and difference limen in hearing and vibration sense," *Laryngoscope*, Vol. 57, pp. 756–777, Dec 1947.

36. Verrillo, R. T., "Temporal summation in vibrotactile sensitivity," *Journal of the Acoustical Society of America*, Vol. 37, pp. 843–846, 1965.

37. Green, G. B., "Vibrotactile temporal summation: Effect of frequency," *Journal of General Psychology*, Vol. 1, pp. 138–149, 1976.

38. Gescheider, G. A., E. J. Beiles, C. M. Checkosky, S. J. Bolanowski, and R. T. Verillo, "The effects of aging on information-processing channels in the sense of touch: Ii. temporal summation in the p channel," *Somatosensory and Motor Research*, Vol. 11, no. 4, pp. 359–365, 1994.

39. Gescheider, G. A., M. E. Berryhill, R. T. Verillo, and S. J. Bolanowski, "Vibrotactile temporal summation: probability summation or neural integration?," *Somatosensory and Motor Research*, Vol. 16, no. 3, pp. 229–242, 1999.

40. Gescheider, G. A., "Evidence in support of the duplex theory of mechanoreception," *Sensory Processes*, Vol. 1, pp. 68–76, 1976.

41. Zwislocki, J. J., F. Maire, A. S. Feldman, and H. Rubin, "Theory of temporal auditory summation," *Journal of the Acoustical Society of America*, Vol. 32, pp. 1046–1059, 1960.

42. Feldman, A. S., and J. J. Zwislocki, "Effect of the acoustic reflex on the impedance at the eardrum," *J Speech Hear Res.*, Vol. 8, no. 3, pp. 213–222, 1965.

43. Gescheider, G. A., and J. M. Joelson, "Vibrotactile temporal summation for threshold and suprathreshold levels of stimulation," *Percept Psychophys*, Vol. 33, no. 2, pp. 156–162, 1983.

44. Gescheider, G. A., B. Güçlü, J. L. Sexton, S. Karalunas, and A. Fontana, "Spatial summation in the tactile sensory system: Probability summation and neural integration," *Somatosensory and Motor Research*, Vol. 22, pp. 255–268, 2005.

45. Güçlü, B., and S. J. Bolanowski, "Vibrotactile thresholds of the non-pacinian i channel: Ii. predicting the effects of contactor location on the phalanx," *Somatosensory and Motor Research*, Vol. 22, pp. 57–68, 2005.

46. Gescheider, G. A., R. D. Frisina, and R. T. Verillo, "Selective adaptation of vibrotactile thresholds," *Sensory Processes*, Vol. 3, no. 1, pp. 37–48, 1979.

47. Foley, J. M., and G. M. Boynton, "Forward pattern masking and adaptation: effects of duration, interstimulus interval, contrast, and spatial and temporal frequency," *Vision Res*, Vol. 33, no. 7, pp. 959–980, 1993.

48. Oxenham, A. J., and C. J. Plack, "Effects of masker frequency and duration in forward masking: further evidence for the influence of peripheral nonlinearity," *Hear Res*, Vol. 150, no. 1, pp. 258–266, 2000.

49. Dalton, P., "Psychophysical and behavioral characteristics of olfactory adaptation," *Chem Senses*, Vol. 25, no. 4, pp. 487–492, 2000.

50. Hamer, R. D., R. T. Verillo, and J. J. Zwislocki, "Vibrotacile masking of pacinian and non-pacinian channels," *J Acoust Soc Am.*, Vol. 73, no. 4, pp. 1293–1303, 1983.

51. Gescheider, G. A., C. L. V. Doren, and R. T. Verillo, "Vibrotactile forward masking: Effects of the amplitude level and duration of the masking stimulus," *Journal of the Acoustical Society of America*, Vol. 78, no. 2, pp. 534–543, 1985.

52. Gescheider, G. A., K. E. Santoro, J. C. Makous, and S. J. Bolanowski, "Vibrotactile forward masking: Effects of the amplitude level and duration of the masking stimulus," *Journal of the Acoustical Society of America*, Vol. 98, pp. 3188–3194, 1995.

53. Kirman, J. H., "Vibrotactile frequency recognition: forward and backward masking effects," *J Gen Psychol*, Vol. 113, no. 2, pp. 147–158, 1986.

54. Güçlü, B., and S. J. Bolanowski, "Vibrotactile thresholds of the non-pacinian i channel: I. methodological issues," *Somatosensory and Motor Research*, Vol. 22, pp. 49–56, 2005.

55. Hoppe, U., K. Schnabel, S. Weiss, and I. Rundshagen, "Representation of somatosensory evoked potentials using discrete wavelet transform," *Journal of Clinical Monitoring and Computing*, Vol. 17, no. 3, pp. 227–233, 2002.

56. Karl, E. M., "Somatosensory evoked potentials," in *Spehlmann's Evoked Potential Primer*, Vol. 1, Butterworth-Heinemann, 3 ed., 2001.

57. Lebedev, M. A., J. M. Denton, and R. J. Nelson, "Vibration-entrained and premovement activitiy in mokey primary somatosensory cortex," *Journal of Neurophysiology*, Vol. 72, no. 4, pp. 1654–1673, 1994.

58. Lebedev, M. A., and R. J. Nelson, "High-frequency vibratory sensitive neurons in monkey primary somatosensory cortex: entrained and nonentrained responses to vibration during the performance of vibratory-cued hand movements," *Exp Brain Res.*, Vol. 111, no. 3, pp. 313–325, 1996.

59. Kelly, F. E., T. Mats, and S. E. Folger, "Models for skin absorption and skin toxicity testing," *Journal of Neurophysiology*, Vol. 77, pp. 137–144, 1997.

60. Kelly, F. E., and S. E. Folger, "Eeg evidence of stimulus-directed response dynamics in human somatosensory cortex," *Brain Research*, Vol. 815, pp. 326–336, 1999.

61. Checkosky, C. M., and S. J. Bolanowski, "Effects of stimulus duration on the response properties of pacinian corpuscles: Implications for the neural code," *Journal of the Acoustical Society of America*, Vol. 91, pp. 3372–3380, 1992.

62. Checkosky, C. M., and S. J. Bolanowski, "The effect of stimulus duration on frequency-response functions in the pacinian (p) channel," *Somatosensory and Motor Research*, Vol. 11, pp. 47–56, 1994.

63. Verrillo, R. T., and S. J. Bolanowski, "The effects of skin temperature on the psychophysical responses to vibration on glabrous and hairy skin," *Journal of the Acoustical Society of America*, Vol. 80, pp. 528–532, 1986.

64. Güçlü, B., and Ç Öztek, "Tactile sensitivity of children: Effects of frequency, masking, and the non-pacinian i psychophysical channel," *Journal of Experimental Child Psychology*, Vol. 98, pp. 113–130, 2007.

65. Cauna, N., and G. Mannan, "The structure of human digital pacinian corpuscles and its functional significance," *Muscle and Nerve*, Vol. 92, pp. 1–20, 1958.

66. Knibestol, M., and A. B. Vallbo, "Single unit analysis of mechanoreceptor activity from the human glabrous skin area," *Acta Physiologica Scandinavica*, Vol. 80, pp. 178–195, 1970.

67. Johannson, R. S., "Receptive field sensitivity profile of mechanosensitive units innervating the glabrous skin of the human hand," *Brain Research*, Vol. 104, pp. 330–334, 1976.

68. Vallbo, A. B., and R. S. Johansson, "The tactile sensory innervation of the glabrous skin of the human hand," in *Active Touch: The Mechanism of Recognition of Objects by Manipulation* (Gordon, G., ed.), pp. 29–54, New York, USA: Oxford: Pergamon Press., 1978.

69. Sato, M., "Response of pacinian corpuscles to sinusoidal vibration," *Journal of Physiology*, Vol. 159, pp. 391–409, 1961.

70. Freides, D., "Human information processing and sensory modality: cross-modal functions, information complexity, memory, and deficit," *Psychological Bulletin*, Vol. 81, pp. 284–310, 1974.

71. Bolanowski, S. J., and J. J. Zwislocki, "Intensity and frequency characteristics of pacinian corpuscles. ii. receptor potentials," *Journal of Neurophysiology*, Vol. 51, pp. 812–830, 1984b.

72. Lamore, P. J. J., H. Muijser, and C. J. Keemink, "Envelope detection of amplitude-modulated high-frequency sinusoidal signals by skin mechanoreceptors," *Journal of the Acoustical Society of America*, Vol. 79, pp. 1082–1085, 1986.

73. Bensmaia, S., M. Hollins, and J. Yau, "Vibrotactile intensity and frequency information in the pacinian system: A psychophysical model," *Perception and Psychophysics*, Vol. 67, pp. 828–841, 2005.

74. Verillo, R. T., "Investigation of some parameters of the cutaneous threshold for vibration," *Journal of the Acoustical Society of America*, Vol. 34, pp. 1768–1773, 1962.

75. Mountcastle, V. B., R. H. LaMotte, and G. Carli, "Detection thresholds for stimuli in humans and monkeys: Comparison with threshold events in mechanoreceptive afferent fibers innervating the monkey hand," *Journal of Neurophysiology*, Vol. 159, pp. 122–136, 1972.

76. Whitehouse, J. D., M. Miyuki, and M. J. Griffin, "Effect of contact location on vibrotactile thresholds at the finger," *Somatosensory and Motor Research*, Vol. 23, pp. 73–81, 2006.

77. Verrillo, R. T., "Vibrotactile thresholds measured at the finger," *Perception and Psychophysics*, Vol. 9, pp. 329–330, 1971.

78. Johannson, R. S., and A. B. Vallbo, "Tactile sensibility in the human hand: Relative and absolute densities of four types of mechanoreceptive units in glabrous skin," *Journal of Physiology*, Vol. 286, pp. 283–300, 1979.

79. Moore, T. J., "A survey of the mechanical characteristics of skin and tissue in response to vibratory stimulation," *IEEE Transactions on Man-Machine Systems*, Vol. 11, pp. 79–84, 1970.

80. Moore, T. J., and J. R. Mundie, "Measurement of specific mechanical impedance of the skin: effects of static force, site of stimulation, area of probe, and presence of a surround," *The Journal of the Acoustical Society of America*, Vol. 52, pp. 577–584, 1972.

81. Pubols, B. H., "Effects of mechanical stimulus spread across glabrous skin of raccoon and squirrel monkey hand on tactile primary afferent fiber discharge," *Somatosensory and Motor Research*, Vol. 4, pp. 273–308, 1987.

82. Bermudez, F. V., and K. O. Johnson, "Surround suppression in the responses of primate sa1 and ra mechanoreceptive afferents mapped with a probe array," *Journal of Neurophysiology*, Vol. 81, pp. 2711–2719, 1999.

83. Wang, Q., and V. Hayward, "In vivo biomechanics of the fingerpad skin under local tangential traction," *Journal of Biomechanics*, Vol. 40, pp. 851–860, 2007.

84. Gilmer, B. V. H., "The measurements of the sensitivity of the skin to mechanical vibration," *Journal of General Psychology*, Vol. 13, pp. 42–61, 1935.

85. Lundström, R., "Local vibrations-mechanical impedance of the human handâs glabrous skin," *Journal of Biomechanics*, Vol. 17, pp. 137–144, 1984.

86. Srinivasan, M. A., and K. Dandekar, "An investigation of the mechanics of tactile sense using two-dimensional models of the primate fingertip," *Transactions of the ASME*, Vol. 118, pp. 48–55, 1996.

87. Cohen, J. C., J. C. Makous, and S. J. Bolanowski, "Under which conditions do the skin and probe decouple during sinusoidal vibrations?," *Experimental Brain Research*, Vol. 129, pp. 211–217, 1999.

88. Bell, J., S. Bolanowski, and M. H. Holmes, "Models for skin absorption and skin toxicity testing," *Progress in Neurobiology*, Vol. 42, pp. 79–128, 1994.

89. Silver, F. H., "Coding of sensory information," in *Biological materials structure, mechanical properties and modeling of soft tissues*, Vol. 1, New York: NYU Press, 4 ed., 1987.

90. Boyer, G., H. Zahouani, A. L. Bot, and L. Laquiezee, "In vivo characterization of viscoelastic properties of human skin using dynamic micro-indentation," *Proceedings of the 29th Annual International Conference of IEEE EMBS*, pp. 4584–4587, 2007.

91. Hakansson, B., P. Carlsson, and A. Tjesllstrom, "The mechanical point impedance of the human head, with and without skin penetration," *Journal of the Acoustical Society of America*, Vol. 80, pp. 1065–1075, 1986.

92. Pereira, J. M., J. M. Mansour, and B. R. Davis, "Dynamic measurement of the viscoelastic properties of skin," *Journal of Biomechanics*, Vol. 24, pp. 157–162, 1991.

93. Kirkpatrick, S. J., D. D. Duncan, and L. Fang, "Low-frequency surface wave propagation and viscoelastic behavior of porcine skin," *Journal of Biomedical Optics*, Vol. 9, pp. 1311–1319, 2004.

94. Xu, F., and T. J. Lu, "Skin biothermomechanics: Modeling and experimental characterization. in: Aref h, van der giessen e, editors. advances in applied mechanics volume 43," *San Diego: Academic Press*, pp. 148–249, 2008.

95. Hendrix, F. M., D. Brokken, C. W. J. Oomens, D. L. Bader, and F. P. T. Baaijens, "The relative contributions of different skin layers to the mechanical behavior of human skin in vivo using suction experiments," *Medical Engineering and Physics*, Vol. 28, pp. 259–266, 2006.

96. Hubbard, S. J., "A study of rapid mechanical events in a mechanoreceptor," *Journal of Physiology*, Vol. 141, pp. 198–218, 1958.

97. Lowenstein, W. R., and R. Skalak, "Mechanical transmission in a pacinian corpuscle. an analaysis and a theory," *Journal of Physiology*, Vol. 182, no. 4, pp. 346–378, 1966.

98. Mouraux, A., and G. D. Iannetti, "Across-trial averaging of event-related eeg responses and beyond," *Magnetic Resonance Imaging*, Vol. 26, no. 7, pp. 1041–1054, 2008.

99. Mallat, S. G., "A theory for multiresolution signal decomposition: The wavelet representation," *IEEE Trans Pattern Anal Machine*, Vol. 11, pp. 674–692, 1989.

100. Prasher, D. K., and M. Cohen, "The selective effects of central masking on brain stem potentials," *Br J Audiol*, Vol. 18, no. 2, pp. 79–83, 1984.

101. Stechison, M. T., S. G. Panagis, and S. S. Reinhart, "Somatosensory evoked potential. monitoring during spinal surgery," *Acta Neurochir*, Vol. 135, pp. 56–61, 1995.

102. Yildiz, M., Y. Kahya, and B. Güçlü, "Reconstruciton of somatosensory evoked potentials by using discrete wavelet transforms, x. international conference on cognitive neuroscience," *Abstract Book*, p. 449, 2008.

103. Mountcastle, V. B., W. H. Sakata, and J. Hyvarinen, "Cortical neuronal mechanisms in flutter-vibration studied in unanesthetized monkeys. neuronal periodicity and frequency discrimination," *J Neurophysiology*, Vol. 32, no. 3, pp. 452–484, 1969.

104. Ferrington, D. G., and M. J. Rowe, "Differential contributions to coding of cutaneous vibratory information by cortical somatosensory areas i and ii," *J Neurophysiology*, Vol. 43, no. 2, pp. 310–331, 1980.

105. Talbot, W. H., I. D. Smith, H. H. Kornhuber, and V. B. Mountcastle, "The sense of flutter-vibration: comparison of the human capacity with response patterns of mechanoreceptive afferents from the monkey hand," *J Neurophysiology*, Vol. 31, no. 2, pp. 301–334, 1968.

106. Marasco, P. D., K. Kim, J. E. Colgate, M. A. Peshkin, and T. A. Kuiken, "Robotic touch shifts perception of embodimentto a prosthesis in targeted reinnervation amputees," *Brain*, Vol. 134, pp. 747–758, 2011.